UNIVERSITY OF CALIFORNIA
SANTA CRUZ

NO CHROMOSOME LEFT BEHIND: MECHANISMS THAT ALLOW LAGGING CHROMOSOMES TO ENTER DAUGHTER NUCLEI

A dissertation submitted in partial satisfaction
of the requirements for the degree of

DOCTOR OF PHILOSOPHY

in

MOLECULAR, CELL AND DEVELOPMENTAL BIOLOGY

by

Brandt B. Warecki

June 2019

The Dissertation of Brandt Warecki is approved:

_____
Professor William Sullivan, chair

_____
Professor Needhi Bhalla

_____
Professor John Tamkun

_____
Lori Kletzer
Vice Provost and Dean of Graduate Studies

Table of Contents

List of Figures and Tables

Abstract

NO CHROMOSOME LEFT BEHIND: MECHANISMS THAT ALLOW LAGGING CHROMOSOMES TO ENTER DAUGHTER NUCLEI

Brandt Warecki

Cells that divide with lagging chromosomes risk losing key genetic information if those chromosomes are not incorporated into daughter nuclei. When the nuclear envelope reforms a physical barrier around the daughter nucleus, lagging chromosomes are expected to be locked out of the nucleus and form damage-prone micronuclei. While micronuclei occur fairly frequently in cancer cells, lagging chromosomes can still sometimes enter telophase daughter nuclei to preserve euploidy. However, very little is known about the cellular mechanisms that allow lagging chromosomes to reintegrate into daughter nuclei and maintain genome integrity. In *Drosophila*, lagging chromosome fragments lacking a centromere, called acentrics, are capable of efficient reintegration into telophase daughter nuclei. Acentrics remain connected to daughter nuclei through a DNA tether. The tether is coated with Polo kinase, BubR1 kinase, Aurora B kinase, and INCENP, but the function of the tether is poorly understood. Here, I use *Drosophila* as a model system to identify mechanisms that promote lagging chromosome reintegration. I find that dividing with lagging chromosomes triggers the formation of highly localized gaps in the nascent nuclear envelope surrounding daughter nuclei. These gaps form channels through which acentrics pass to enter into daughter nuclei. Channel formation requires the pool of Aurora B kinase localized to the tether. Aurora B kinase

phosphorylates chromatin on the acentric and at the site of acentric entry, keeping this chromatin in a mitotic state that prevents the recruitment of nuclear envelope components, leading to gap formation. Furthermore, I find that while acentrics are free of lamin and nuclear pore complexes, nuclear membrane frequently contacts acentrics during reintegration. Fusion between membrane on the acentric and membrane on the nucleus guides the acentric through the channel. The membrane fusion protein Comt/NSF and the ESCRT-III component Shurb/CHMP4B are required for these fusion events and efficient acentric entry into daughter nuclei. Taken together, these results uncover novel mechanisms by which lagging chromosomes can rejoin daughter nuclei to preserve the integrity of the genome.

Dedication and Acknowledgments

I would like to thank Dr. Sullivan for his expert mentorship, for being enthusiastic about my research, and for providing me the support and to present at diverse conferences. I would like to thank my thesis committee, Dr. Bhalla and Dr. Tamkun, for their input, guidance, and support—both with my research projects and with my development as a scientist. I would like to thank the current and past members of the Sullivan Lab for their advice and always being open to have a conversation about anything. In particular, I would like to thank Travis, Lotti, Laura, and Simon for being not just labmates but also friends. I would like to thank the entire MCD Department at UCSC for welcoming me into their community. Finally, I would like to thank my family, Anna, Jack, Rebecca, and Rachael, without whose unwavering support this would not have been possible.

The text of this dissertation includes reprints of the following previously published material: Karg, T., Warecki, B.*, and Sullivan, W. (2015). Aurora B-mediated localized delays in nuclear envelope formation facilitate inclusion of late-segregating chromosome fragments*. Molecular Biology of the Cell. *26: 2227-2241 and Warecki, B., and Sullivan, W. (2018). Micronuclei Formation is Prevented by Aurora B-Mediated Exclusion of HP1a from Late-Segregating Chromatin in* Drosophila. Genetics. *210: 171-187. * Indicates equal contribution. The co-author (William Sullivan) listed on these publications directed and supervised the research which forms the basis for the dissertation*.

CHAPTER 1: Aurora B-mediated localized delays in nuclear envelope formation facilitate inclusion of late-segregating chromosome fragments

Abstract

To determine how chromosome segregation is coordinated with nuclear envelope formation (NEF), we examined the dynamics of NEF in the presence of lagging acentric chromosomes in *Drosophila* neuroblasts. Acentric chromosomes often exhibit delayed but ultimately successful segregation and incorporation into daughter nuclei. However, it is unknown whether these late segregating acentric fragments influence NEF to ensure their inclusion in daughter nuclei. Through live analysis, we show that acentric chromosomes induce highly localized delays in the reassembly of the nuclear envelope. These delays result in a gap in the nuclear envelope that facilitates the inclusion of lagging acentrics into telophase daughter nuclei. Localized delays of nuclear envelope reassembly require Aurora B kinase activity. In cells with reduced Aurora B activity, there is a decrease in the frequency of local nuclear envelope reassembly delays, resulting in an increase in the frequency of acentric-bearing lamin-coated micronuclei. These studies reveal a novel role of Aurora B for maintaining genomic integrity by promoting the formation of a passageway in the nuclear envelope through which late segregating acentric chromosomes enter the telophase daughter nucleus.

Introduction

The eukaryotic cell has evolved a number of mechanisms to maintain genome integrity. In response to damaged or improperly replicated DNA, cell cycle checkpoints activate signaling pathways that influence the activity of both positive and negative cell cycle regulators, providing time for repair or elimination of the damaged cell (Abbas et al., 2013). The molecular basis of these signaling pathways has been extensively investigated, with much of the work focused on the action of DNA damage/replication checkpoints during interphase (G1, S, and G2) (Rhind and Russell, 2012). Recent studies provide convincing evidence that cells entering metaphase with damaged chromosomes delay anaphase entry, suggesting the activation of DNA damage checkpoints during metaphase. Support for this interpretation comes from studies in a number of cell types, demonstrating that these DNA damage induced metaphase delays depend on the spindle assembly and DNA damage checkpoints (Cipressa and Cenci, 2013; Zhang and Hunter, 2014; Mikhailov et al., 2002; Fasulo et al., 2012). For example, in *Drosophila chk1/grp* is required for delaying anaphase entry in response to double-strand breaks (Royou et al., 2005).

In spite of these safeguards, cells occasionally exit metaphase with damaged DNA. Unrepaired double-strand breaks (DSBs) are particularly problematic because they produce chromosome fragments lacking either a centromere or a telomere (Kaye et al., 2004). The former, known as acentrics, are incapable of forming normal attachments with the mitotic spindle and are thus expected to exhibit segregation defects. For example, acentrics often fail to properly segregate, resulting in their

exclusion from daughter nuclei and inclusion in cytoplasmic micronuclei (Fenech et al., 2011; LaFountain et al., 2001; Kanda and Wahl, 2000). In *Drosophila*, the behavior of acentrics has been examined by taking advantage of transgenic lines bearing an inducible I-CreI endonuclease (Royou et al., 2010; Rong et al., 2002). I-CreI specifically targets the rDNA locus near the base of the X chromosome (Rong et al., 2002; Maggert and Golic, 2005; Paredes and Maggert, 2009**;** Golic and Golic, 2011)**.** Surprisingly, I-CreI induced acentrics segregate in a delayed but otherwise normal fashion due to the action of DNA tethers connecting the fragments to their centric partners (Royou et al., 2010; Kotadia et al., 2012). The DNA tether contains histones and is coated with BubR1, Polo, and the chromosome passenger proteins Aurora B and INCENP (Royou et al., 2010). During metaphase, acentrics localize to the outer edge of the metaphase plate, separated from the main mass of chromosomes. Upon entry into anaphase, they remain in this position while the main mass of sister chromosomes separate. Only during late anaphase do sister acentrics segregate to opposing poles. Polo and BubR1 are not necessary for tether formation but are required for the normal poleward movement of the acentrics (Royou et al., 2010).

The extensive delay in acentric segregation raises a number of questions regarding the spatial and temporal control of events during the anaphase-telophase transition, including the timing of NEF with respect to chromosome segregation. *Drosophila* cells undergo "semi-closed" mitosis in which the nuclear envelope only breaks down completely in early anaphase before reassembling again during late anaphase/early telophase (Katsani et al., 2008). Current models of NEF propose that

the nuclear envelope forms from mitotic endoplasmic reticulum (ER) extensions, which initiate interactions between chromatin and inner nuclear membrane proteins (Anderson and Hetzer, 2008; Lu et al., 2011). Membrane fusion of nuclear envelope microdomains and nuclear pore complex assembly complete NEF to build a fully functioning nuclear envelope (Baur et al., 2007; Dultz et al., 2008). Chromatin decondensation is concomitant with NEF and Aurora B has been shown to inhibit both decondensation and NEF on a global scale (Ramadan et al., 2007; Meyer et al., 2010; Afonso et al., 2014).

Understanding the mechanisms by which chromosome segregation and NEF are coordinated is of particular interest. Specifically, how would delayed segregation of acentric chromosomes influence the dynamics of nuclear envelope reformation during telophase? Here, we directly address this issue through live and fixed analyses of chromosome segregation and NEF in *Drosophila* larval neuroblasts bearing normal and lagging acentric chromosomes. Our analysis reveals a highly localized delay of the reassembly of NE components around the lagging acentrics that result in the formation of large gaps in the nascent nuclear envelope. Live analysis reveals that these gaps provide a means for late segregating acentrics to be included in the newly formed telophase nuclei. Aurora B kinase activity is required for these local nuclear envelope component reassembly delays. If Aurora B levels are reduced, the frequency of cells with delays in the reassembly of NE components upon I-CreI induction is greatly decreased. As a result, reduced Aurora B levels result in a dramatic increase in lamin-coated acentric-bearing micronuclei. Thus, in addition to its well-

established role in the spindle midzone assembly, kinetochore-microtubule attachments, and the abscission checkpoint (Douglas et al., 2010; Tanaka et al., 2002; Norden et al, 2006), we find that Aurora B also plays an important role in maintaining genomic integrity by facilitating the entry of late segregating acentrics into daughter nuclei through highly localized delays in the reassembly of nuclear envelope.

Results

Acentric chromosomes induce highly localized delays in the reassembly of the nuclear envelope during telophase

To examine the impact of severely delayed acentric chromosome segregation on nuclear envelope formation (NEF), we visualized NEF in third instar *Drosophila* neuronal stem cells (neuroblasts) in which lagging acentrics were induced by I-CreI. Third instar neuroblasts divide asymmetrically to produce a large self-renewing neuroblast and a smaller ganglion mother cell, which divides once more giving rise to a post-mitotic neuron (Doe, 2008). Transgenic *Drosophila* bearing the heat-inducible I-CreI endonuclease produce DSBs specifically at the rDNA repeats on the X-chromosome (Maggert and Golic, 2005; Rong et al., 2002). The resulting acentrics localize to the edge of the metaphase plate and eventually segregate to the poles late in anaphase through the action of a DNA tether attaching each acentric fragment to its centric partner (Royou et al., 2010). In addition to I-CreI, these transgenic lines express the Histone 2 variant (H2Av) labeled with RFP, (H2Av)-RFP, and lamin B-

GFP, facilitating live analysis of chromosome and nuclear envelope dynamics in neuroblasts (see materials and methods).

Live imaging of chromosome segregation and reformation of the nuclear lamina in neuroblasts with undamaged chromosomes (no I-CreI expression) is shown in the top panel of Figure 1A (see Movie 1). In neuroblasts with undamaged chromosomes, NEF occurs rapidly after sister chromatid segregation (Figure 1A, top panel; Movie 1). Time 0 marks the onset of anaphase as defined by separation of sister chromosomes. Once NEF is initiated, it proceeds until it is fully completed, as visualized by lamin B-GFP signal completely surrounding the segregated chromatin (compare time points 180-240). On average, initiation and completion of NEF occurred approximately 217 +/- 102 sec (N=6) and 327 +/- 116 sec (N=6) respectively after anaphase onset. Despite neuroblast divisions being asymmetric with respect to their cell size (Jiang and Reichert, 2014), centrosome morphology (Rebollo et al., 2007), microtubule aster size (Giansanti et al., 2001) and cortical components (Doe, 2008), we found that timing of NEF initiation and completion were synchronous in the two daughter nuclei, which is consistent with previous reports (Katsani et al., 2008).

We next imaged chromosome separation and NEF in neuroblasts bearing I-CreI induced acentrics (Figure 1A, bottom panel; see Movie 2). While initiation of NEF was slightly delayed in divisions with acentrics (298 +/- 65 sec (N=32)), we observed significant delays in completion of NEF (681 +/- 248 sec (N=14)) (Figure 1A, bottom panel, compare timepoints 280-680). The delay in NEF completion, as

visualized by a gap in the lamin B-GFP signal, was highly localized, consistently occurring at the site of acentric entry (Figure 1A green arrows). These gaps in the nuclear envelope serve as passageways for late segregating acentrics to enter the telophase nuclei. Our analysis revealed that the width of these nuclear envelope gaps did not undergo significant changes in diameter as the acentric passed through to rejoin the main nuclear mass. We found that the localized nuclear envelope gaps have an average width of 0.92μm +/- 0.27 (N=7). This is approximately 6 fold larger than the physical diameter of a nuclear pore (Wente and Rout, 2010). It should be pointed out that these localized delays in nuclear envelope reassembly only occur in the presence of an acentric and are not present in heat-shocked larvae without I-CreI.

To quantify the presence of localized delays in nuclear envelope reassembly induced by acentric chromosomes, we measured the fluorescence intensity of lamin B-GFP across the surface of the nuclear envelope during telophase (Figure 1B). Compared to regions on the same telophase nucleus without local delays in nuclear envelope reassembly (blue line), fluorescence intensity of lamin B-GFP was markedly lowered across the site where acentrics entered through local delays in nuclear envelope reassembly (red line) (Figure 1B, left panel). We did not observe the same lowered intensity of lamin B-GFP signal on the midzone face in non-I-CreI expressing control telophase neuroblasts (Figure 1B, right panel). We found that the lowered intensity of lamin B-GFP signal persisted until after the acentric had passed through the gap, at which point nuclear envelope assembly resumed, as visualized by an increase in lamin B-GFP signal (Figure 1C).

To further demonstrate that these gaps in the nuclear envelope were induced by acentrics, we performed live 3D rendering of telophase nuclei expressing I-CreI to determine the position of acentrics relative to the nuclear envelope gaps. This analysis revealed that the acentric is positioned within the channel formed by the gap in the nuclear envelope (Figure 1D).

Figure 1. Acentric chromosome fragments enter nascent daughter nuclei through highly localized delays in assembly of the nuclear envelope**.** (A) Still images from time-lapse movies of mitotic neuroblasts without (top panel, see Movie 1) and with (bottom panel see Movie 2) I-CreI-induced acentrics (red arrows). Acentrics enter daughter nuclei through nuclear envelope gaps (green arrows). The chromosomes are labeled with H2Av-RFP (red) and the nuclear envelope with lamin B-GFP (green). These gaps do not form when acentric fragments are not present. Dashed lines represent cell outlines. Scale bars are 2 μm. (B) Quantification of lamin B-GFP signal across the surface of the nuclear envelope gaps during NEF. Shown are graphs of the lamin B-GFP fluorescence intensity along pole facing (blue line) and midzone facing (red line) sections of the newly formed telophase nuclear envelopes with (left panel) and without acentrics (right panel). Each graph represents an average of three measurements. Error bars indicate standard deviations. Green brackets indicate the presence of a nuclear envelope gap. Scale bars are 2 μm. (C) Quantification of lamin B-GFP signal across the midzone face of a newly formed nuclear envelope before and after an acentric enters the daughter nucleus. Shown are graphs of the lamin B-GFP fluorescence intensity along pole facing (blue line) and midzone facing (red line) sections of the telophase nuclear envelope before (top) and after (bottom) an acentric has entered the daughter nucleus. Each graph represents an average of three measurements. Error bars indicate standard deviations. Green brackets indicate the presence of a nuclear envelope gap. Scale bar is 2 μm. (D) Multi-plane 3D rendering of an I-CreI-induced acentric entering a nascent daughter nucleus through a nuclear envelope gap (green arrow). Red channel depicts H2Av-RFP. Green channel represents lamin B-GFP.

Figure 1

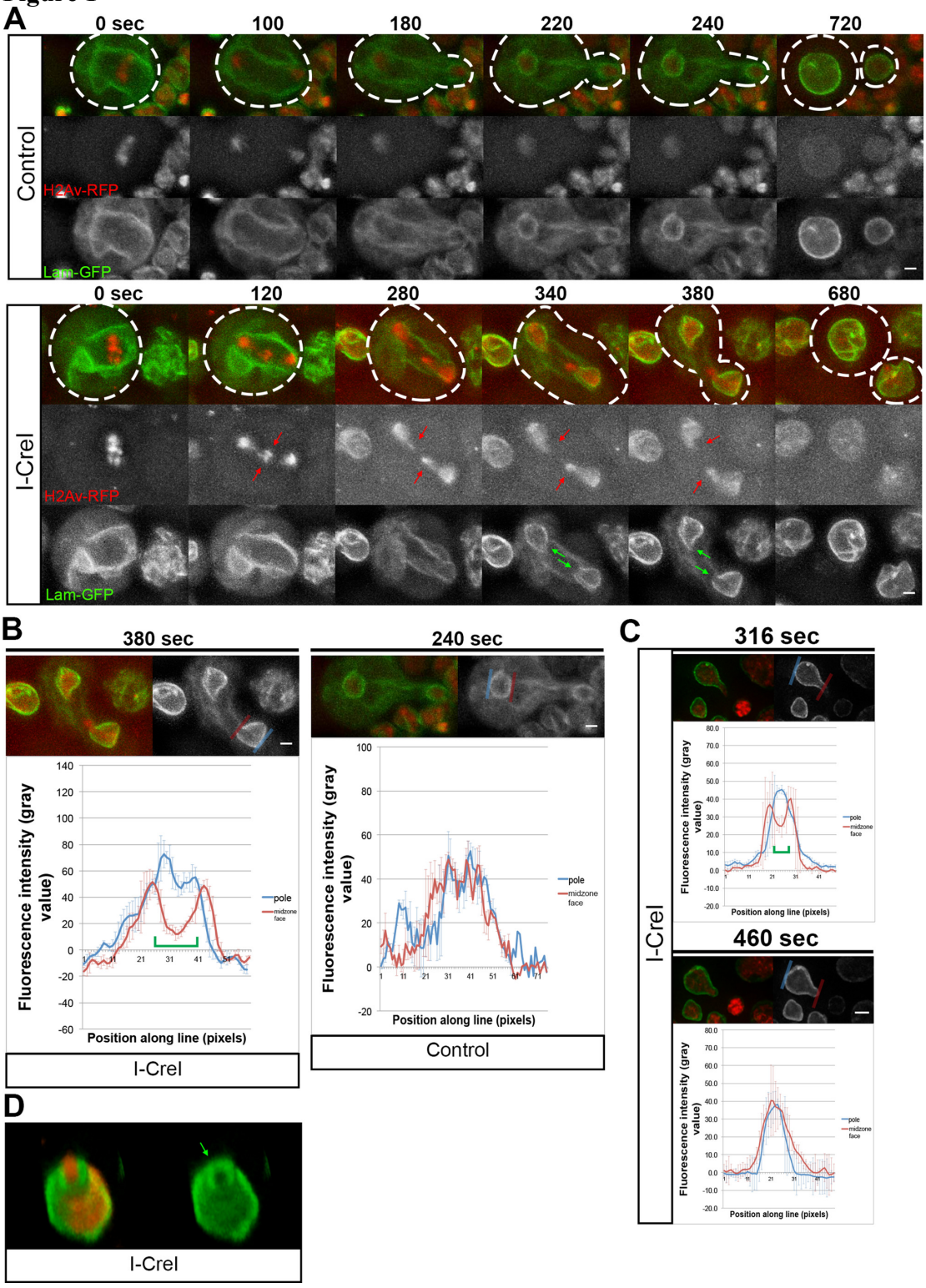
A
0 sec
100
180
220
240
720
Control
H2Av-RFP
Lam-GFP
0 sec
120
280
340
380
680
I-Crel
H2Av-RFP
Lam-GFP
B
380 sec
240 sec
Fluorescence intensity (gray value)
Position along line (pixels)
pole
midzone face
I-Crel
Control
C
316 sec
460 sec
I-Crel
D
I-Crel

To determine whether these localized gaps in nuclear envelope involve nuclear envelope proteins in addition to lamin B, we examined dividing non-I-CreI expressing control neuroblasts (Movie 3) and neuroblasts with I-CreI induced acentrics (Movie 4) that co-expressed a GFP-tagged nuclear pore complex protein, Nup107 (Figure 2). Embedded in the nuclear membrane, nuclear pore complexes are a highly conversed component of the nuclear envelope (Doucet and Hetzer, 2010). Similar to our live imaging analysis with lamin B-GFP, we observed localized delays and gaps in the reassembly of the nuclear envelope with GFP-Nup107 (Figure S1A, bottom panel, green arrow, see Movie 4). Similar to our experiments with lamin B-GFP, quantification of GFP-Nup107 fluorescence intensity along the nuclear envelope showed a decrease at the site of acentric entry compared to regions on the same nucleus where nuclear envelope reassembly was not delayed (compare Figure 2B to Figure 1B). Staged-matched control and I-CreI expressing neuroblasts in telophase demonstrate that using GFP-Nup107 to image the nuclear envelope reveal acentric generated gaps in the nuclear envelope (Figure 2C). Taken together with the lamin imaging, these studies suggest an absence of the nuclear envelope in the acentric-induced gaps but do not formally exclude the possibility that other components of the nuclear envelope have completely reassembled.

Figure 2. Nuclear envelope gaps are imaged using a GFP-tagged nuclear pore protein. (A) Still frames from time-lapse movies of mitotic neuroblasts expressing GFP-Nup107 and H2Av-RFP without (top panel, Movie 33) and with (bottom panel, Movie 4) I-CreI-induced acentrics. Red arrows indicate acentric chromosomes. Green arrow indicates the nuclear envelope gaps. Dashed lines outline the cell. Scale bars are 2 μm. (B) Quantification of GFP-Nup107 signal across the surface area of nuclear envelope gaps during NEF. Shown are graphs of the GFP-Nup107 fluorescence intensity along pole opposing and midzone facing sections of the newly formed telophase nuclear envelopes with (left and middle panel) and without acentrics (right panel). Depicted in each panel are merged RFP and GFP signals, GFP signal alone, and graphical representation of GFP fluorescence intensity measured along a line tangent to the nuclear envelope at the polar (blue line) and midzone (red line) faces of the nucleus. Each graph represents an average of three measurements. Error bars indicate standard deviations. Green brackets indicate the presence of a nuclear envelope gap. Scale bars are 2 μm. (C) Stage-matched telophase nuclei from neuroblasts with (right panel) and without (left panel) I-CreI-induced acentrics. Red arrow indicates acentric. Green arrow indicates nuclear envelope gap. Scale bars are 2 μm.

Figure 2

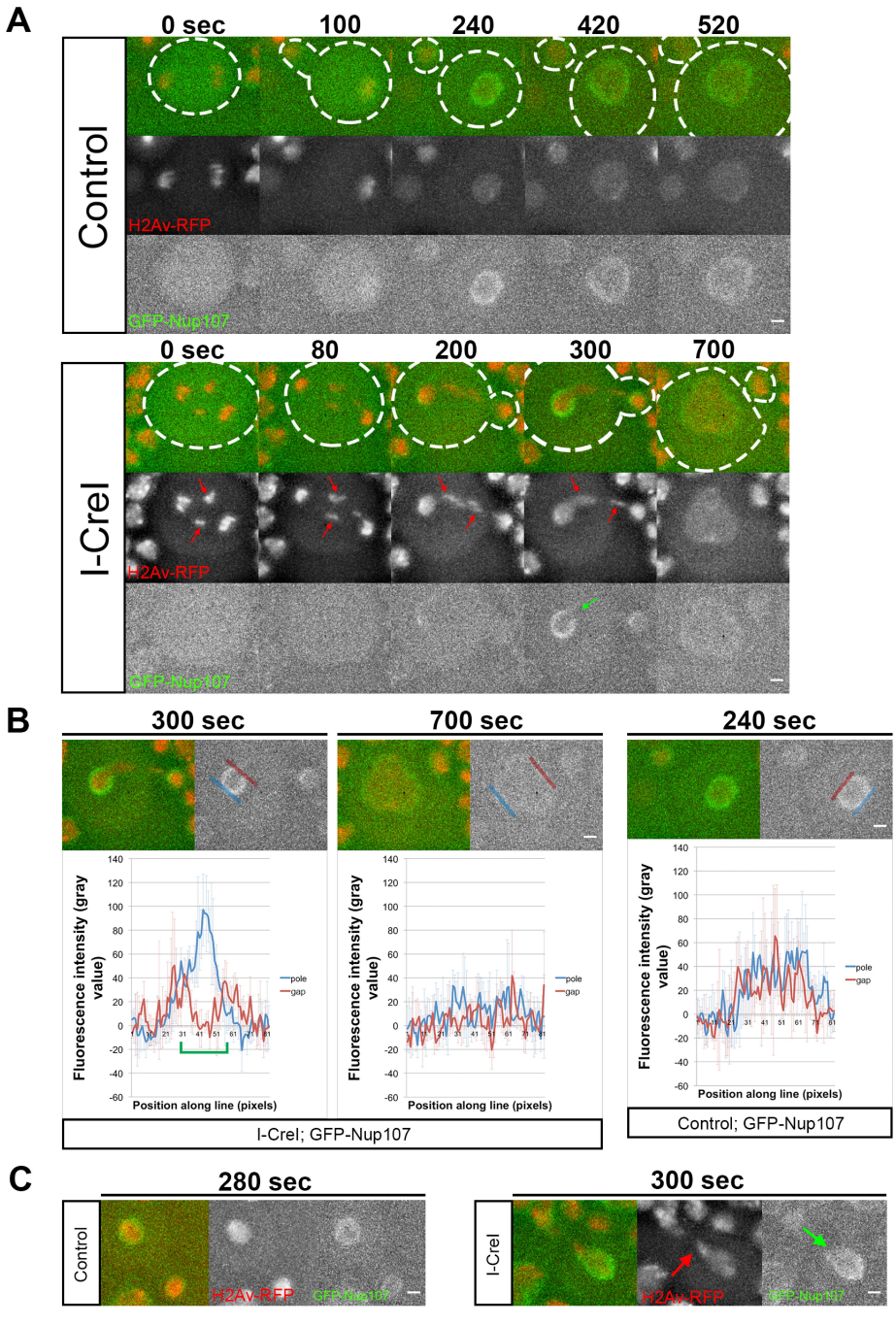
A
0 sec
100
240
420
520
Control
H2Av-RFP
GFP-Nup107
0 sec
80
200
300
700
I-CreI
H2Av-RFP
GFP-Nup107
B
300 sec
700 sec
240 sec
Fluorescence intensity (gray value)
Position along line (pixels)
pole
gap
I-CreI; GFP-Nup107
Control; GFP-Nup107
C
280 sec
300 sec
Control
I-CreI
H2Av-RFP
GFP-Nup107

Localized delays and gaps in nuclear envelope formation are determined by the timing of acentric chromosome segregation

To further define the relationship between acentric chromosome segregation and localized gaps in the nuclear envelope, we investigated whether the timing of acentric segregation correlates with gap formation. The initiation of acentric chromosome segregation occurs at varying times following the onset of anaphase segregation of the undamaged autosomes (Royou et al., 2010). In theory, acentrics that segregate soon after the undamaged sister chromatids separate should be more associated with the nascent daughter nuclei than acentrics that segregate much later. Therefore, early-segregating acentrics should be able to rejoin the nucleus before NEF is initiated, while late-segregating acentrics will remain as discrete entities at this time, necessitating the localized delay in nuclear envelope reformation to allow these late-segregating acentrics to rejoin the nucleus.

To determine whether or not the timing of acentric segregation is correlated with the presence of localized gaps in the nuclear envelope, we induced I-CreI and imaged live the neuroblast divisions as described above. We found that formation of localized gaps is highly correlated with late segregating acentric chromosomes (Figure 3, A-D). In contrast, early segregating acentrics were less likely to form localized gaps in the nuclear envelope and rejoined telophase nuclei well before completion of NEF (Figure 3, A-D). To further demonstrate the importance of time and distance of acentric segregation relative to the separation of undamaged chromosomes, we plotted both the time of acentric segregation and the distance of

acentrics from the separated sisters (Figure 3F). As expected, this analysis showed that delayed acentric segregation was correlated (r=0.73) with a greater distance of acentrics from the main mass of separated sisters. For divisions in which acentrics segregate later and thus at a greater distance from the main mass of separated sisters, the formation of a nuclear envelope gap allowed acentric entry into daughter nuclei (Figure 3F, blue diamonds), while a lack of gap formation resulted in acentrics forming micronuclei (Figure 3F, green triangles). We interpret these results as evidence that the presence of an acentric fragment separated from the main chromosome mass causes a localized delay in nuclear envelope reassembly, providing a gap for the inclusion of the acentric into the daughter telophase nucleus.

Figure 3. Local inhibition of nuclear envelope assembly is determined by acentric segregation timing. (A) Time lapse images of a larval neuroblast division expressing H2Av-RFP and lamin B-GFP with I-CreI-induced acentrics segregating soon after anaphase initiation. Acentrics (red arrows) lag on the metaphase plate for 40 sec after anaphase initiation before they begin their poleward segregation. Nuclear envelope formation begins 340 sec after anaphase initiation and is completed at 400 sec after anaphase initiation. Nuclear envelope assembly proceeds normally with no nuclear envelope gap present. (B) Time lapse images of a larval neuroblast division expressing H2Av-RFP and lamin B-GFP with I-CreI-induced acentrics segregating well after anaphase initiation and segregation of the main chromosome complement. Acentrics (red arrows) lag on the metaphase plate for an extended period of 260 sec after anaphase initiation and then undergo poleward segregation. Nuclear envelope formation begins 400 sec after anaphase initiation and is completed at 1060 sec after anaphase initiation. Nuclear envelope assembly is marked by the presence of a nuclear envelope gap (green arrow) through which the acentric fragment enters the daughter nucleus. This gap persists until acentrics have rejoined the nucleus. (C) Schematic depicting the timing and distances of acentric segregation relative to the timing and distance of the main chromosome mass were measured. Time of acentric segregation was measured from sister chromatid separation to separation of the last acentric pair. Distance of acentrics from main nuclear masses was measured from the center of the acentric to the center of the main nuclear mass at the time of last acentric segregation. (D, E and F) Graphs demonstrating that nuclear envelope gaps are more likely to form in neuroblasts with late segregating acentrics. (D) Acentrics that do not form gaps (red squares) segregate less than 100 sec after anaphase initiation (50 +/- 11, N=8). Acentrics that form gaps (blue diamonds) segregate at least 100 sec after anaphase initiation (220 +/- 90, N=23). p values calculated by independent t-test with equal variances not assumed. (E) Acentrics that do not form gaps (red squares) are separated from the main chromosome mass by a shorter distance (3.14 +/- 0.8 μm, N=10) compared to acentrics that do form gaps (blue diamonds) (5.38 +/- 1.06 μm, N=30) following anaphase initiation. p values calculated by independent t-test with equal variances assumed. (F) A plot showing the correlation between the timing of acentric segregation following anaphase initiation the distance between acentrics from the main chromosome mass after anaphase (r=0.73). Red squares indicated acentrics that rejoin nuclei without gap formation. Blue diamonds represent acentrics that rejoin nuclei through nuclear envelope gaps. Green triangles represent acentrics that do not form gaps rejoin nuclei and form micronuclei. Acentrics that segregate at a shorter time and distance after anaphase initiation are able to reenter daughter nuclei before NEF initiation and do not form gaps (red shaded area). In contrast, acentrics that segregate later and further from undamaged chromosomes require a nuclear envelope gap to reenter daughter nuclei (blue shaded area). Solid line represents line of best fit for data ($R^2 = 0.5$). Time and distances are represented as averaged values +/- SD. Dotted lines outline the plasma membrane of the cell. All scale bars are 2μm.

Figure 3

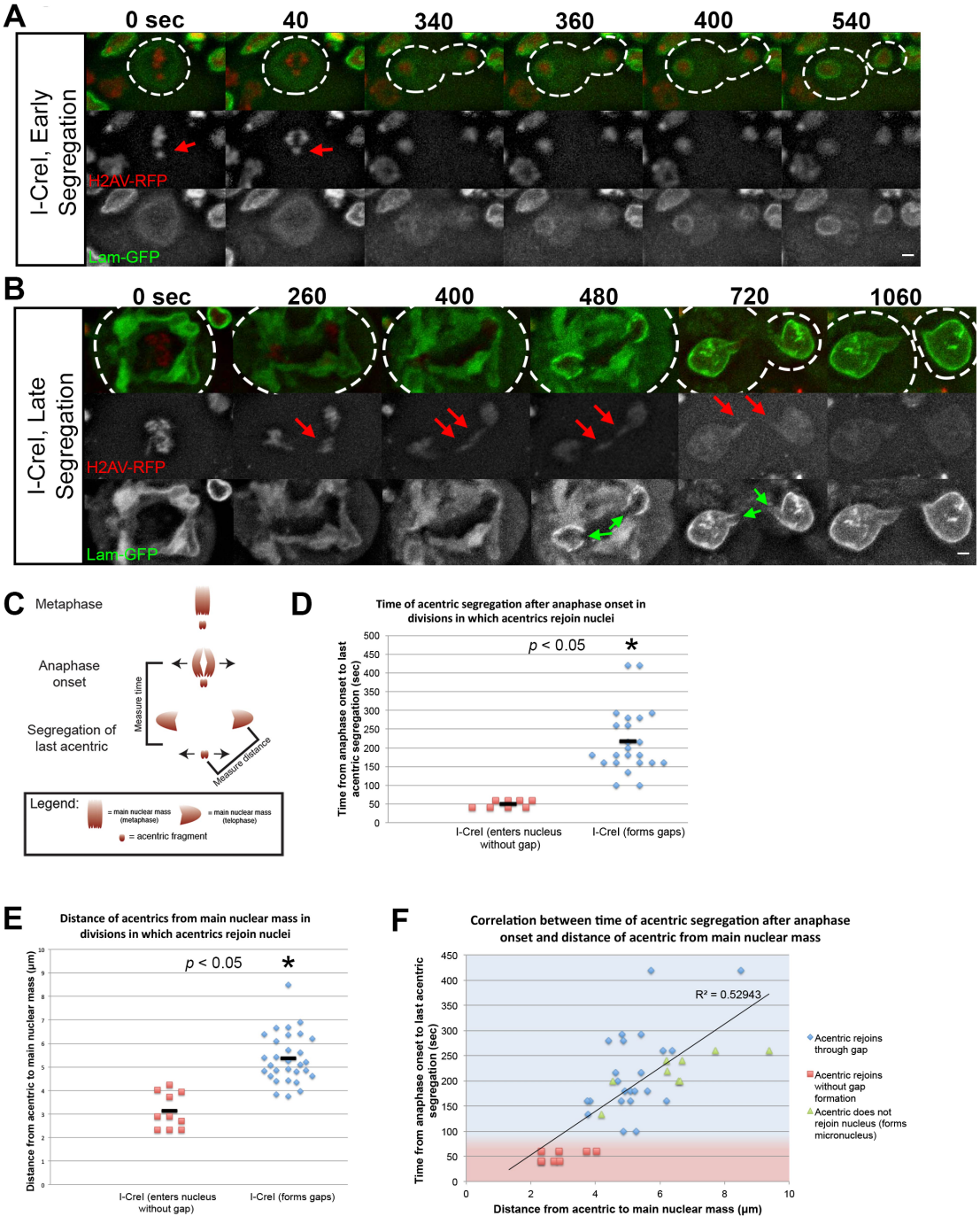
A
0 sec
40
340
360
400
540
I-CreI, Early Segregation
H2AV-RFP
Lam-GFP
B
0 sec
260
400
480
720
1060
I-CreI, Late Segregation
H2AV-RFP
Lam-GFP
C
Metaphase
Anaphase onset
Segregation of last acentric
Measure time
Measure distance
Legend:
= main nuclear mass (metaphase)
= main nuclear mass (telophase)
= acentric fragment
D
Time of acentric segregation after anaphase onset in divisions in which acentrics rejoin nuclei
p < 0.05
*
Time from anaphase onset to last acentric segregation (sec)
I-CreI (enters nucleus without gap)
I-CreI (forms gaps)
E
Distance of acentrics from main nuclear mass in divisions in which acentrics rejoin nuclei
p < 0.05
*
Distance from acentric to main nuclear mass (µm)
I-CreI (enters nucleus without gap)
I-CreI (forms gaps)
F
Correlation between time of acentric segregation after anaphase onset and distance of acentric from main nuclear mass
R² = 0.52943
Time from anaphase onset to last acentric segregation (sec)
Distance from acentric to main nuclear mass (µm)
Acentric rejoins through gap
Acentric rejoins without gap formation
Acentric does not rejoin nucleus (forms micronucleus)

X-irradiation-induced acentrics also produce localized delays and gap formation in nuclear envelope formation

The foregoing results demonstrate that I-CreI induced late segregating acentric chromosomes no longer associated with the main mass of segregating chromosomes result in localized delays in nuclear envelope formation. To determine if acentrics formed by others sources of DSBs also produce localized delays in nuclear envelope formation, we exposed neuroblasts to X-irradiation (Figure 4). X-irradiation produces both single and double-stranded breaks, resulting in acentric fragments and BubR1-coated DNA tethers (Royou et al., 2005; Royou et al., 2010). In divisions with X-irradiation induced acentrics, nuclear envelope formation was specifically delayed at the site of acentric entry, resulting in gaps in the nuclear envelope (Figure 4, A-B, green arrow). As seen in an additional irradiated neuroblast, these gaps were strikingly similar to those observed with I-CreI induced acentrics (compare Figure 4B to Figure 1A, bottom panel). Of 25 neuroblast divisions examined from irradiated larvae, 15 exhibited chromosome segregation defects (Figure 4C, grey bar). Of these 15 divisions, 8 possessed acentric fragments (Figure 4C, red bar) and gaps in nuclear envelope formation were observed in 4 of these (Figure 4C, blue bar).

Figure 4. X-ray induced acentric chromosome fragments also enter nascent daughter nuclei through highly localized delays in assembly of the nuclear envelope. (A) Time-lapse images of acentric fragments in the neuroblast division of an X-ray irradiated larva expressing H2Av-RFP (red) and lamin B-GFP (green). Acentrics resulting from X-ray irradiation (red arrows) enter the daughter nuclei through a gap in the nuclear envelope (green arrow). Initiation to completion of NEF requires 220 seconds (sec). (B) A still frame from a time-lapse movie of a nuclear envelope gap forming in a telophase nucleus with irradiation-induced acentrics (different neuroblast than shown in A) expressing H2Av-RFP (red), and lamin B-GFP (green). As seen in Panel A, the irradiation-induced acentric (red arrow) rejoins the main nuclear mass by entering the nucleus through a gap in the nuclear envelope (green arrow). (C) A graphical representation quantifying the percentage of irradiated neuroblasts that had chromosome segregation defects (grey bar), the percentage of neuroblasts with chromosome segregation defects that were acentrics (red bar), and the percentage of neuroblasts with acentrics that formed nuclear envelope gaps (blue bar).

Figure 4

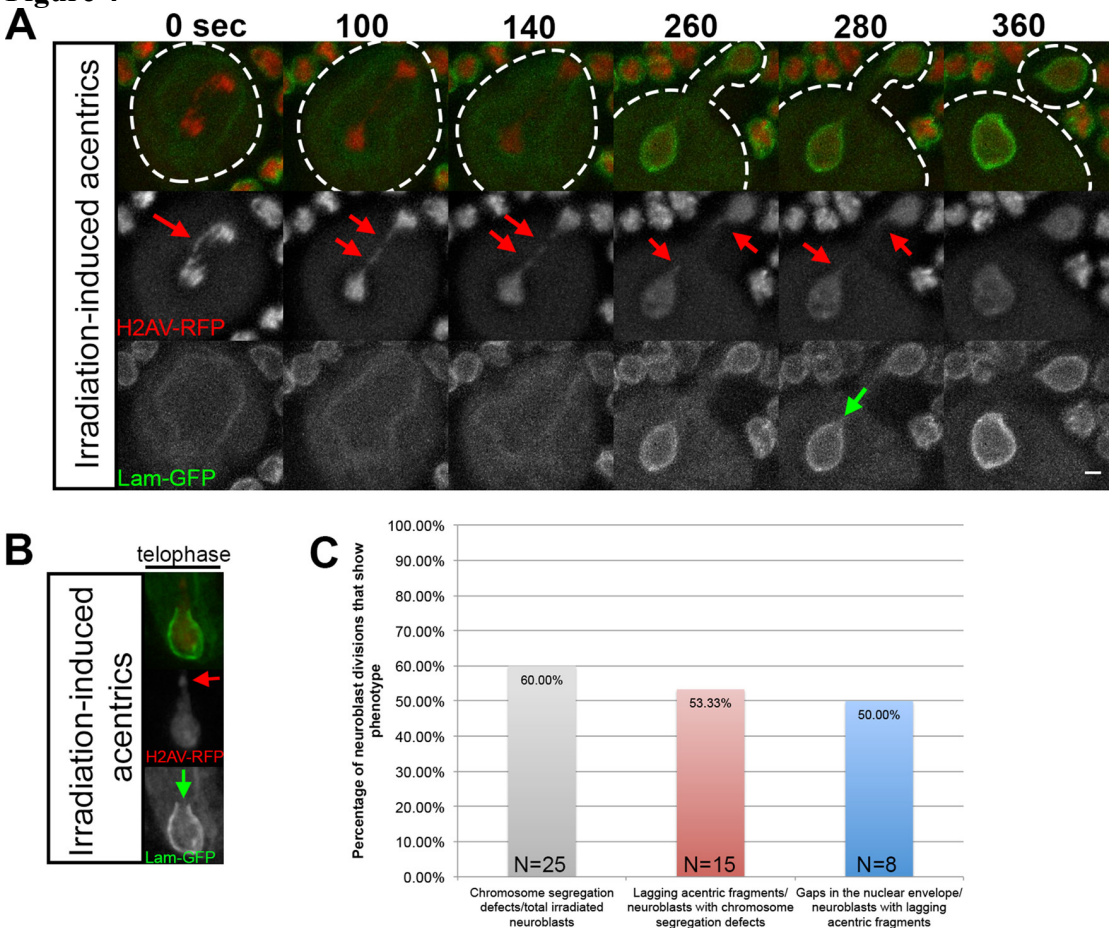

Nuclear envelope gaps are specific to acentric chromosomes and not intact lagging chromosomes

To determine if nuclear envelope gaps are a result of a physical barrier due to the presence of a lagging chromosome that blocks complete reformation of the nuclear envelope, or if these gaps are specific to acentrics, we visualized lamin reassembly in neuroblasts bearing a long compound second chromosome, (C(2)EN). Created by attaching both second chromosome homologs to a common centromere, these artificial chromosomes possess chromosome arms twice the normal length and exhibit extensive lagging during anaphase, but are not coated with the tether component BubR1 (Novitski et al., 1981; Gonzalez et al., 1991; Sullivan et al., 1993; Kotadia et al., 2012; Martins et al., 2013). Nuclear envelope formation was examined by immunofluorescence in dividing larval neuroblasts expressing either I-CreI or bearing C(2)EN (Figure 5). The panels in Figure 5A depict fixed neuroblasts in which I-CreI has been induced. As described in the previous sections, these images clearly show the lagging acentric chromosomes (red arrows, Figure 5A) during anaphase and telophase. During telophase a distinct gap in the nuclear envelope is observed (green arrow, Figure 5A).

We used the same fixed protocol to examine whether lagging compound chromosome arms also produce nuclear envelope gaps. Similar to the I-CreI results, fixed and stained neuroblasts bearing the compound chromosome exhibited extensive chromosome lagging during anaphase and telophase (red arrowheads, Figure 5B). However, no gaps in the nuclear envelope were observed. Instead, lamin formed

around the nucleus and the entire length of the outstretched lagging arm (green arrowhead, Figure 5B). Recent studies demonstrated that the compound chromosome undergoes extensive stretching at heterochromatic linker regions (Oliveira et al., 2014). Significantly, the lamin signal could be visualized around these highly stretched regions of the elongated chromosome. We interpret these results as suggesting, but not excluding the possibility, that lagging chromatin by itself is not sufficient to induce nuclear envelope gaps through a physical blockage of nuclear envelope reassembly.

Figure 5. Unlike acentric chromosome fragments, intact lagging chromosomes do not form nuclear envelope gaps. Images of fixed neuroblasts bearing I-CreI-induced acentrics (A) and neuroblasts with long compound second chromosome (C(2)EN) (B) stained with DAPI (red) and anti-Lamin antibody (green). (A) I-CreI-induced acentrics (red arrows) rejoin the main nuclear mass through a nuclear envelope gap (green arrow) during telophase. (B) In contrast, the compound second chromosome (red arrowheads) is entirely encapsulated by lamin (green arrowhead) at telophase. All scale bars are 2 μm.

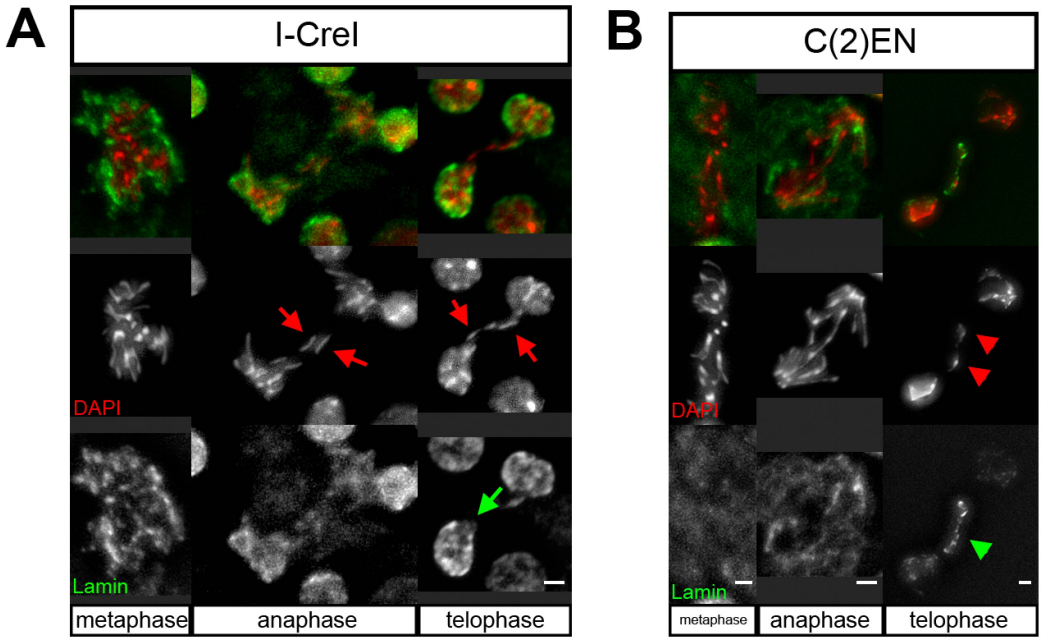

Aurora B kinase is required for highly localized delays in nuclear envelope formation and acentric entry into daughter nuclei

Previous studies demonstrated that injection of chromatin into *Xenopus* egg extracts resulted in the association of lamins and formation of a nuclear envelope encompassing the outer periphery of the ectopic chromatin mass (Forbes et al., 1983). Given the propensity of lamin to form around chromatin, the highly localized delays in nuclear envelope formation in response to acentric fragments suggest the presence of factors preventing lamin-chromatin association specifically at the site of localized delays and acentric entry. Insight into the mechanism of highly localized delays in nuclear envelope formation comes from the observation that these delays often form in the presence of tethered acentrics. Previous studies demonstrated that Aurora B kinase is an established negative regulator of lamin assembly (Ramadan et al., 2007; Meyer et al., 2010; Afonso et al., 2014). As shown in Figure 6, we observed that Aurora B specifically associated with the tether as previously reported (Royou et al., 2010). Aurora B is a chromosome passenger protein that concentrates at the midzone microtubules once sister chromosome segregation is initiated (Gruenberg et al., 2004). Recent studies demonstrate that a gradient of Aurora B originating from the midzone globally prevents NEF (Afonso et al., 2014). Once the chromosomes have segregated away from the high Aurora B concentrations, NEF is initiated. Here we investigated whether Aurora B associated with the tether during late anaphase/telophase acts to locally prevent lamin assembly and NEF leading to the formation of highly localized gaps in the reassembly of the nuclear envelope.

Figure 6. Aurora B is highly associated with acentric fragments and their DNA tethers. (A) Still frames of a control neuroblast (no I-CreI expression) movie show GFP-tagged Aurora B (cyan) on kinetochores during metaphase and at the cleavage furrow during anaphase. Dotted lines outline the plasma membrane of the cell. All scale bars are 2µm. (B) Still frames from a movie of a dividing neuroblast during the same mitotic stages with I-CreI induced acentrics that are decorated with GFP-tagged Aurora B (cyan arrows). Undamaged chromosomes (cyan arrowheads) are not associated with Aurora B (bottom panel). These results are in accord with Royou et al (2010). Dotted lines outline the plasma membrane of the cell. All scale bars are 2µm.

Figure 6

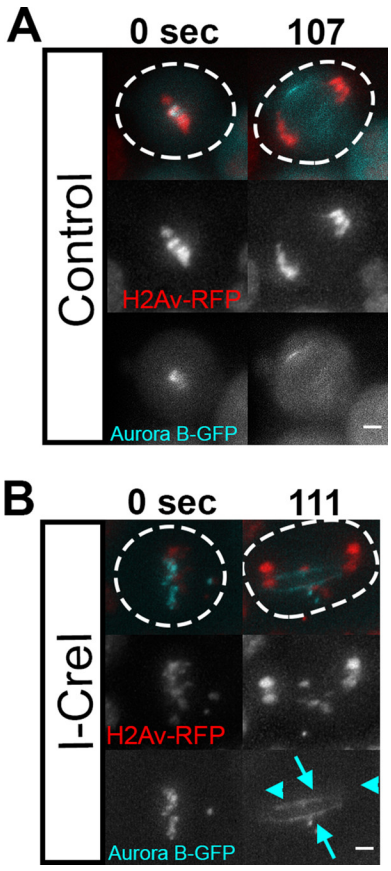

Because Aurora B provides a number of essential functions in the mitotic cell cycle, in order to investigate its role specifically in highly localized nuclear envelope gap formation, we used RNAi to reduce but not eliminate Aurora B levels in neuroblasts. We achieved conditions in which chromosome morphology, condensation, alignment on the metaphase plate and segregation proceeded normally. We measured chromosome compaction in I-CreI expressing control and I-CreI with Aurora B RNAi neuroblasts. Chromosome compaction was determined by measuring the area occupied by the metaphase chromosomes at the time when the last acentric began poleward segregation. This corresponds to the point of maximum chromosome compaction in the cell cycle. We found no difference between the measured areas of the chromosomes in I-CreI expressing control and I-CreI with Aurora B RNAi neuroblasts (Figure 7A). In addition, Aurora B RNAi expressing neuroblasts without the I-CreI transgenes revealed no discernable defects in chromosome segregation or any evidence of chromosome bridging. In control and Aurora B RNAi neuroblasts, 0/10 and 0/13 divisions respectively exhibited chromosome bridging.

To determine if our Aurora B RNAi conditions caused specific defects in acentric morphology, we measured the area of acentrics of I-CreI expressing control and I-CreI with Aurora B RNAi neuroblasts at the beginning of NEF (Figure 7B). We found no difference between the measured area of acentrics in I-CreI expressing control and I-CreI with Aurora B RNAi neuroblasts. We also measured the distance from acentrics to the main nuclear mass at the time of acentric segregation in I-CreI control and I-CreI with Aurora B RNAi neuroblasts. We found no difference in the

distance of acentrics from the main chromosome mass in I-CreI control and I-CreI with Aurora B RNAi neuroblasts (Figure 7C). To determine whether induction of Aurora B RNAi influences acentric segregation, we compared the timing and dynamics of acentric poleward segregation in both I-CreI with Aurora B RNAi and I-CreI-expressing control neuroblasts. We found that acentrics began their poleward segregation within similar time frames during anaphase in both I-CreI-expressing control and I-CreI with Aurora B RNAi neuroblasts (Figure 7D). Likewise, there was a small, but not statistically significant increase in the frequency of unequal versus equal acentric segregation in I-CreI-expressing neuroblasts with Aurora B RNAi compared to I-CreI alone control neuroblasts (Figure 7E). To ensure that induction of Aurora B RNAi reduced Aurora B levels in the neuroblasts, we assayed the frequency of binucleate cells, a result of failed cytokinesis and previously described phenotype in Drosophila using RNAi knockdown of Aurora B (Giet and Glover, 2001). We observed a dramatic increase in bi-nucleate neuroblasts (Aurora B RNAi (22% N=18) compared to I-CreI-expressing controls (2.7% N=37) (Figure 7F). Taken together, these results indicate that reducing Aurora B levels through RNAi does not disrupt chromosome morphology, condensation, or segregation of the normal chromosomes or the acentric fragment.

Figure 7. Aurora B RNAi does not lead to gross changes in chromosome behavior or structure. (A) Graph of the measured size of undamaged chromosomes in I-CreI-expressing control (cyan triangles) and I-CreI; Aurora B RNAi neuroblasts (red squares) at the moment of maximal metaphase compaction. (B) A graph of the measured size of acentrics generated in I-CreI neuroblasts (cyan triangles) and I-CreI; Aurora B RNAi neuroblasts (red squares) at the beginning of NEF. (C) Graph of the distance between acentrics and the main chromosome mass in gap forming I-CreI alone (control) neuroblasts (cyan triangles) and non-gap forming I-CreI, Aurora B RNAi neuroblasts (red squares) following the completion of anaphase. (D) Graph of the timing of the initiation of acentric poleward segregation following the onset of anaphase in both I-CreI alone (control) and I-CreI; Aurora B RNAi neuroblasts. The timing of the initiation of acentric poleward segregation was grouped into two categories: 0-4 min (cyan bars), and 4-7 min (red bars). (E) Still images from time-lapse movies of equal (top panel) and unequal (bottom panel) segregation of acentrics during anaphase in neuroblasts expressing I-CreI alone (top panel) or I-CreI plus Aurora B RNAi (bottom panel). Red arrows show acentrics. Scale bar is 2 μm. Graph of the percentage of unequal segregation in both types of neuroblasts is shown on the right. A statistically non-significant increase in unequal segregation of acentrics in I-CreI with Aurora B RNAi neuroblasts versus I-CreI alone (control) neuroblasts was observed. (F) Single frame pictures of third instar neuroblasts from wild type larvae (top panel) and larvae in which Aurora B is reduced (bottom panel). To the right is a graph of the percentage of binucleate neuroblasts in both types of larvae. Cyan arrows point to binucleate cells. Red channel is H2Av-RFP. Grey channel is differential interface contrast (DIC). Scale bar is 6 μm. p values were calculated by independent t-test with equal variances not assumed.

Figure 7

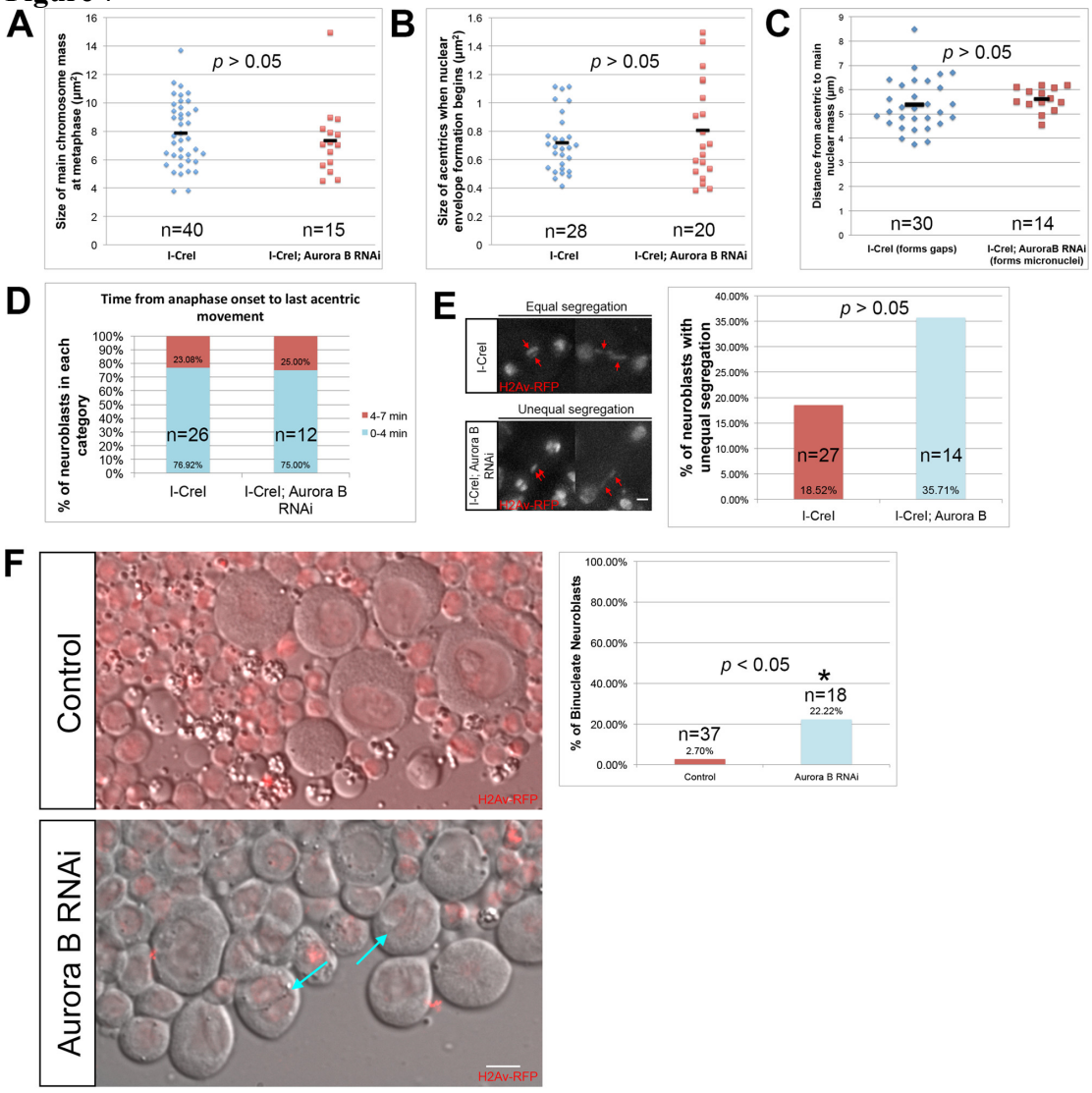
A
Size of main chromosome mass at metaphase (μm²)
p > 0.05
n=40
n=15
l-CreI
l-CreI; Aurora B RNAi
B
Size of acentrics when nuclear envelope formation begins (μm²)
p > 0.05
n=28
n=20
l-CreI
l-CreI; Aurora B RNAi
C
Distance from acentric to main nuclear mass (μm)
p > 0.05
n=30
n=14
l-CreI (forms gaps)
l-CreI; AuroraB RNAi (forms micronuclei)
D
Time from anaphase onset to last acentric movement
% of neuroblasts in each category
23.08%
25.00%
n=26
n=12
76.92%
75.00%
4-7 min
0-4 min
l-CreI
l-CreI; Aurora B RNAi
E
Equal segregation
Unequal segregation
l-CreI
l-CreI; Aurora B RNAi
H2Av-RFP
% of neuroblasts with unequal segregation
p > 0.05
n=27
18.52%
n=14
35.71%
l-CreI
l-CreI; Aurora B
F
Control
Aurora B RNAi
H2Av-RFP
% of Binucleate Neuroblasts
p < 0.05
*
n=37
2.70%
n=18
22.22%
Control
Aurora B RNAi

To determine if Aurora B is necessary for the highly localized delays in nuclear envelope formation, we compared divisions in I-CreI-expressing control and I-CreI with Aurora B RNAi neuroblasts for the presence of gaps in the nuclear envelope. Through fixed analysis, we discovered that the frequency of gap formation was greatly reduced in neuroblasts bearing an I-CreI induced acentric with reduced levels of Aurora B (Figure 8A). As seen in Figure 6A, I-CreI induced acentrics are free of lamins and a distinct gap is present in the nuclear envelope (green arrow). In contrast, when Aurora B levels are reduced there is a dramatic increase in the number of acentrics coated with lamins (green arrowheads). Nuclear envelope gaps were formed at a frequency of 79% (N=13) and 14% (N=25) in I-CreI-expressing control and I-CreI with Aurora B knockdown neuroblasts respectively (Figure 8B). In addition, the percentage of telophase cells with lamins ectopically localized to the acentrics increased two-fold (from 21%, N=13 to 41% N=25) in the Aurora B knockdown neuroblasts (Figure 8C).

In accord with these fixed results, live imaging of acentrics in I-CreI-expressing control neuroblasts formed nuclear envelope gaps (Figure 8D, green arrow) through which the acentrics passed to join daughter nuclei. Strikingly, acentric fragments in divisions with reduced Aurora B were associated with ectopic lamin (Figure 8D, green arrowheads, Movie 5). Presumably, because of this absence of highly localized delays in nuclear envelope formation, acentric fragments in I-CreI with Aurora B RNAi expressing neuroblasts were not able to rejoin daughter nuclei

and therefore formed micronuclei at a higher rate compared to controls (see below) (Figure 8E).

Increased failure of nuclear envelope gap formation when Aurora B levels are reduced indicates that gap formation is dependent on Aurora B. Because our Aurora B RNAi conditions did not affect whole or acentric chromosome segregation or geometry, our results suggest that nuclear envelope gap formation is likely mediated by Aurora B through prevention of local nuclear envelope reassembly specifically at the site of acentric entry into daughter nuclei as opposed to altering chromosome segregation or compaction. In addition, the ectopic assembly of lamins on acentric fragments in reduced Aurora B conditions shows that the formation of nuclear envelope gaps is not due to an inability of the acentrics to recruit nuclear envelope components.

Failure to form highly localized delays in nuclear envelope formation results in increased rates of micronuclei formation

As described previously, when I-CreI induction results in late segregation of acentrics, there is a local delay in completion of NEF. In contrast, when Aurora B levels are reduced, these delays are eliminated (Figure 8F). In neuroblasts expressing I-CreI and Aurora B RNAi, acentrics form micronuclei at a higher rate (67% N=9) than acentrics in I-CreI expressing controls (15% N=33). Therefore, formation of micronuclei appears to be a direct consequence of the failure to form highly localized delays in nuclear envelope formation when Aurora B levels are reduced.

A small molecule inhibitor of Aurora B prevents nuclear envelope gap formation

To further demonstrate that Aurora B is responsible for gap formation, we treated neuroblasts with the Aurora B small molecule inhibitor Binucleine-2 (Afonso et al., 2014). Similar to our results with Aurora B RNAi, the inhibition of Aurora B by Binucleine-2 decreased nuclear envelope gap formation and increased the rate of lamin-coated acentric-bearing micronuclei (Figure 8G). To test whether or not Aurora B inhibition diminished tether function, we examined the localization of the tether component BubR1 (Royou et al., 2010) to I-CreI Induced DNA tethers. We found that Binucleine-2 inhibition of Aurora B did not disrupt tether integrity as evidenced by the ectopic localization of BubR1 on the acentric and tether in control (Figure 9A) and Binucleine-2 (Figure 9B) treated neuroblasts. Altogether, this suggests that a key function of Aurora B is to locally prevent lamin assembly, resulting in a nuclear envelope gap through which late segregating chromatin separated from the main chromosome mass can enter the telophase nucleus (Figure 10).

Figure 8. Local inhibition of nuclear envelope assembly is mediated by Aurora B kinase. (A) Fixed images of telophase nuclei from I-CreI-expressing control and I-CreI with Aurora B depleted neuroblasts bearing I-CreI induced acentrics stained with anti-lamin (green) and DAPI (red). Acentrics induced in I-CreI-expressing controls show little to no association with lamin B and form a nuclear envelope gap (green arrow). In contrast, acentrics in neuroblasts with reduced Aurora B result in both the absence of a nuclear envelope gap and clear associations with lamins on acentrics (green arrowheads). (B) I-CreI induced acentrics in control neuroblasts resulted in nuclear envelope gaps in 79% (N=13) of telophase nuclei. In contrast, acentrics in neuroblasts depleted of Aurora B resulted in a significant reduction (14%; $p < 0.05$; N=25) in the formation of nuclear envelope gaps in telophase nuclei. (C) Acentrics in I-CreI-expressing control neuroblasts were coated with lamin B in 21% (N=13) of telophase nuclei. In contrast, telophase nuclei of neuroblasts depleted of Aurora B resulted in an increase (41%; N=25) of acentrics coated with lamins (not significant). (D) Time-lapse images of dividing neuroblasts from I-CreI-expressing controls (top) and I-CreI with Aurora B RNAi (bottom, see Movie 5) expressing lamin B-GFP (green) and H2Av-RFP (red). I-CreI induced acentrics are present in both. In I-CreI expressing controls, acentrics (red arrows) enter telophase nuclei through nuclear envelope gaps (green arrow). In contrast, neuroblasts bearing acentrics with reduced Aurora B show no gaps. Consequently, acentrics (red arrows) in Aurora B depleted neuroblasts remain outside of the nucleus and form micronuclei coated with lamin B (green arrowheads). (E) Bar graphs of micronuclei frequencies in I-CreI-expressing control, I-CreI with Aurora B RNAi, and Aurora B RNAi without I-CreI control neuroblasts. (F) Box plots showing the time elapsed from the onset of anaphase to the completion of NEF in neuroblasts expressing I-CreI and I-CreI with Aurora B RNAi. Early-segregating I-CreI induced acentrics do not form gaps, whereas late-segregating I-CreI induced acentrics do form gaps. Late-segregating acentrics in neuroblasts with reduced Aurora B expression fail to form gaps and complete NEF in a similar time frame to early segregating wild-type acentrics. These results indicate that Aurora B mediates the local inhibition of NEF in neuroblasts. Asterisks in panels indicate statistical significance. (G) Time-lapse images of dividing neuroblasts from I-CreI-expressing DMSO treated controls (left) and I-CreI-expressing Binucleine-2 treated neuroblasts (right) expressing lamin B-GFP (green) and H2Av-RFP (red). In DMSO treated controls, acentrics (red arrows) enter telophase nuclei through nuclear envelope gaps (green arrows). In contrast, Binucleine-2 treated neuroblasts show no gaps. Consequently, acentrics (red arrows) in Aurora B depleted neuroblasts remain outside of the nucleus and form micronuclei coated with lamin B (green arrowhead).

Figure 8

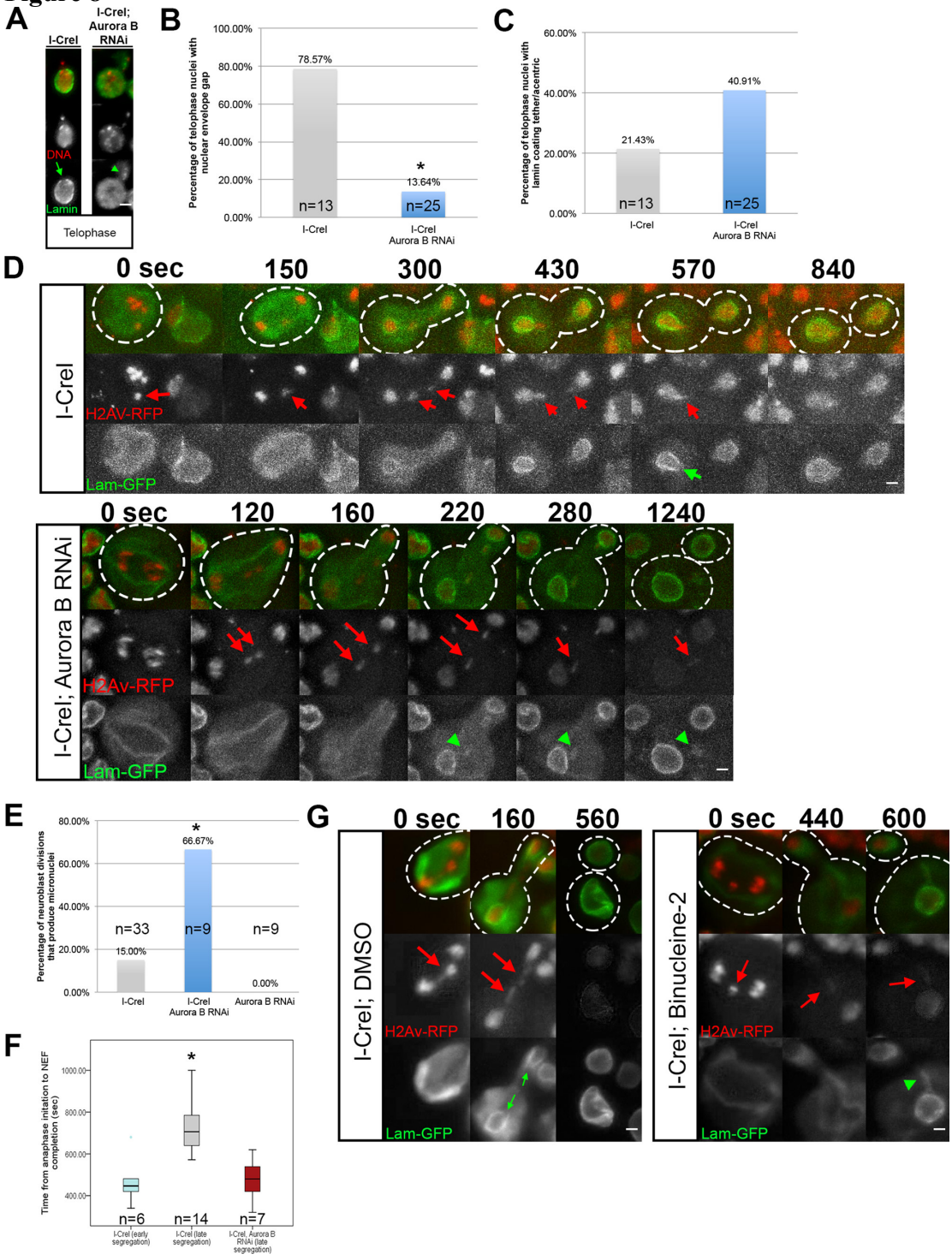
A
I-CreI
I-CreI; Aurora B RNAi
DNA
Lamin
Telophase
B
Percentage of telophase nuclei with nuclear envelope gap
100.00%
80.00%
60.00%
40.00%
20.00%
0.00%
78.57%
n=13
*
13.64%
n=25
I-CreI
I-CreI Aurora B RNAi
C
Percentage of telophase nuclei with lamin coating tether/centric
60.00%
40.00%
20.00%
0.00%
21.43%
n=13
40.91%
n=25
I-CreI
I-CreI Aurora B RNAi
D
0 sec
150
300
430
570
840
I-CreI
H2AV-RFP
Lam-GFP
0 sec
120
160
220
280
1240
I-CreI; Aurora B RNAi
H2Av-RFP
Lam-GFP
E
Percentage of neuroblast divisions that produce micronuclei
80.00%
60.00%
40.00%
20.00%
0.00%
n=33
15.00%
*
66.67%
n=9
n=9
0.00%
I-CreI
I-CreI Aurora B RNAi
Aurora B RNAi
F
Time from anaphase initation to NEF completion (sec)
1000.00
800.00
600.00
400.00
*
n=6
n=14
n=7
I-CreI (early segregation)
I-CreI (late segregation)
I-CreI, Aurora B RNAi (late segregation)
G
0 sec
160
560
I-CreI; DMSO
H2Av-RFP
Lam-GFP
0 sec
440
600
I-CreI; Binucleine-2
H2Av-RFP
Lam-GFP

Figure 9. Aurora B inhibition does not disrupt tether formation. Time-lapse images of dividing larval neuroblasts expressing H2Av-RFP and BubR1-GFP with I-CreI-induced acentrics treated with DMSO alone (A) or with the Aurora B small molecule inhibitor Binucleine-2 (B). BubR1 localization on I-CreI induced tethers is similar in both DMSO alone and Binucleine-2 treated neuroblasts. Red arrows indicate acentrics. Green arrows indicate ectopic BubR1. Dotted lines show cell outline. All scale bars are 2 μm.

Figure 9

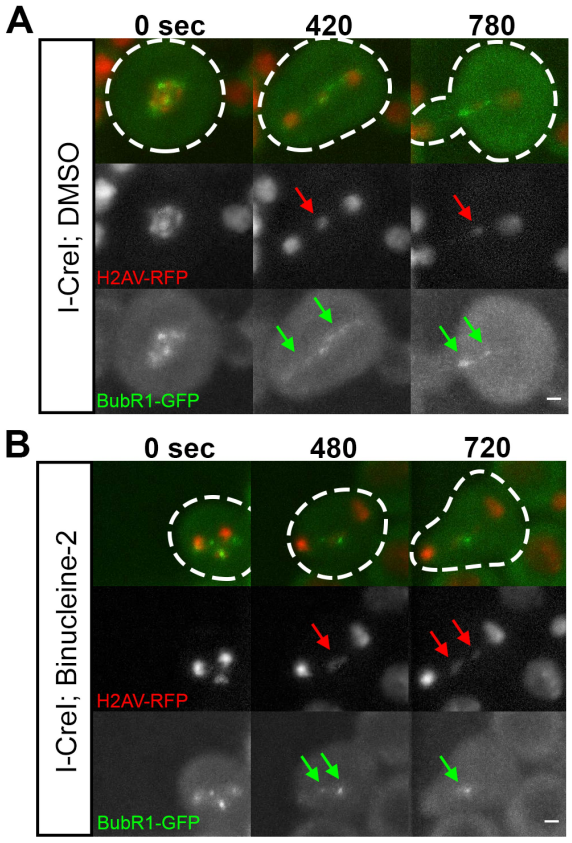

Figure 10. A model of Aurora B dependent formation of nuclear envelope gaps. (A) Nuclear envelope formation (NEF) is completed within 349 seconds following the metaphase-to-anaphase transition in non-I-CreI expressing control neuroblasts with undamaged chromosomes. NEF initiates 60 seconds after cessation of poleward movement of the chromosomes and is quickly completed to form an intact nuclear envelope. In neuroblasts with acentrics (B and C), the initiation of NEF is slightly delayed relative to neuroblasts with undamaged chromosomes (A). In the event of early acentric segregation (B), acentrics have sufficient time to rejoin daughter nuclei before the initiation of NEF, thus localized delays in NEF are not induced and no nuclear envelope gap is observed. In contrast, late segregating acentrics (C) have less time with respect to the initiation of NEF to rejoin daughter nuclei and are more likely to exist as distinct entities when NEF initiates. This results in localized delays in NEF at the site where Aurora B decorated acentrics facilitate entry into daughter telophase nuclei through the formation of nuclear envelope gaps.

Figure 10

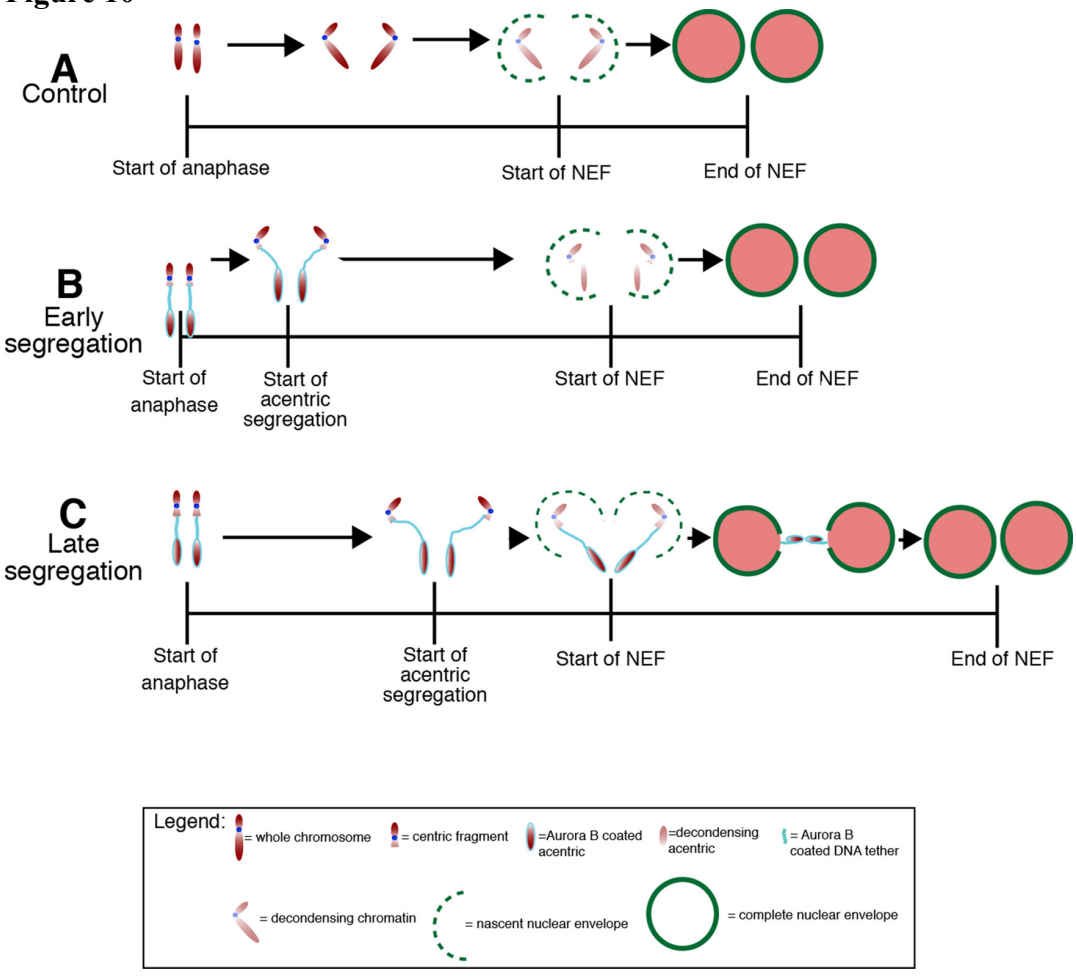

Discussion

Much remains unknown concerning the cellular response to defects and delays in chromosome segregation during anaphase and telophase. The anaphase-telophase transition is a complex process requiring the coordination of chromosome movements with cytoskeletal and membrane dynamics. Upon completion of chromosome segregation during anaphase, extensive chromosome reorganization and decondensation occurs while reassembly of the nuclear envelope is initiated (Güttinger et al., 2009; Katsani et al., 2008). Spindle disassembly is completed and the centrosome re-associates with the newly formed nuclear envelope (Robinson et al., 1999). Directly after the chromosomes have cleared the plate during anaphase, cytokinesis is initiated. Because of the complexity and speed of these events, compensating for delays and defects in chromosome segregation is particularly challenging. A number of studies demonstrate that some cells respond to delays in chromosome segregation by delaying initiation of cytokinesis (Norden et al., 2006) or alternatively elongating the spindle and daughter cells to accommodate increased arm length (Kotadia et al., 2012).

In the studies presented here, we focus on the effects of lagging acentric chromosomes on nuclear envelope formation (NEF). Recent work has shown that delayed chromosome segregation induces a delay in NEF initiation (Afonso et al., 2014). Here, we specifically investigated whether severely delayed acentric segregation results in corresponding delays in NEF completion as well. We reasoned that severely delayed acentric fragments must be able to enter daughter nuclei by a

mechanism distinct from delayed NEF initiation, as acentric segregation occurs around the same time as the nuclear envelope starts to reform. By using a subset of nuclear envelope components (Lamin B and Nup107) to visualize nuclear envelope reassembly, we found that severely lagging acentrics induce highly localized delays in NEF completion specifically at the site where lagging acentrics rejoin the main chromosome mass.

As previously reported, delays in the time interval between anaphase initiation (sister chromosome segregation) and initiation of NEF occur in acentric bearing cells compared to controls (Afonso et al., 2014). While we observed delays in NEF initiation in the presence of lagging chromosomes, we also observed significant highly localized delays in the completion of NEF that are required for acentric entry into daughter nuclei.

Previous studies revealed that acentric chromosomes segregate to daughter nuclei using a DNA tether-like structure connecting, and perhaps pulling, an acentric fragment to its centric partner (Royou et al., 2010). Segregation of these acentric fragments is severely delayed. The tethers are coated with the spindle checkpoint components BubR1 and Polo, and the chromosome passenger proteins INCENP and Aurora B (Royou et al., 2010). Of these, the Aurora B kinase is particularly interesting because it is responsible for maintaining the chromosomes in a condensed state and preventing nuclear envelope assembly until after the chromosomes have completed segregation (Ramadan et al., 2007; Afonso et al., 2014).

To investigate whether Aurora B plays a role in the formation of the acentric induced gaps in nuclear envelope formation, we reduced Aurora B in neuroblasts by RNAi. We found that the frequency of acentric-induced nuclear envelope gaps were reduced in neuroblasts depleted of Aurora B. In addition, we found that acentrics in neuroblasts depleted of Aurora B were coated with lamins and left outside of the main nuclei as micronuclei. Increased failure of nuclear envelope gap formation when Aurora B levels are reduced indicates that gap formation is dependent on Aurora B. Because our partial knockdowns of Aurora B did not affect normal or acentric chromosome segregation or compaction, our results suggest that nuclear envelope gap formation is mediated by Aurora B through prevention of nuclear envelope reassembly specifically at the site of acentric entry into daughter nuclei as opposed to altering chromosome segregation or compaction. In addition, the ectopic assembly of lamins on acentric fragments in reduced Aurora B conditions shows that the formation of nuclear envelope gaps is not due to an inability of the acentrics to recruit nuclear envelope components. Furthermore, lamin association along the outstretched arms of compound chromosomes suggests but does not exclude that gaps in the nuclear envelope are not simply due to a physical blockage of nuclear envelope formation created by the tether.

Recent studies have shown that the nuclear envelope reforms around separated sister chromosomes once they have segregated outside of the highly concentrated Aurora B gradient in the mitotic midzone (Afonso et al., 2014). In these studies, lagging acentrics remained free of nuclear envelope components during anaphase

despite the initiation of nuclear envelope reformation around the intact chromosomes at the poles. That is, the nuclear envelope cannot reform around lagging acentrics that remain in the highly concentrated Aurora B gradient in the midzone. Although we have not specifically ruled out the role of the midzone gradient of Aurora B in nuclear envelope gap formation, we believe that the localized formation of gaps in the nuclear envelope is the specific result of acentrics and tethers coated with ectopic Aurora B. The rationale for this view is that nuclear envelope gaps do not occur in neuroblasts with undamaged chromosomes, despite the presence of an Aurora B midzone gradient. That is, nuclear envelope gaps are only observed with acentrics associated with highly-localized and concentrated levels of Aurora B at the site where a gap is needed to include acentrics in daughter nuclei. Our studies complement the work showing an Aurora B gradient in regulating nuclear envelope formation on a global scale (Afonso et al., 2014) by suggesting that an increased local concentration of Aurora B can induce a corresponding local delay in nuclear envelope reformation to ensure the inclusion of acentrics in daughter nuclei.

Because Aurora B phosphorylation of histone H3 inhibits HP1 recruitment to the chromatin (Hirota et al., 2005) and HP1 is known to interact with the nuclear lamina (Ye and Worman, 1996), it would be interesting to test whether or not this Aurora B mediated prevention of lamin-tether interaction is the effect of disrupted HP1 recruitment to histone H3. Alternatively, the Aurora B mediated regulation of the state of chromosome condensation at telophase may influence local lamin-chromatin interactions and gap formation (Ramadan et al., 2007).

One of the most striking consequences of reducing Aurora B levels in the presence of I-CreI induced double stranded breaks is the formation of large numbers of micronuclei. This appears to be a direct consequence of the failure to form a nuclear envelope gap, blocking the acentric chromosome from entering the daughter telophase nucleus. Historically, micronuclei have been used as biomarkers for genomic instability, and their increased presence of micronuclei in human cells is typically associated with cancer (Bonassi et al., 2011; Santos et al., 2010; Celik et al., 2013). As such, there has been much interest in understanding the cellular response to micronuclei formation and subsequent micronuclei fate (Hatch et al., 2013; Ji et al., 2013; Huang et al., 2011; Kirsch-Volders et al.; 2011, Fenech et al.; 2011). Previous studies have shown a direct correlation between Aurora B levels and micronuclei frequency (Tatsuka et al., 1998). Here, we find that reducing Aurora B levels can also lead to an increased frequency of micronuclei in the presence of double-stranded breaks. Taken together, these results suggest multiple distinct mechanisms by which micronuclei can form. Furthermore, we provide an easy method for generating large amounts of micronuclei, which can then be used for further studies into micronuclei contribution toward genomic instability.

Taken together, our results suggest that Aurora B-mediated highly localized delays in the final stages of NEF result in a portal through which the tethered acentrics pass to rejoin the daughter telophase nuclei, preserving genomic integrity. Whether this portal is a novel structure of the nuclear envelope remains to be determined.

Materials and Methods

Fly Stocks

All stocks were raised on standard *Drosophila* media (Sullivan et al., 2000) at room temperature and then incubated at 29^{o}C for at least 24 hours before imaging. The following Gal4 drivers were used: elav-Gal4 (Lin and Goodman, 1994), Wor-Gal4 (Cabernard and Doe, 2009), Actin-Gal4 (Bloomington stock #25708) (Ito et al., 1997). Using these drivers the following larvae were constructed: elav-Gal4; H2Av-RFP/UAS-lamin-GFP; I-CreI, Sb (Figures 1A-D, 3A-B, 5E, 8D, G), Wor-Gal4; I-CreI, Sb (Figure 5A), Actin-Gal4; I-CreI, Sb (Figure 8A), elav-Gal4; H2Av-RFP/UAS-GFP-Nup107; I-CreI, Sb (Figure 2A-C), elav-Gal4; H2Av-RFP (Figure 7F). For Aurora B RNAi experiments, ial RNAi (#28691 from Bloomington) was introduced to create the following larvae: Actin-Gal4; I-CreI/ial (Figure 8A), elav-Gal4; H2Av-RFP/UAS-lamin-GFP; I-CreI/ial (Figure 7E, 8D), elav-Gal4l H2Av-RFP; ial (Figure 5F). lamin-GFP (#7376) and GFP-Nup107 (#35514) were obtained from the Bloomington Stock center. The Aurora B-GFP lines, kindly provided by the Lipsick lab, were used to create the following larvae: elav-Gal4; H2Av-RFP/UAS-AuroraB-GFP (Figure 6A) and elav-Gal4; H2Av-RFP/UAS-AuroraB-GFP; Icre, Sb (Figure 6B). For the experiments with the compound chromosome (Figure 5B), a yw; C(2)EN,bw,sp (Novitski et al., 1981) stock was obtained from Bloomington (#2974). GFP-BubR1 lines previously characterized by Buffin et al. (2005) were used to create elav-Gal4; H2Av-RFP/GFP-BubR1; I-CreI, Sb larvae (Figure 9).

I-CreI and X-irradiation induced chromosome breaks

I-CreI expression was induced in elav-Gal4; H2Av-RFP/lamin-GFP; I-Cre, Sb larvae with I-CreI driven by a heat shock 70 promoter. Female 3rd instar larvae were subjected to a 1 hour 37°C heat shock followed by a 1 hour recovery period at room temperature. The larval brains were then dissected and imaged as described below. To induce more generalized DNA damage, female 3rd instar larvae were exposed to X-irradiation using a Torrex X-ray generator. This was followed by a 1 to 6 hour recovery period (higher doses required a longer recovery period). The larval brains were then dissected and imaged as described below.

Live and fixed neuroblast cytology

For live imaging, female *Drosophila* 3rd instar larval brains were dissected in PBS (pH=7.4) and placed between a slide and coverslip. The resulting capillary forces resulted in a gentle squashing of the preparation (Buffin et al., 2005). The preparation was imaged immediately and for a maximum period of 60 minutes. Best imaging was achieved using neuroblasts along the periphery of the squashed brain.

Fixed images were obtained by dissecting female 3rd instar larval brains in 0.7% NaCl then soaking them for 5 minutes in 0.5% Na Citrate to induce brain cell swelling. Brains were squashed in fixative (1.85% formaldehyde, 45% acetic acid) then slides were frozen in liquid nitrogen. After washing in PBS, samples were immersed in a 5% dried milk, 0.2% TX-100 solution for 1h before being incubated

overnight at 4°C with anti-lamin antibody (1:1000 dilution in the milk solution). Samples were then washed three times in PBST (PBS + 0.2% TX-100) and incubated at room temperature with Alexa 546-conjugated anti-rabbit secondary antibody (1:300 dilution). The samples were washed three more times in PBS before the addition of DAPI in vectashield. This fixing and staining procedure was adapted from (Cenci et al., 2003).

Microscopy and image acquisition

Figure 1D was acquired with a 60X 1.4 NA objective on an inverted spinning disk microscope (Improvision) equipped with a Hamamatsu C9100-50 EM CCD camera. Three-dimensional reconstruction and brightness adjustments were performed with Volocity Image Analysis software. Figure 1C and Figure 4B were acquired with a Leica DN5500B wide-field upright microscope equipped with a Leica DFC360 FX camera using a 63X objective with an NA of 1.4. All other images were acquired with a Leica DMI6000B wide-field inverted microscope equipped with a Hamamatsu EM charge-coupled device (CCD) camera (ORCA C9100-02) with a binning of 1 and obtained using a 100X Plan-Apochromat objective with a NA of 1.4. Time-lapse movies were composed of images taken at 20 seconds intervals unless otherwise indicated. All movie images were then deconvolved with LeicaAF software using 6 iterations of a blind deconvolution algorithm with a 1.5 refractive index except with Figure 1C 4B, which were deconvolved with Autoquant X3 and Figures S3A-B and 6G, which were deconvolved with Autoquant X2. Both movies and fixed images

were projected 2D images (maximum intensity). All images were assembled using ImageJ software (http://rsb.info.nih.gov/ij/), Adobe Photoshop (Figures 1, 2, 3, 4, 5, 7, 8, 9), and Adobe Illustrator (Figures 3C, 6, 10). Selected stills (both experimental and control) were processed with Adobe Photoshop to increase brightness.

Measurements

Anaphase initiation was determined in time-lapse movies as the last frame before sister chromatid separation. Initiation of poleward movement by the final acentric fragment was measured as the last frame before the final two acentric chromosomes segregated. The measured distance from the center of the acentrics to the center of the main nuclear masses at this time was used as the distance of the acentrics from the main nuclear mass. The start of nuclear envelope formation was measured as the first frame in which a nuclear envelope reappeared around segregating sister chromatids. Complete nuclear envelope formation was scored as the first frame in which quantification of GFP-signal intensities along lines tangent to polar and opposing faces of daughter nuclei were of similar shape and magnitude. These measurements as well as those appearing in Figure 1B-C and Figure 2B were obtained in ImageJ by plotting the profile of signal intensity along regions of interest tangent to polar and opposing faces of daughter nuclei.

The diameter of the nuclear envelope gap was measured as the distance of the width of the gap in the lamin B-GFP signal using frames from time-lapse movies in which the acentric is passing through the gap. Pooled data calculated from fixed

images required the presence of two nuclei in the same decondensaton state on the same Z-plane with an acentric fragment between them that was also on the same Z-plane. Presence or absence of a nuclear envelope gap or lamin association with the acentric was then scored. The frequency of micronuclei formation was determined in time-lapse movies in which both the segregating chromosomes and nuclear envelope were clearly visible throughout the length of the movie.

Measurements for I-CreI values from Figure 3D-F, Figure 7A-E, Figure 8E-F were taken from the same pool of data. Measurements for I-CreI; Aurora B RNAi values from Figure 7A-E, Figure 8E-F were taken from the same pool of data.

All measurements were made using ImageJ software. Statistical analysis was calculated using SPSS. Bonferroni one-way ANOVA tests were used to calculate *p*-values for Figure 8F. Independent sample t-tests were used to calculate *p*-values for Figure 2D-E, Figure 8B, C, E and Figure 7A, B, C, E, F. Final graphic representations were created in SPSS (Figure 6F) and Excel (Figures 3C-E, 7A-F, 8B, C, E; Figure 2B). For box plots, boxes represent data within the 25th to 75th range. Black bar is data median and whiskers represent the 95th percentile range. Circles in box plot are outliers.

CHAPTER 2: Micronuclei Formation Is Prevented by Aurora B-Mediated Exclusion of HP1a from Late-Segregating Chromatin in *Drosophila*

Abstract

While it is known that micronuclei pose a serious risk to genomic integrity by undergoing chromothripsis, mechanisms preventing micronucleus formation remain poorly understood. Here, we investigate how late-segregating acentric chromosomes that would otherwise form micronuclei instead reintegrate into daughter nuclei by passing through Aurora B kinase-dependent channels in the nuclear envelope of *Drosophila melanogaster* neuroblasts. We find that localized concentrations of Aurora B preferentially phosphorylate H3(S10) on acentrics and their associated DNA tethers. This phosphorylation event prevents HP1a from associating with heterochromatin and results in localized inhibition of nuclear envelope reassembly on endonuclease and X-irradiation-induced acentrics, promoting channel formation. Finally, we find that HP1a also specifies initiation sites of nuclear envelope reassembly on undamaged chromatin. Taken together, these results demonstrate that Aurora B-mediated regulation of HP1a-chromatin interaction plays a key role maintaining genome integrity by locally preventing nuclear envelope assembly and facilitating incorporation of late-segregating acentrics into daughter nuclei.

Introduction

Eukaryotic cells have evolved sophisticated mechanisms that maintain genome integrity. Checkpoints halt cell cycle progression in response to damaged DNA to allow for repair or elimination of compromised cells (Abbas *et al.* 2013). For example, the G1-S and the G2-M checkpoints prevent entry into S-phase and mitosis respectively when DNA is damaged (Elledge 1996). An additional checkpoint at the metaphase-anaphase transition delays progression into anaphase if DNA is damaged once a cell commits to mitosis (Mikhailov *et al.* 2002; Royou *et al.* 2005). Despite these checkpoints, cells sometimes enter anaphase with damaged DNA. Unrepaired double-stranded DNA breaks are particularly problematic, as they result in chromosome fragments lacking either a telomere or centromere (Kaye *et al.* 2004). The latter, called acentrics, are unable to form traditional microtubule-kinetochore attachments and are therefore expected to fail to segregate and to be excluded from the nascent daughter nuclei, leading to the formation of micronuclei (Kanda and Wahl 2000; LaFountain *et al.* 2001; Fenech *et al.* 2011). Historically, micronuclei have been a biomarker for cancer (Santos *et al.* 2010; Bonassi *et al.* 2011), and recent studies reveal that micronuclei drive genomic instability either through their loss during subsequent cell divisions or through chromothripsis, the dramatic shattering and rearrangement of micronuclear DNA that is then incorporated into the genome (Crasta *et al.* 2012; Vázquez-Diez *et al.* 2016; Zhang *et al.* 2015; Ly *et al.* 2017).

While the formation of micronuclei from lagging chromosomes has been widely documented, in some instances, lagging chromosomes avoid micronuclei

formation by rejoining daughter nuclei before mitosis is completed. For example, in human colorectal cancer cells, a proportion of lagging whole chromosomes that would otherwise form micronuclei instead reincorporate into the daughter nuclei in late anaphase (Huang *et al.* 2012). In fission yeast, lagging chromatids that remain distinct from the main segregating chromosomes during anaphase eventually reunite with daughter nuclei in telophase (Pidoux *et al.* 2000; Sabatinos *et al.* 2015). In addition, in *Drosophila* neuroblast and papillar divisions, late-segregating acentric fragments induced by endonuclease activity or irradiation successfully rejoin daughter nuclei in late telophase (Royou *et al.* 2010; Bretscher and Fox 2016). Therefore, the fate of lagging acentric chromosomes is an important but underexplored area of cell biology. Here, we specifically examine the mechanisms that facilitate incorporation of late-segregating acentric chromosomes into daughter nuclei, avoiding micronuclei formation.

In *Drosophila*, acentric behavior has been studied using transgenic flies containing a heat-shock inducible I-CreI endonuclease (Rong *et al.* 2002; Royou *et al.* 2010; Kotadia *et al.* 2012; Karg *et al.* 2015; Derive *et al.* 2015; Bretscher and Fox, 2016; Karg *et al.* 2017), which targets rDNA near the base of the X chromosome (Rong *et al.* 2002; Maggert and Golic 2005; Paredes and Maggert 2009; Golic and Golic 2011). I-CreI-mediated double-stranded DNA breaks result in γH2Av foci that persist through mitosis and chromosome fragments that do not recruit canonical centromere components and thus are considered acentrics (Royou *et al.* 2010). Even though I-CreI-induced acentrics initially lag on the metaphase plate while undamaged

chromosomes segregate, acentrics ultimately undergo delayed but successful segregation (Royou *et al.* 2010). Acentric segregation is achieved through protein-coated DNA tethers connecting acentrics to their centric partners and microtubule bundles that encompass acentrics, enabling their poleward movement (Karg *et al.* 2017). The histone-based DNA tether is associated with Polo, BubR1, and the chromosome passenger proteins Aurora B and INCENP (Royou *et al.* 2010).

Because lagging and acentric chromosome segregation is significantly delayed, occurring late in anaphase, they often remain distinct from the main mass of chromosomes when nuclear envelope reassembly initiates (Fenech 2000; Cimini *et al.* 2002; Afonso *et al.* 2014; Karg *et al.* 2015). Despite the presence of the nascent nuclear envelope surrounding the main nuclear mass, in *Drosophila* neuroblasts, lagging acentrics are not "locked out" of daughter nuclei and do not form micronuclei. Rather, the late-segregating acentrics bypass the nuclear envelope barrier and enter telophase nuclei through channels in the nuclear envelope that are formed by highly localized delays in the completion of nuclear envelope reassembly (Karg *et al.* 2015). Nuclear envelope channel formation is dependent upon the Aurora B kinase activity associated with the acentric and DNA tether. When Aurora B activity is reduced, acentrics are unable to enter daughter nuclei and instead form lamin-coated micronuclei. The pool of Aurora B responsible for channel formation likely comes from Aurora B persisting on the DNA tethers and acentrics, as channel formation is not observed in divisions which lack both acentrics and their associated Aurora B-coated tethers (Karg *et al.* 2015).

The formation of nuclear envelope channels suggests localized inhibition of important steps in nuclear envelope reassembly. Key events in nuclear envelope reassembly include reformation of nuclear pore complexes, reestablishment of connections between chromatin and inner nuclear membrane proteins that are disrupted in early mitosis, and fusion of nuclear envelope membrane microdomains (Baur *et al.* 2007; Dultz *et al.* 2008; Anderson and Hetzer 2008; Lu *et al.* 2011; Olmos *et al.* 2015; Vietri *et al.* 2015). Additionally, the nuclear lamina reassembles once nuclear pore complexes and inner nuclear membrane proteins are recruited to daughter nuclei (Newport *et al.* 1990; Chaudhary and Courvalin 1993; Daigle *et al.* 2001; Katsani *et al.* 2008).

Regulation of nuclear envelope reassembly is achieved through the global activity of mitotic kinases, among which Aurora B is a known negative regulator (Ramadan *et al.* 2007; Afonso *et al.* 2014; Karg *et al.* 2015). One mechanism by which Aurora B activity may inhibit nuclear envelope reassembly is through disrupting chromatin interactions with the heterochromatin component HP1α/HP1a (Schellhaus *et al.* 2015). In interphase, HP1α/HP1a binds both methylated histone H3 and nuclear envelope components (Ye and Worman, 1996; Ye *et al.* 1996; Kourmouli *et al.* 2000; Polioudaki *et al.* 2001). As cells enter mitosis, Aurora B-mediated phosphorylation of H3(S10) acts as a switch to remove HP1α/HP1a from chromosomes (Hirota *et al.* 2005; Fischle *et al.* 2005; Dormann *et al.* 2006). During anaphase, when Aurora B relocalizes to the spindle midzone and H3(S10) phosphate groups are removed (Carmena *et al.* 2012), HP1α/HP1a is reloaded onto segregating

chromosomes and subsequently reestablishes connections with nuclear envelope-associated components (Sugimoto *et al.* 2001; Poleshko *et al.* 2013), which is a possible early step in reformation of the nuclear envelope (Kourmouli *et al.* 2000).

Understanding the mechanisms by which Aurora B kinase activity locally alters the events of nuclear envelope reassembly to mediate channel formation is of particular interest. Specifically, understanding the pathway through which Aurora B acts to allow incorporation of late-segregating acentrics into daughter nuclei would reveal new mechanisms by which Aurora B prevents micronuclei formation and maintains genome integrity. In addition, studying the mechanisms by which nuclear envelope channel formation is regulated may provide a system for understanding how global nuclear envelope reassembly is regulated in wild-type divisions. Here, we explore these issues by generating acentrics using both the I-CreI endonuclease and X-irradiation and find that Aurora B excludes HP1a from late-segregating acentrics and that HP1a exclusion allows late-segregating acentrics to reincorporate into daughter telophase nuclei.

Results

Aurora B kinase preferentially phosphorylates H3(S10) on acentrics and on chromatin near sites of channel formation

Aurora B kinase, a component of the chromosome passenger complex, initially localizes to chromosomes in early mitosis and then localizes to the spindle midzone during anaphase (Carmena *et al.* 2012). Aurora B modifies mitotic chromatin by

phosphorylating histone H3 on serine 10 (Hsu *et al.* 2000), and previous studies demonstrated that the midzone-based pool of Aurora B phosphorylates segregating chromosomes in a spatial manner so that lagging whole chromosomes have relatively high phospho-H3(S10) levels (Fuller *et al.* 2008). In *Drosophila* neuroblasts bearing I-CreI-induced acentrics, Aurora B kinase persists on DNA tethers stretching from the lagging acentrics to the newly formed daughter nuclei after Aurora B removal from the main mass of segregating chromosomes (Royou *et al.* 2010; Karg *et al.* 2015). This highly localized Aurora B activity mediates nuclear envelope channel formation to allow acentric entry into telophase nuclei (Karg *et al.* 2015). Thus, we hypothesized that the Aurora B localized on the acentric and its associated tether might locally prohibit nuclear envelope formation.

We tested if Aurora B-dependent phosphorylation of H3(S10) persists on acentrics, tethers, and channel sites despite this mark having been removed from the rest of the main nuclei by fixing I-CreI-expressing mitotic neuroblasts from female 3rd instar larvae and staining with an antibody that specifically recognizes phospho-H3(S10) (Figure 11). In neuroblasts fixed in metaphase, we observed phospho-H3(S10) present along the length of all chromosomes, consistent with data from (McManus *et al.* 2006) (Figure 11A, left panel). In anaphase neuroblasts, we observed a weak phospho-H3(S10) signal on segregating intact chromosomes. In contrast, late-segregating acentrics that remained at or had just segregated from the metaphase plate (Figure 11A, middle panels, red arrows) exhibited a strong phospho-H3(S10) signal (Figure 11A, middle panels, cyan arrows). In neuroblasts fixed in

telophase, the stage at which acentrics begin to rejoin daughter nuclei, we observed a continued strong phospho-H3(S10) signal on acentrics. The phospho-H3(S10) signal abruptly ended at the point of contact between the acentric and daughter nucleus (Figure 11A, right panel).

To quantify these observations, we measured the fold change of the phospho-H3(S10)/DNA signal intensity from the main nuclei to the acentrics for each fixed neuroblast division imaged (Figure 11B). For 31 out of the 32 neuroblast divisions scored, we observed an increase in phospho-H3(S10)/DNA intensity on acentrics compared to main nuclei (mean fold change = 4.13; SD = 2.65; N=32), consistent with previous reports (Fuller *et al.* 2008; de Castro *et al.* 2016).

Intriguingly, in a large proportion (47%; N=19) of anaphase- or telophase-fixed neuroblast divisions in which at least one acentric remained distinct from the main nuclei, we clearly detected localized "hotspots" of strong phospho-H3(S10) intensity on one of the newly formed nuclei at presumptive sites of acentric entry. These hotspots correspond to the location where tethers contact the nuclei and nuclear envelope channel formation is generally observed (Figure 11A, yellow arrowheads). Taken together, these data demonstrate that acentrics, tethers, and the chromatin at sites of channel formation remain preferentially phosphorylated on H3(S10) even though phosphorylation of H3(S10) is broadly reduced on the chromatin in newly formed telophase nuclei.

Figure 11. H3(S10) is preferentially phosphorylated on acentrics and tethers. (A) Fixed mitotic neuroblasts expressing I-CreI in metaphase (left panel), anaphase (middle panels), and telophase (right panel) (red = DNA; blue = phospho-H3(S10)). Acentrics are indicated by red arrows. Increased phosphorylation of H3(S10) is indicated by cyan arrows. phospho-H3(S10) "hotspots" are indicated by yellow arrowheads. (B) Graphical comparison of fold increases in the average phopsho-H3(S10)/DNA pixel intensity ratio for the areas of the acentrics vs. the areas of the main nuclei for I-CreI-expressing neuroblasts. Each circle represents one anaphase/telophase cell. Values above 1 (green box) indicate increased phospho-H3(S10)/DNA pixel intensity ratio on acentrics. Values below 1 (red box) indicate increased phospho-H3(S10)/DNA pixel intensity ratio on main nuclei. Black bar indicates mean fold change. Scale bars are 2 µm.

Figure 11

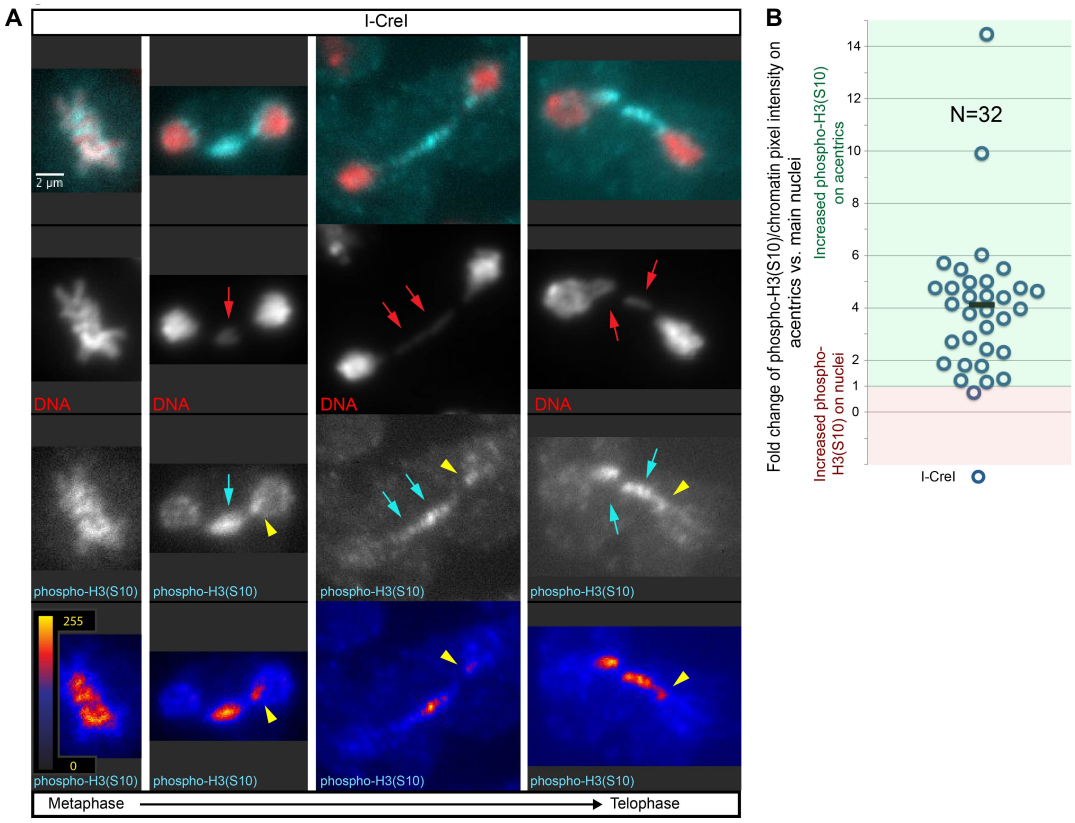

To determine whether Aurora B kinase activity is responsible for the observed preferential phosphorylation of H3(S10) on acentrics and tethers, we compared the fold changes of phospho-H3(S10)/DNA intensity from the main nuclei to the acentrics between neuroblasts with normal and RNAi-reduced levels of Aurora B. In I-CreI-expressing neuroblasts fixed in anaphase and telophase (Figure 12A), we observed an average fold change of phospho-H3(S10)/DNA signal from main nuclei to acentrics of 6.39 (SD = 6.56; N=23) with 78% of divisions showing a greater than 2-fold increase of phospho-H3(S10)/DNA intensity on acentrics compared to the main nuclei (and 57% of divisions showing a greater than 4-fold increase of phospho-H3(10)/DNA intensity on acentrics compared to the main nuclei) (Figure 12C).

In contrast, upon reduction of Aurora B (Figure S1B), we observed a decreased average fold change of phospho-H3(S10)/DNA signal on acentrics compared to main nuclei of 2.34 (SD = 2.15; N=20) (statistically significant by two-sided independent t-test $p = 0.01$) with only 40% of divisions showing a greater than 2-fold increase of phospho-H3(S10)/DNA intensity on acentrics to main nuclei (compare to 78% of acentrics in wild-type conditions, significant by chi-square test p=0.0105) (and only 20% of divisions showing a greater than 4-fold increase of phospho-H3(S10)/DNA intensity on acentrics compared to the main nuclei) (Figure 12C). These findings indicate that Aurora B kinase is responsible for the observed persistent phosphorylation of H3(S10) on acentric fragments during anaphase and telophase.

Figure 12. Aurora B kinase preferentially phosphorylates H3(S10) on acentrics and tethers. Images of acentrics in (A) wild-type and (B) Aurora B-depleted anaphase neuroblasts stained for DNA (red) and phospho-H3(S10) (cyan). (C) Graph comparing fold increase in the average phopsho-H3(S10)/DNA pixel intensity ratio for the areas of the acentrics vs. the areas of the main nuclei for I-CreI-expressing neuroblasts (left) and I-CreI- and Aurora B RNAi-expressing neuroblast. Each circle represents one anaphase/telophase cell. Scale bars are 2 µm.

Figure 12

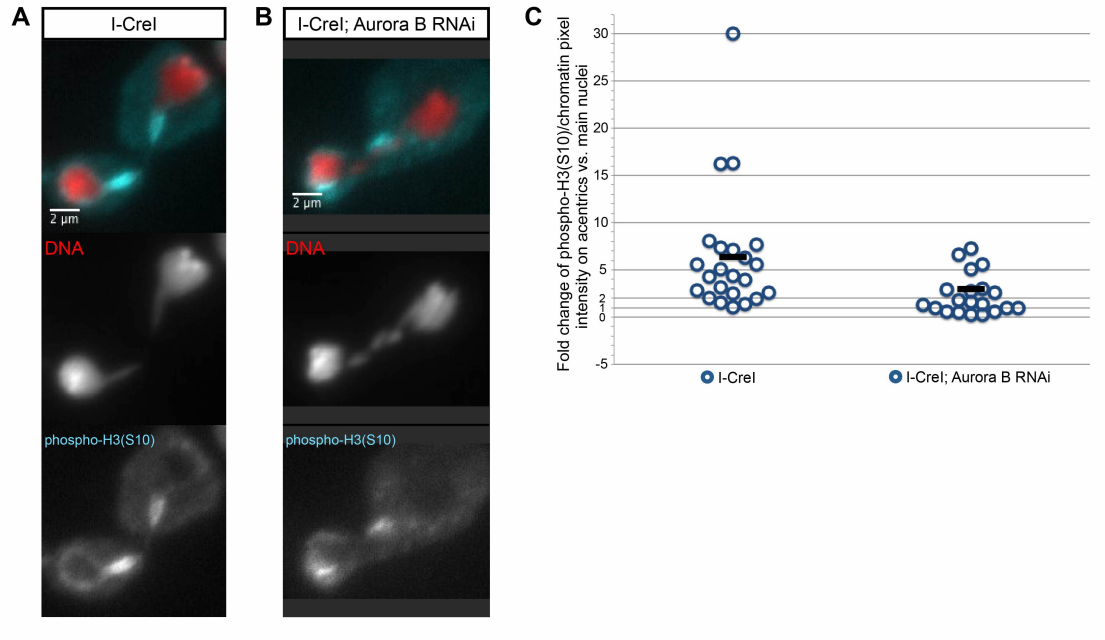

Aurora B kinase activity blocks HP1a association on late-segregating acentrics

Since phosphorylation of H3(S10) by Aurora B kinase is known to prevent H3 interaction with the heterochromatin component HP1α (the mammalian ortholog of HP1a) (Hirota *et al.* 2005; Fischle *et al.* 2005), we hypothesized that the observed increase in phosphorylation of H3(S10) on acentrics with respect to the main nuclei would lead to an Aurora B-dependent preferential exclusion of HP1a on late-segregating acentrics. To test this hypothesis, we performed live imaging of dividing neuroblasts from female larvae expressing I-CreI, H2Av-RFP, and GFP-HP1a in control conditions (Dimethyl sulfoxide (DMSO)-treated neuroblasts) and conditions in which Aurora B kinase activity was partially inhibited through introduction of the Aurora B-specific small molecule inhibitor Binucleine-2 (Smurnyy *et al.* 2010) (Figure 13).

In control DMSO-treated mitotic neuroblasts (Figure 13A, see Movie 6), we observed the following patterns of HP1a association: in metaphase, little or no HP1a was detected on the chromosomes; and in anaphase, a strong HP1a signal was detected on the main segregating chromosomes, primarily on the pericentric heterochromatin (Figure 13A, green arrowheads). These results are consistent with previous data showing that a large proportion of HP1α/HP1a dissociates from chromosomes in early mitosis and re-associates with segregating chromosomes in anaphase (Hirota *et al.* 2005; Fischle *et al.* 2005; Dormann *et al.* 2006; Poleshko *et al.* 2013). Interestingly, in contrast to the anaphase recruitment of HP1a on the main chromosomes, little or no HP1a was detected on late-segregating acentrics, despite

the expected high heterochromatin content of I-CreI induced acentrics (Figure 13A, red arrows). In total, we only clearly detected HP1a on acentrics in about 22% of neuroblast divisions we imaged (N=37) (Figure 13C).

In mitotic neuroblasts that were treated with the Aurora B inhibitor Binucleine-2 dissolved in DMSO (Figure 13B, see Movie 7), we observed a similar pattern of HP1a association on the main intact nuclei: little or no HP1a on metaphase chromosomes followed by anaphase recruitment of HP1a on the main segregating chromosomes (Figure 2B, green arrowheads). However, in contrast to DMSO-treated neuroblasts, in which HP1a was not detected on late-segregating acentrics, we observed strong HP1a association on anaphase acentrics in neuroblasts treated with DMSO + Binucleine-2 (Figure 13B, green arrows). In all the DMSO + Binucleine-2-treated neuroblasts imaged, clear HP1a association was observed 55% of the time (N=31) (Figure 13C) (compare to 22% of the time in control divisions, a statistically significant difference determined by a chi-square test $p = 0.005$).

To more stringently quantify the levels of HP1a associated with segregating acentrics in wild-type and Aurora B inhibited conditions, we measured the pixel intensity of GFP-HP1a on acentrics as they began to segregate poleward in both DMSO- and DMSO + Binucleine-2-treated neuroblasts imaged using spinning disk confocal microscopy (Figure 13D). This analysis revealed two key differences: 1) in Aurora B inhibited neuroblasts (red line), segregating acentrics were associated with higher levels of HP1a than acentrics from control neuroblasts (blue line); and 2) HP1a association with acentrics from Aurora B inhibited neuroblasts increased over time

while HP1a association with acentrics from control neuroblasts slightly decreased. Taken together, these results indicate that Aurora B activity preferentially excludes HP1a from late-segregating acentrics.

Additionally, we observed that acentrics from DMSO-treated control neuroblasts segregated normally and rejoined daughter nuclei in telophase (Figure 13A). We observed micronucleation in 40% of divisions (N=30) (Figure 13E). Micronuclei were defined as acentrics that failed to enter daughter nuclei, remaining either physically distinct from nuclei or directly adjacent to nuclei but moving independently. However, In DMSO + Binucleine-2-treated neuroblasts, acentrics mostly failed to rejoin daughter nuclei, instead forming micronuclei (Figure 13B, red arrowheads). When we inhibited Aurora B activity, we observed micronucleation 71% of the time (N=28) (Figure 13E) (a statistically significant increase compared to the 40% micronucleation observed in control divisions, determined by a chi-square test $p = 0.02$).

We next determined whether HP1a association with acentrics was correlated with micronucleation. We scored individual acentrics for the presence of HP1a and whether the acentric formed a micronucleus (Figure 13F). We grouped the scored acentrics into four categories: 1) acentrics that were HP1a-free and formed micronuclei (Figure 13F, blue box); 2) acentrics that were HP1a-free and rejoined daughter nuclei (Figure 13F, green box); 3) acentrics that were HP1a-coated and formed micronuclei (Figure 13F, red box); and 4) acentrics that were HP1a-coated and rejoined daughter nuclei (Figure 13F, yellow box). Overall, we found that 79%

of acentrics that were HP1a-free (N=58) rejoined daughter nuclei, while only 16% of acentrics that were HP1a-coated were able to rejoin daughter nuclei (N=32) (statistical significance determined by chi-square test $p=5.34 \times 10^{-9}$). The remaining 84% of acentrics that were HP1a-coated formed micronuclei. Thus, the absence or presence of HP1a is a strong predictor of the fate of the I-CreI-induced acentric, either entering the daughter nucleus or forming a micronucleus.

Figure 13. Aurora B kinase activity blocks HP1a association with late-segregating acentrics**.** (A) Stills from a time-lapse movie of a mitotic neuroblast expressing I-CreI, H2Av-RFP (red), and GFP-HP1a (green) treated with DMSO (control) (see Movie S1). GFP-HP1a detected on the centric heterochromatic region of segregating intact chromosomes is indicated by green arrowheads. Acentrics are indicated by red arrows. (B) Stills from a time-lapse movie of a mitotic neuroblast expressing I-CreI, H2Av-RFP (red), and GFP-HP1a (green) treated with the Aurora B inhibitor Binucleine-2 dissolved in DMSO (see Movie S2). GFP-HP1a observed on acentric chromosomes is indicated by green arrows. Micronuclei are indicated by red arrowheads. (C) Comparison of the percentage of divisions in which GFP-HP1a was detected on acentrics in DMSO-treated (left) and DMSO + Binucleine-2-treated (right) I-CreI-expressing neuroblasts. Asterisk indicates statistical significance by a chi-square test ($p = 0.005$). (D) Comparison of GFP-HP1a pixel intensity on acentrics from DMSO-treated neuroblasts (blue line) and DMSO + Binucleine-2-treated neuroblasts (red line). Error bars represent 2 SE. (E) Comparison of the percentage of divisions in which acentrics formed micronuclei in DMSO-treated (left) and DMSO + Binucleine-2-treated (right) I-CreI-expressing neuroblasts. Asterisk indicates statistical significance by a chi-square test ($p = 0.02$). (F) Graph depicting a strong correlation between the lack of HP1a on the acentric and the ability of the acentric to rejoin the daughter nucleus. Each circle represents one acentric: blue and red circles depict single acentrics derived from DMSO and DMSO + Binucleine-2 treated I-CreI-expressing neuroblasts respectively. Asterisk indicates statistical significance by a chi-square test ($p = 5.34 \times 10^{-9}$). Time is written as min:sec after anaphase onset. Scale bars are 2 μm.

Figure 13

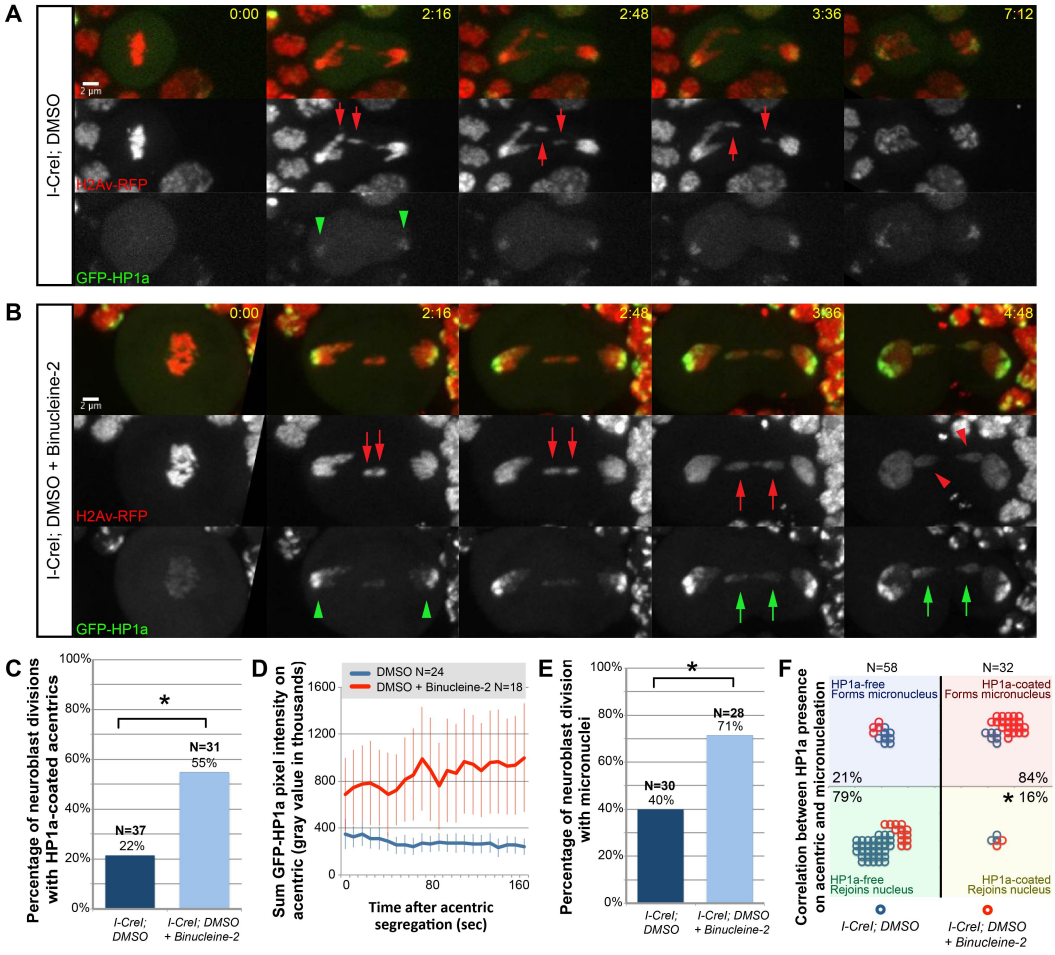
A
I-CreI; DMSO
0:00
2:16
2:48
3:36
7:12
2 µm
H2Av-RFP
GFP-HP1a
B
I-CreI; DMSO + Binucleine-2
0:00
2:16
2:48
3:36
4:48
2 µm
H2Av-RFP
GFP-HP1a
C
Percentage of neuroblast divisions with HP1a-coated acentrics
100%
80%
60%
40%
20%
0%
*
N=31
55%
N=37
22%
I-CreI; DMSO
I-CreI; DMSO + Binucleine-2
D
Sum GFP-HP1a pixel intensity on acentric (gray value in thousands)
DMSO N=24
DMSO + Binucleine-2 N=18
1600
1200
800
400
0
0
80
160
Time after acentric segregation (sec)
E
Percentage of neuroblast division with micronuclei
100%
80%
60%
40%
20%
0%
*
N=28
71%
N=30
40%
I-CreI; DMSO
I-CreI; DMSO + Binucleine-2
F
Correlation between HP1a presence on acentric and micronucleation
N=58
N=32
HP1a-free Forms micronucleus
HP1a-coated Forms micronucleus
21%
84%
79%
* 16%
HP1a-free Rejoins nucleus
HP1a-coated Rejoins nucleus
I-CreI; DMSO
I-CreI; DMSO + Binucleine-2

Aurora B kinase activity promotes nuclear envelope channel formation through HP1a exclusion from acentrics and tethers

Due to the correlation of HP1a-acentric association and the formation of micronuclei as well as the ability of HP1α/HP1a to interact with and recruit the nuclear envelope (Ye and Wormann 1996; Kourmouli *et al.* 2000), we tested whether Aurora B-mediated HP1a exclusion from acentrics might be a key factor in channel formation through localized inhibition of nuclear envelope reassembly. We performed live imaging of mitotic neuroblasts from female larvae expressing I-CreI, H2Av-RFP, and the nuclear envelope marker Lamin-GFP and asked whether depletion of HP1a rescued the ability to form nuclear envelope channels when Aurora B was inhibited. The rationale is that while chromatin containing H3-HP1a is a strong promoter of nuclear envelope assembly, chromatin containing H3 by itself is only a neutral substrate for assembly, and thus prevention of H3-HP1a formation on the acentric and tether, either through Aurora B-mediated phosphorylation of H3(S10) or through depletion of HP1a, would be conducive to channel formation (Figure 14).

Figure 14. Schematic illustrating logic of HP1a co-depletion with Aurora B inhibition. (A) In wild-type conditions, highly localized Aurora B on the acentric and the tether inhibits recruitment of both HP1a and nuclear envelope components specifically to the acentric and tether, leading to the formation of nuclear envelope channels and the reincorporation of acentrics into daughter nuclei. (B) When Aurora B is inhibited, HP1a and nuclear envelope components can now be recruited to acentric and tether and channels do not form. Therefore, acentrics are "locked out" as micronuclei. (C) If Aurora B activity mediates nuclear envelope channel formation through the preferential exclusion of HP1a from the acentric and the tether, RNAi depletion of HP1a should rescue nuclear envelope channel formation in conditions in which Aurora B is inhibited, allowing acentrics to reintegrate into daughter nuclei. NER = nuclear envelope reassembly.

Figure 14

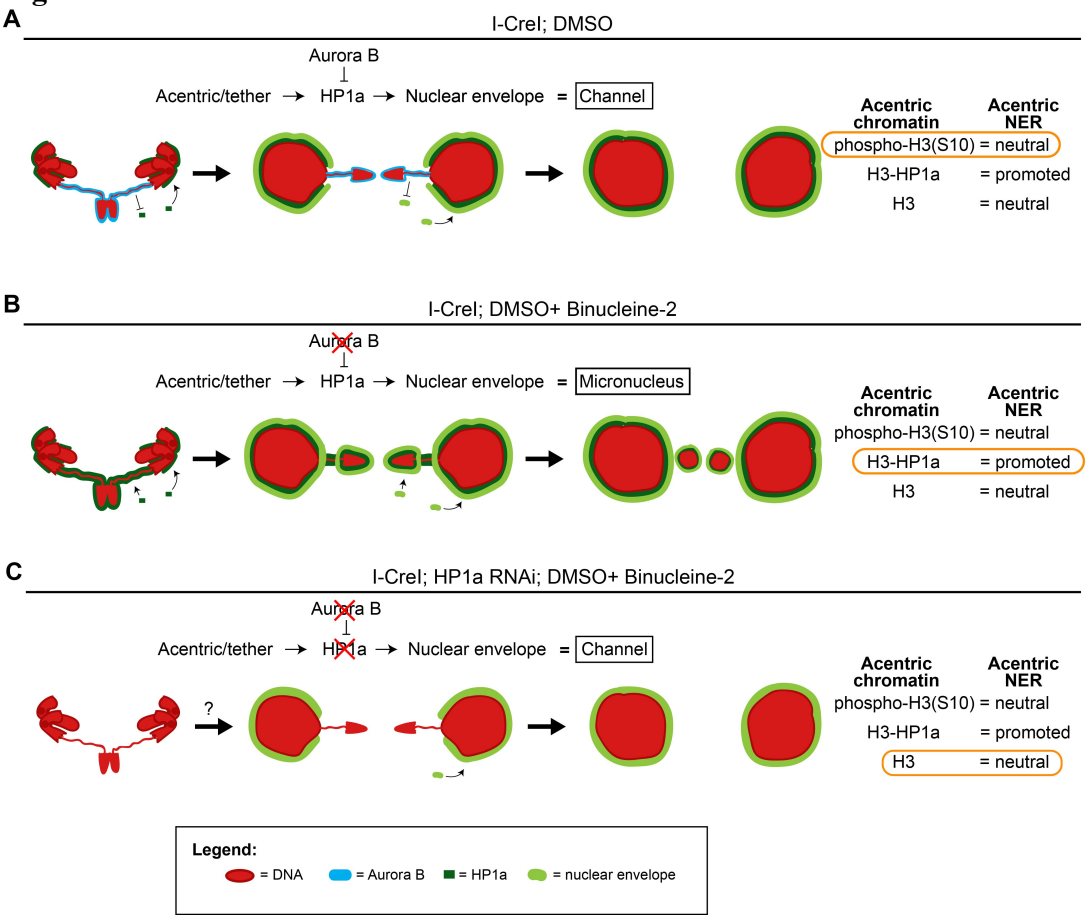

HP1α/HP1a is essential: homozygous null mutants result in embryonic lethality in *Drosophila* (Kellum and Alberts 1995). Therefore, to address the role of HP1a in nuclear envelope channel formation, we made use of the transgenic UAS/Gal4 system (for review, see Duffy 2002) to deplete HP1a through RNA interference (RNAi). In our setup, we expressed UAS-HP1a-dsRNA in the larval central nervous system. One of the additional benefits of using the transgenic UAS/Gal4 system is the ability to fine-tune the degree of Gal4 activity by altering the temperature at which flies are grown (Duffy 2002). Using this property, we found that HP1a depletion was stronger when larvae were grown at 29^{o}C as opposed to a more mild depletion when larvae were grown at room temperature (measured as 22^{o}C) (Figure 15). When larvae were grown at 29^{o}C, we observed an increase in chromosome segregation errors (Figure 15A-A'), a previously observed phenotype in HP1a mutants (Kellum and Alberts 1995) and a decrease in survivability (Figure 15B) compared to larvae grown at 22^{o}C.

Figure 15. Growth temperature influences strength of HP1a depletion. (A) Stills from time-lapse movies of a wild-type neuroblast expressing H2Av-RFP (top panel) and a neuroblast expressing H2Av-RFP and HP1a RNAi (bottom panel) from larvae grown at 29ºC. In the wild-type neuroblast, chromosomes separate normally. In the HP1a RNAi-expressing neuroblast, there are lagging chromosomes (arrow) and a chromosome bridge (arrowhead). (A') Comparison of the percentage of chromosome segregation errors in wild-type neuroblasts (dark blue bars) and HP1a RNAi-expressing neuroblasts (light blue bars) from larvae grown at 22ºC (left bars) and 29ºC (right bars). 14% (N=7) and 13% (N=8) of wild-type neuroblast divisions had chromosome segregation errors when larvae were grown at 22ºC and 29ºC respectively. 29% (N=7) and 45% (N=20) of HP1a RNAi-expressing neuroblast divisions had chromosome segregation errors when larvae were grown at 22ºC and 29ºC respectively. (B) Comparison of the mean survival of wild-type larvae (dark blue bars) and larvae expressing HP1a RNAi (light blue bars) when grown at 22ºC (left bars) and 29ºC (right bars). Error bars represent standard deviation. On average, wild-type larvae developed into adults 85% (SD = 30%, N=13) and 78% (SD = 21%, N=13) when grown at 22ºC and 29ºC respectively. On average, HP1a RNAi-expressing larvae developed into adults 73% (SD = 23%, N=13) and 29% (SD= 31%, N=13) when grown at 22ºC and 29ºC respectively. Asterisks indicate statistical significance by unpaired one-sided t-tests (HP1a RNAi-expressing larvae at 22ºC and 29ºC: $p=0.0002$; and wild-type and HP1a RNAi-expressing larvae at 29ºC: $p=5.5 \times 10^{-5}$). Time is written as min:sec after anaphase onset. Scale bars are 2 μm.

Figure 15

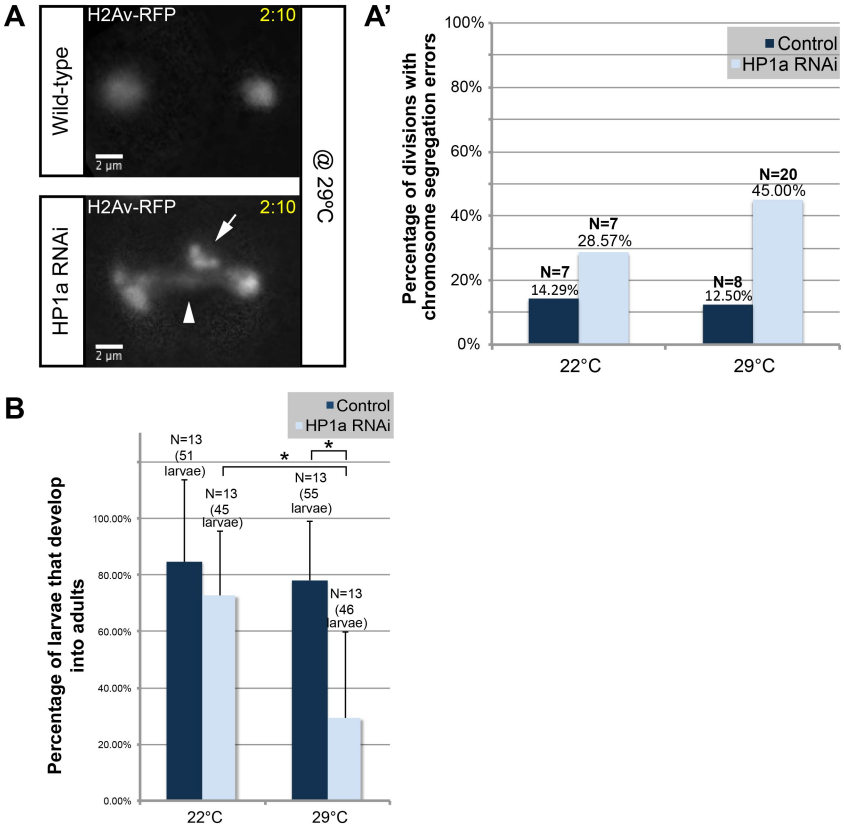
A
Wild-type
H2Av-RFP
2:10
2 µm
HP1a RNAi
H2Av-RFP
2:10
2 µm
@ 29ºC
A'
Percentage of divisions with chromosome segregation errors
Control
HP1a RNAi
100%
80%
60%
40%
20%
0%
N=7
14.29%
N=7
28.57%
N=8
12.50%
N=20
45.00%
22°C
29°C
B
Percentage of larvae that develop into adults
Control
HP1a RNAi
N=13 (51 larvae)
N=13 (45 larvae)
N=13 (55 larvae)
N=13 (46 larvae)
*
*
100.00%
80.00%
60.00%
40.00%
20.00%
0.00%
22°C
29°C

To determine the role of Aurora B-mediated exclusion of HP1a from acentrics/tethers in nuclear envelope channel formation, we performed live imaging on neuroblasts from female larvae in which levels of Aurora B and HP1a were modulated, and compared the rates of nuclear envelope channel formation and micronucleation. All larvae were grown in conditions of mild HP1a depletion (22^{o}C). In DMSO-treated neuroblasts (Figure 16A-A', see Movie 8), we observed that late-segregating acentrics (red arrows) entered daughter nuclei through channels in the nuclear envelope (green arrows) and successfully rejoined the main nuclear mass, consistent with previously reported data (Karg *et al.* 2015). In DMSO + Binucleine-2-treated neuroblasts (Figure 16B-B', see Movie 9), we observed that late-segregating acentrics (red arrows) failed to form channels in the daughter nuclear envelope and were subsequently locked out of the nuclei to form micronuclei (red arrowheads), as previously reported (Karg *et al.* 2015). In DMSO-treated HP1a RNAi-expressing neuroblasts (Figure 16C-C', see Movie 10), we observed that late-segregating acentrics (red arrows) entered daughter nuclei through channels in the nuclear envelope (green arrows), successfully rejoining the intact DNA. However, in contrast to the decreased rates of nuclear envelope channel formation and increased micronucleation observed upon inhibition of Aurora B in neuroblasts with wild-type HP1a levels, in DMSO + Binucleine-2-treated HP1a RNAi-expressing neuroblasts (Figure 16D-D', see Movie 11), we observed that late-segregating acentrics (red arrows) were once again capable of forming nuclear envelope channels (green arrows), through which acentrics rejoined daughter telophase nuclei.

In total, 67% of DMSO-treated control neuroblasts divisions (N=21) resulted in visible nuclear envelope channels, and inhibition of Aurora B resulted in a decrease in divisions with visible nuclear envelope channels (36%; N=45) (significance determined by a chi-square test $p = 0.02$) (Figure 16E). In contrast, RNAi depletion of HP1a alone (73%; N=22) or in combination with Aurora B inhibition (63%; N=35) showed no difference in the percentage of divisions with visible nuclear envelope channels (no statistical significance determined by a chi square test $p = 0.44$) (Figure 16E). In accord with these observations, we also measured an increase in micronucleation from DMSO-treated control neuroblasts (26%; N=19) to Aurora B inhibited neuroblasts (74%; N=42) (statistical significance determined by a chi-square test $p = 0.003$), while there was no difference in the rate of micronucleation when HP1a was depleted alone (33%; N=18) or in combination with Aurora B inhibition (34%; N=32) (no statistical significance determined by a chi-square test $p = 0.94$) (Figure 16F). Taken together, these results indicate that forming an H3-HP1a complex along the acentric and tether promotes local nuclear envelope assembly, and preventing the formation of this complex, either through Aurora B-dependent H3 phosphorylation or depletion of HP1a, reduces nuclear envelope assembly and facilitates channel formation.

Figure 16. Aurora B-mediated HP1a exclusion from acentrics/tethers results in nuclear envelope channel formation**.** (A-A') Stills from time-lapse movies of two different mitotic neuroblasts expressing I-CreI, H2Av-RFP (red), and Lamin-GFP (green) treated with DMSO (see Movie 8). Acentrics are indicated by red arrows. Channels are indicated by green arrows. (B-B') Stills from time-lapse movies of two different mitotic neuroblasts expressing I-CreI, H2Av-RFP, and Lamin-GFP treated with DMSO + Binucleine-2 (see Movie 9). Micronuclei are indicated by red arrowheads. (C-C') Stills from time-lapse movies of two different mitotic neuroblasts expressing I-CreI, H2Av-RFP, Lamin-GFP, and HP1a RNAi treated with DMSO (see Movie 10). (D-D') Stills from time-lapse movies of two different mitotic neuroblasts expressing I-CreI, H2Av-RFP, Lamin-GFP, and HP1a RNAi treated with DMSO + Binucleine-2 (see Movie 11). (E) Comparison of the percentage of neuroblast divisions in which nuclear envelope channels were observed when I-CreI-expressing neuroblasts were treated with DMSO or DMSO + Binucleine-2 (asterisk indicates statistically significant to I-CreI; DMSO neuroblasts; $p = 0.02$, determined by a chi-square test) and when I-CreI- and HP1a RNAi-expressing neuroblasts were treated with DMSO or DMSO + Binucleine-2 (asterisk indicates statistically significant to I-CreI; DMSO + Binucleine-2 neuroblasts; $p = 0.01$, determined by a chi-square test). NS indicates no statistical significance. (F) Comparison of the percentage of neuroblast divisions in which micronuclei were observed when I-CreI-expressing neuroblasts were treated with DMSO or DMSO + Binucleine-2 (asterisk indicates statically significant to I-CreI; DMSO neuroblasts; $p = 0.0005$, determined by a chi-square test) and I-CreI- and HP1a RNAi-expressing neuroblasts were treated with DMSO or DMSO + Binucleine-2 (asterisk indicates statistical significance to I-CreI; DMSO + Binucleine-2 neuroblasts; $p = 0.0006$, determined by a chi-square test). NS indicates no statistical significance. Time is written as min:sec after anaphase onset. Scale bars are 2 μm.

Figure 16

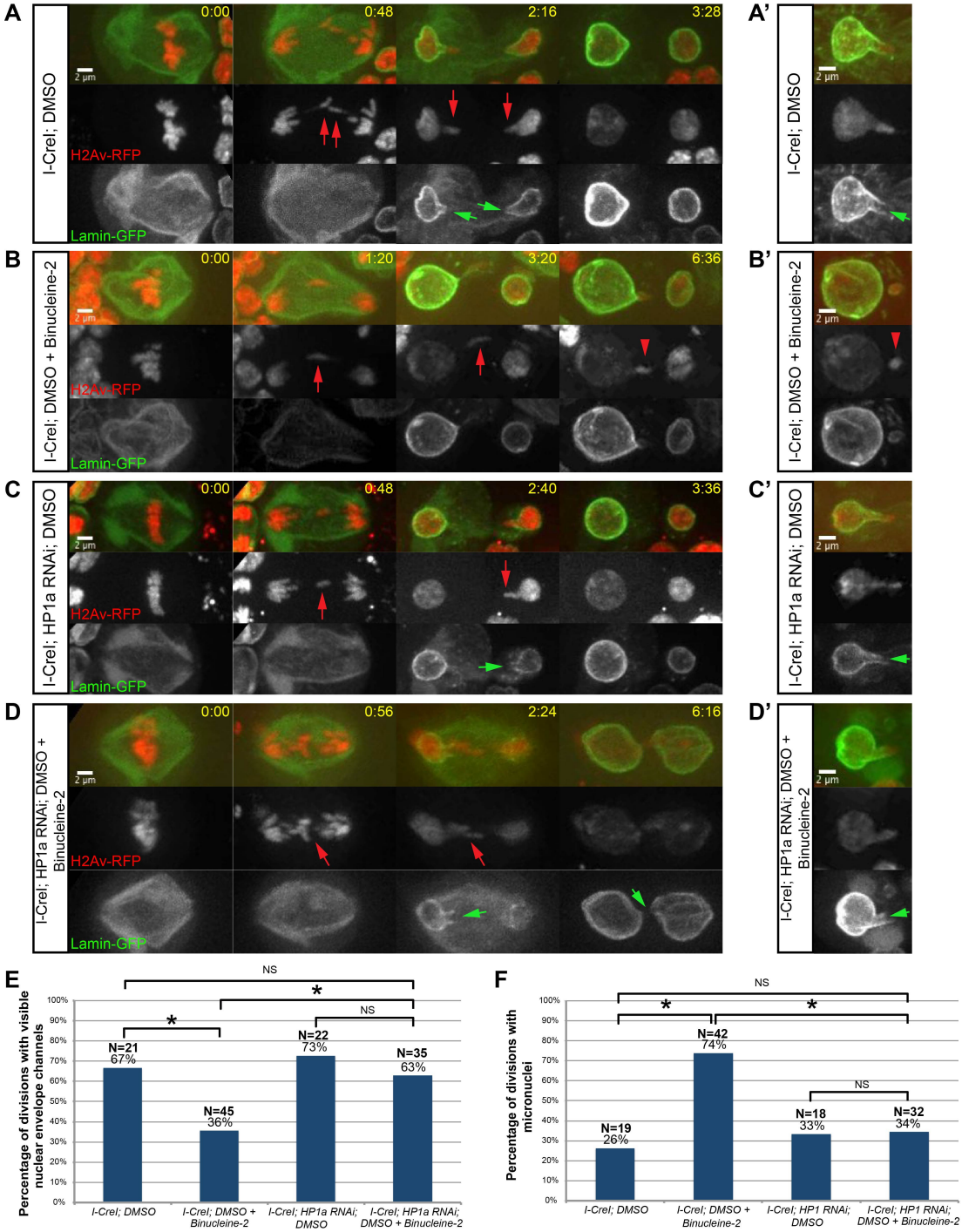
A
I-CreI; DMSO
0:00
0:48
2:16
3:28
H2Av-RFP
Lamin-GFP
2 µm
A'
B
I-CreI; DMSO + Binucleine-2
0:00
1:20
3:20
6:36
B'
C
I-CreI; HP1a RNAi; DMSO
0:00
0:48
2:40
3:36
C'
D
I-CreI; HP1a RNAi; DMSO + Binucleine-2
0:00
0:56
2:24
6:16
D'
E
Percentage of divisions with visible nuclear envelope channels
N=21 67%
N=45 36%
N=22 73%
N=35 63%
NS
*
I-CreI; DMSO
I-CreI; DMSO + Binucleine-2
I-CreI; HP1a RNAi; DMSO
I-CreI; HP1a RNAi; DMSO + Binucleine-2
F
Percentage of divisions with micronuclei
N=19 26%
N=42 74%
N=18 33%
N=32 34%
I-CreI; HP1 RNAi; DMSO
I-CreI; HP1 RNAi; DMSO + Binucleine-2

HP1a exclusion and Aurora B-mediated channel formation are important to prevent micronuclei formation in response to irradiation-induced acentrics

All of the above experiments relied on I-CreI-induced double-stranded breaks specifically in the centric heterochromatin of the X chromosome (Rong *et al.* 2002; Maggert and Golic 2005; Paredes and Maggert 2009; Golic and Golic 2011). We next sought to determine whether similar results would be obtained regarding HP1a-acentric association and channel formation when the acentrics were generated through X-irradiation (Figure 4). Unlike I-CreI-induced double-stranded breaks, ionizing radiation produces single- and double-stranded DNA breaks in both euchromatin and heterochromatin to yield late-segregating acentrics that vary both in size and chromatin composition (Bajer 1957; Roots *et al.* 1985; Puerto *et al.* 2001). Despite these differences between I-CreI and irradiation-induced acentrics, acentrics generated by X-irradiation also form BubR1-coated tethers, undergo delayed poleward segregation, and enter daughter telophase nuclei through nuclear envelope channels (Royou *et al.* 2010, Karg *et al.* 2015).

To test if Aurora B activity preferentially inhibited HP1a recruitment to X-irradiation-induced acentrics and their tethers, we X-irradiated H2Av-RFP- and GFP-HP1a-expressing female larvae. We observed a similar pattern of HP1a-acentric dynamics during neuroblast division as we did upon I-CreI expression. In control conditions (DMSO-treated neuroblasts), we observed GFP-HP1a exclusion (yellow arrows) from X-irradiation-induced late-segregating chromatin (red arrows) despite

its recruitment to main nuclei (green arrowheads) in 8/8 divisions (Figure 17A), with 2/8 divisions resulting in micronuclei. Upon Aurora B inhibition (DMSO + Binucleine-2-treated neuroblasts), we observed a small increase in GFP-HP1a association (3/11 divisions with detectable GFP-HP1a on acentrics (green arrows)) and a decreased ability for acentrics to rejoin daughter nuclei (6/9 divisions resulting in micronuclei) (red arrowheads) (Figure 17B-B'). It should be noted that the sample of X-irradiated acentric data is much smaller than that of I-CreI-induced acentrics, because the ionizing radiation was much less efficient at generating double-strand breaks that would result in detectable acentrics in dividing neuroblasts than I-CreI expression.

Intriguingly, we observed one way in which the recruitment of HP1a to X-irradiation-induced acentrics differed from that of I-CreI-induced acentrics: whereas I-CreI-induced acentrics recruited HP1a upon Aurora B inhibition in a majority of divisions (55%, N=31) (Figure 17C), X-irradiation-induced acentrics only recruited HP1a upon Aurora B inhibition in a minority of divisions (27%, N=11) (Figure 17B' green arrow). Nevertheless, these X-irradiation-induced HP1a-free acentrics still formed micronuclei (4/6 observed micronuclei were HP1a-free) (Figure 17B red arrowhead), suggesting that exclusion of HP1a from acentrics is one of several pathways through which Aurora B mediates channel formation and acentric entry into daughter nuclei.

We additionally monitored nuclear envelope channel formation in response to X-irradiation-induced acentrics by X-irradiating H2Av-RFP- and Lamin-GFP-

expressing neuroblasts. In X-irradiated DMSO-treated neuroblasts, we observed X-irradiation-induced lagging chromatin (red arrow) reintegrate into telophase daughter nuclei by passing through channels in the nuclear envelope (green arrow) in 6/9 divisions (Figure 17C), with only 3/8 divisions resulting in micronuclei, similar to previous results (Karg *et al.* 2015). Treatment of neuroblasts with DMSO + Binucleine-2 to inhibit Aurora B resulted in decreased channel formation (4/9 divisions with detectable channels) and increased micronucleation (5/9 divisions resulting in micronuclei) (red arrowheads) (Figure 17D). Furthermore, upon reduction of HP1a by RNAi and Aurora B inhibition (DMSO + Binucleine-2-treated neuroblasts), we once again observed increased channel formation (9/12 divisions with detectable channels) (green arrows) and reduced micronucleation (2/12 divisions resulting in micronuclei), suggesting that Aurora B-mediated HP1a exclusion from lagging chromatin to promote channel formation is not simply limited to I-CreI-induced acentrics.

Figure 17. X-irradiation-induced acentrics fail to recruit HP1a and re-enter daughter nuclei through Aurora B-mediated nuclear envelope channels**.** (A) Stills from a time-lapse movie of an X-irradiated neuroblast expressing H2Av-RFP (red) and GFP-HP1a (green) and treated with DMSO. Acentrics are indicated by red arrows. HP1a association with the main daughter nuclei is indicated by green arrowheads. Lack of HP1a on segregating acentrics is depicted by yellow arrows. (B-B') Stills from a time-lapse movie of an X-irradiated neuroblast expressing H2Av-RFP (red) and GFP-HP1a (green) and treated with DMSO + Binucleine-2. (B) A micronucleus is indicated by a red arrowhead. (B') A micronucleus is indicated by a red arrowhead and coated with GFP-HP1a (indicated by a green arrow). (C) Stills from a time-lapse movie of an X-irradiated neuroblast expressing H2Av-RFP (red) and Lamin-GFP (green) and treated with DMSO. (D) Stills from a time-lapse movie of an X-irradiated neuroblast expressing H2Av-RFP (red) and Lamin-GFP (green) and treated with DMSO + Binucleine-2. (E) Stills from a time-lapse movie of an X-irradiated neuroblast expressing H2Av-RFP (red), Lamin-GFP (Green), and RNAi against HP1a and treated with DMSO + Binucleine-2. Time is written as min:sec after anaphase onset. Scale bars are 2 μm.

Figure 17

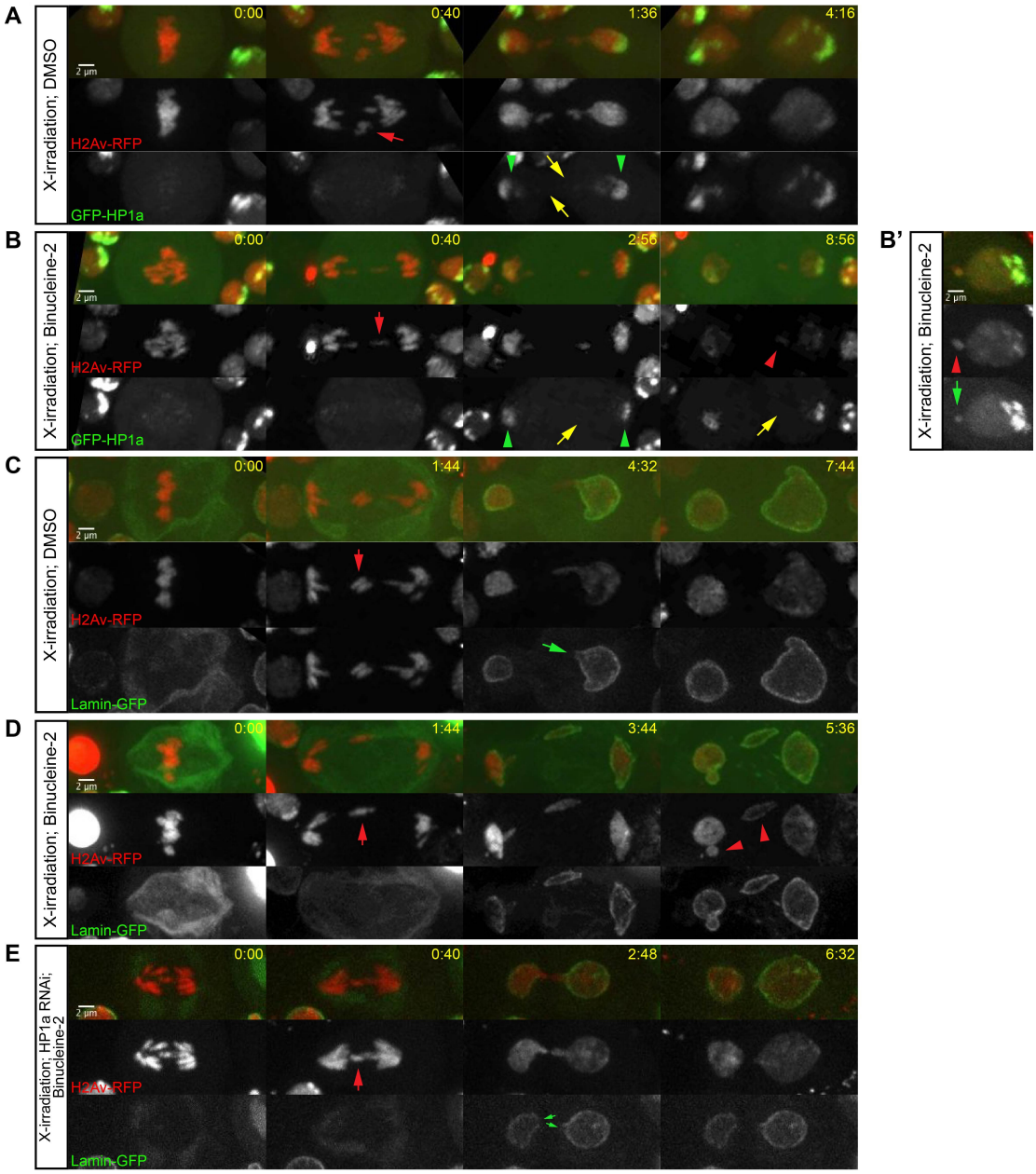
A
X-irradiation; DMSO
0:00
0:40
1:36
4:16
2 µm
H2Av-RFP
GFP-HP1a
B
X-irradiation; Binucleine-2
0:00
0:40
2:56
8:56
2 µm
H2Av-RFP
GFP-HP1a
B'
X-irradiation; Binucleine-2
2 µm
C
X-irradiation; DMSO
0:00
1:44
4:32
7:44
2 µm
H2Av-RFP
Lamin-GFP
D
X-irradiation; Binucleine-2
0:00
1:44
3:44
5:36
2 µm
H2Av-RFP
Lamin-GFP
E
X-irradiation; HP1a RNAi; Binucleine-2
0:00
0:40
2:48
6:32
2 µm
H2Av-RFP
Lamin-GFP

HP1a specifies preference for nuclear envelope reassembly initiation on the leading edge of segregating chromosomes of the self-renewing neuroblast daughter nucleus

Given that the association of HP1a on acentrics influences local nuclear envelope reassembly at the site of nuclear envelope channels, we hypothesized that HP1a might also play a direct role in global nuclear envelope reassembly in wild-type *Drosophila* neuroblast divisions. Support for this idea comes from studies demonstrating a requirement for HP1α/HP1a to tether heterochromatin to the nuclear envelope following mitosis (Poleshko *et al.* 2013) and in which the expression of a truncated form of HP1 disrupts artificial nuclear envelope assembly in mammalian cells (Kourmouli *et al.* 2000), leading to speculation that HP1a may promote nuclear envelope reassembly *in vivo* (Schooley *et al.* 2012).

To test this hypothesis, we performed live analyses of neuroblast divisions from female larvae and found GFP-HP1a was always recruited to segregating chromosomes before initiation of nuclear envelope reassembly in the daughter neuroblast (Figure 18A-A'). This is consistent with previous reports of HP1α/HP1a behavior in mitosis (Sugimoto *et al.* 2001; Poleshko *et al.* 2013). On average, we observed that GFP-HP1a was recruited to segregating chromosomes 150 (SD = 50 sec; N=16) after anaphase onset and 210 (SD = 100 sec; N=15) before nuclear envelope reassembly (Figure 18B). Furthermore, we observed that GFP-HP1a was recruited to the leading edge of segregating chromosomes (Figure 18C). In *Drosophila* neuroblast divisions, which give rise to a self-renewing neuroblast daughter and a ganglion mother cell daughter (GMC), nuclear envelope reassembly

initiates on the pole-proximal side of chromosomes segregating to the neuroblast daughter (Katsani *et al.* 2008; Karg *et al.* 2015). Therefore, HP1a is located at the proper place and time to mediate nuclear envelope reassembly in neuroblast daughters.

Figure 18. HP1a is recruited to the leading edge of segregating chromosomes prior to nuclear envelope reassembly. (A) Stills from a time-lapse movie of a wild-type neuroblast expressing H2Av-RFP (red) and GFP-HP1a (green). Also shown is DIC (grey). GFP-HP1a recruited to segregating chromatin is indicated by green arrows. Nuclear envelope reformation is indicated by a yellow arrow. (A') Graph of the time (sec) from anaphase onset to HP1a recruitment (left circles), anaphase onset to nuclear envelope reassembly (middle circles), and HP1a recruitment to nuclear envelope reassembly (right circles (B) Graphical representation of the average timeline from anaphase to HP1a recruitment to nuclear envelope reassembly. (C) Still image of a wild-type neuroblast expressing H2Av-RFP (red) and GFP-HP1a (green) (left panel) and a graph of the pixel intensity of both H2Av-RFP (red) and GFP-HP1a (green) of the yellow dashed line. Peaks of GFP-HP1a intensity are on the outside shoulders of the peaks of H2Av-RFP intensity, showing GFP-HP1a is recruited to the leading edge of segregating chromosomes. Time is written as min:sec after anaphase onset. Scale bars are 2 µm.

Figure 18

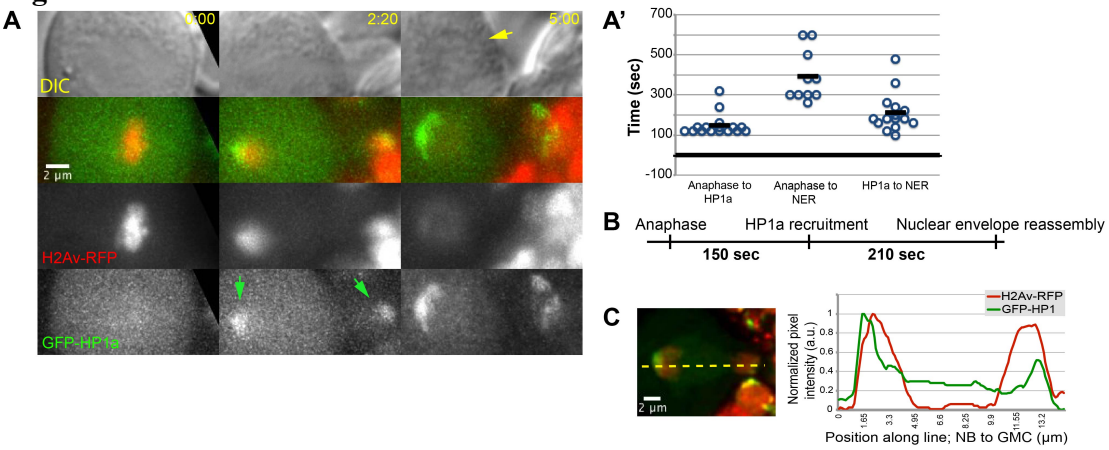

To test the role of HP1a in global nuclear envelope reassembly, we performed live imaging of mitotic neuroblasts from female larvae expressing H2Av-RFP and Lamin-GFP and monitored nuclear envelope reassembly of neuroblast daughters in wild-type conditions or conditions in which HP1a was strongly depleted through RNAi (Figure 19). As previously reported, in wild-type divisions, we observed a dramatic asymmetry in nuclear envelope reassembly initiation on the self-renewing neuroblast daughter cell (Katsani *et al.* 2008). Nuclear envelope reassembly first initiated on the pole-proximal edge of chromosomes segregating to the neuroblast daughter (Figure 19A, green arrows, see Movie 12) before completion on the midzone-proximal face of the segregated chromosomes. As this asymmetry was not as distinct in the differentiating GMC, we focused our studies on the self-renewing neuroblast daughter.

In wild-type neuroblast daughters, we observed nuclear envelope reassembly initiate on the pole-proximal edge of chromosomes 70% of the time, on the midzone-proximal edge of chromosomes 0% of the time, and around all sides of the chromosomes at once 30% of the time (N=37) (Figure 19C). In contrast, in HP1a-depleted neuroblast daughters (Figure 19B, see Movie 13), we observed nuclear envelope reassembly initiate on the pole-proximal edge of chromosomes only 47.5% of the time (statistical significance determined by a chi-square test $p = 0.04$), on the midzone-proximal edge of chromosomes 7.5% of the time, and around all sides of the chromosome at once (Figure 19B, green arrows) 45% of the time (N=40) (Figure 19C).

In spite of this difference in nuclear envelope reassembly initiation preference, we observed no change in the timing of nuclear envelope reassembly initiation (Figure 19D) (no statistical significance determined by an independent two-sided t-test $p = 0.312$) or the amount of nuclear envelope deformities (Figure 19E) (no statistical significance determined by a chi-square test $p = 0.45$) upon HP1a depletion. Taken together, these results suggest that HP1a specifies the pole-proximal location of nuclear envelope reassembly initiation in self-renewing neuroblast daughter cells.

Figure 19. Preferential initiation of nuclear envelope reassembly at the poleward face of segregating chromosomes requires HP1a**.** (A) Stills from a time-lapse movie of a mitotic neuroblast expressing H2Av-RFP (red) and Lamin-GFP (green) (see Movie 12). Nuclear envelope reassembly initiation is indicated by the green arrows. (B) Stills from a time-lapse movie of a mitotic neuroblast expressing H2Av-RFP (red), Lamin-GFP (green), and RNAi against HP1a (see Movie 13). (C) Graph of location frequency for nuclear envelope reassembly initiation in wild-type (left) and HP1a RNAi (right) daughter neuroblasts. Asterisk indicates statistical significance by a chi-square test($p = 0.04$). (D) Graph of the time interval between anaphase onset and initiation of nuclear envelope reassembly in wild-type and HP1a-depleted neuroblast divisions. Each circle represents one division. (E) Graph of the percentage of divisions resulting in nuclear envelope deformities in wild-type and HP1a-depleted divisions. Time is written as min:sec after anaphase onset. Scale bars are 2 µm.

Figure 19

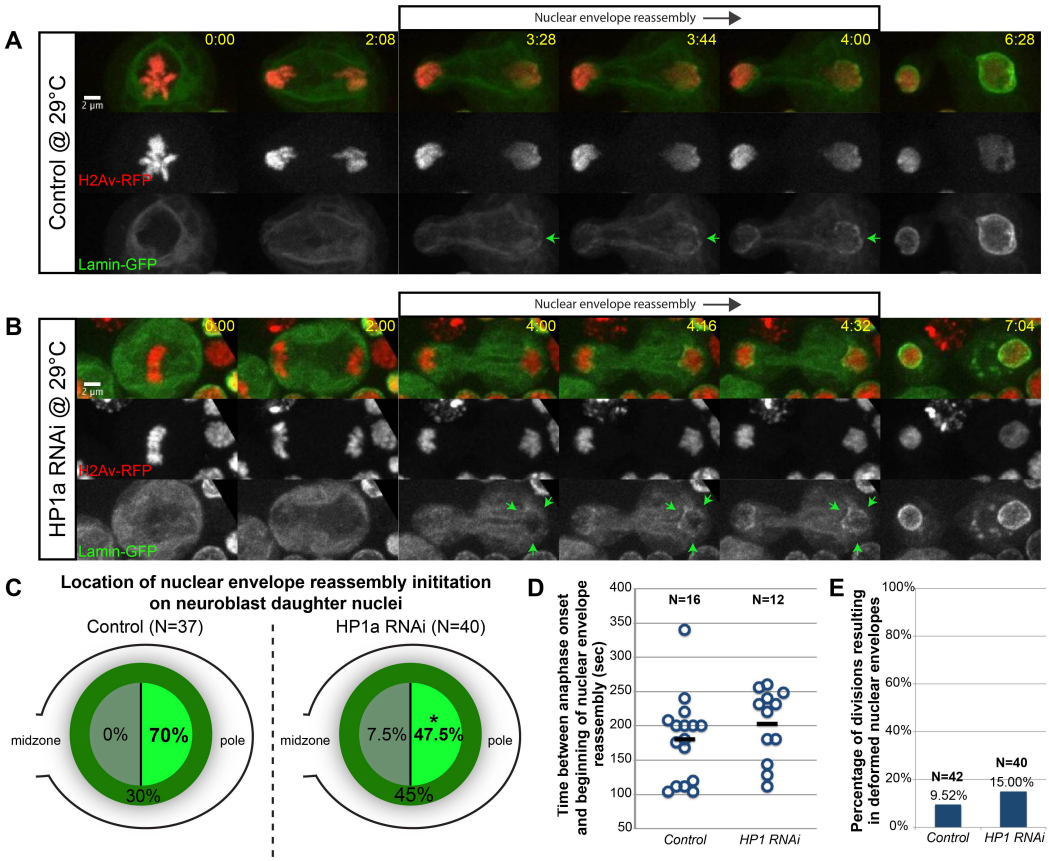

Discussion

Despite the inability of acentric chromosomes to form kinetochore-microtubule attachments, studies show that while some acentrics fail to segregate properly (Fenech *et al.* 2011), others are capable of efficient poleward segregation (Bajer, 1957; Malkova *et al.* 1996; Ahmad and Golic 1998; Galgoczy and Toczyski 2001; Titen and Golic 2008; Royou *et al.* 2010; Bretscher and Fox 2016; Karg *et al.* 2017). Failure of acentrics to reincorporate into daughter telophase nuclei leads to the formation of micronuclei, which result in aneuploidy or DNA damage and are a hallmark of cancer (Santos *et al.* 2010; Bonassi *et al.* 2011; Crasta *et al.* 2012; Zhang *et al.* 2015; Vázquez-Diez *et al.* 2016; Ly *et al.* 2017). In *Drosophila*, I-CreI-induced acentrics avoid this fate by passing through Aurora B-mediated channels in the nuclear envelope (Karg *et al.* 2015).

Here, we observed that late-segregating acentrics in anaphase and telophase neuroblast divisions are marked with strong phospho-H3(S10) signal despite the removal of the majority of this mark from the main nuclei (Figure 11). Consistent with previous reports (Fuller *et al.* 2008), the strength of this signal is dependent upon Aurora B (Figure 12). Intriguingly, in addition to the high phospho-H3(S10) signal on the acentrics, we observed high levels of phospho-H3(S10) on areas of the main nuclei at sites where tethers normally contact the main nuclei. During late anaphase when the normal chromosomes begin to reassemble a nuclear envelope, acentrics and the sites of acentric entry into daughter nuclei remain nuclear envelope-free (Karg *et al.* 2015), suggesting an inverse correlation between nuclear envelope reassembly and

phospho-H3(S10) modification. This finding is consistent with studies suggesting that, in addition to the phosphorylation state of nuclear envelope components (Steen *et al.* 2000; Onischenko *et al.* 2005), nuclear envelope reassembly is also regulated by various chromatin remodeling events, including the removal of phospho-H3(S10) (Vagnarelli *et al.* 2011; Schooley *et al.* 2015).

Our studies also demonstrate that HP1a is excluded from late-segregating I-CreI-induced acentrics despite HP1a recruitment to the main nuclei (Figure 13). We note the chromatin makeup of I-CreI-induced acentrics should be sufficient to recruit HP1a, as I-CreI creates double-stranded breaks in the pericentric region of the X chromosome, resulting in an acentric fragment which contains a large portion of heterochromatin (Rong *et al.* 2002; Maggert and Golic, 2005). Presumably, the difference in recruitment of HP1a to acentrics and the main nuclei is due to the difference in the phosphorylation state of H3(S10) on acentrics and the main nuclei, as Aurora B-mediated phospho-H3(S10) is prohibitive to HP1α/HP1a binding (Hirota *et al.* 2005; Fischle *et al.* 2005). In support of this view, inhibition of Aurora B kinase activity resulted in increased HP1a association with acentrics (Figure 13). However, no increase in HP1a at tether contact sites on the main nuclei was detected upon Aurora B inhibition, possibly due to a limited ability to consistently observe tethers at our imaging resolution.

Furthermore, we found that acentrics possessing high levels of HP1a are largely unable to reintegrate into daughter nuclei and instead form micronuclei (Figure 13). Under the same Aurora B inhibition conditions in which we detected

HP1a association with acentrics and micronucleation, we observed increased nuclear envelope reassembly around acentrics and decreased nuclear envelope channel formation on the main nuclei (Figures 13, 16). We hypothesized that HP1a presence on I-CreI-induced acentrics was prohibitive to acentric entry into daughter nuclei, possibly due to the inability to form a nuclear envelope channel. This hypothesis predicts that 1) in wild-type conditions, Aurora B activity would inhibit formation of an H3-HP1a complex on the acentric and tether and lead to slow nuclear envelope assembly at these sites and the formation of a channel; 2) when Aurora B is inhibited, H3 on the acentric and tether would bind to HP1a which would stimulate nuclear envelope assembly at these sites and prevent channel formation; and 3) when Aurora B is inhibited and HP1a is depleted, no H3-HP1a complex would form on the acentric and tether, leading to slow nuclear envelope assembly at these sites and the formation of a channel, reminiscent of wild-type conditions (Figure 14). Our data show upon co-depletion of HP1a with Aurora B inhibition, nuclear envelope reassembly on acentrics is reduced and channel formation occurs at frequencies similar to those detected in wild-type Aurora B and HP1a conditions (Figure 16). Essentially, depletion of HP1a masks the phenotype of Aurora B inhibition, evocative of a classic epistatic relationship in which Aurora B mediates nuclear envelope channel formation through preferentially excluding HP1a from acentrics and their tethers.

Therefore, we propose a model for nuclear envelope channel formation in which highly localized concentrations of Aurora B kinase phosphorylate H3(S10) specifically on acentrics, their associated tethers, and at sites where the tethers contact

the main nuclei. This prevents local heterochromatic recruitment of HP1a and subsequent recruitment of nuclear envelope lamina on the acentrics and at the sites where acentrics rejoin daughter nuclei, leading to the formation of channels through which acentrics pass to maintain genome integrity (Figure 20).

Figure 20. Model for Aurora B-mediated nuclear envelope channel formation**.** (A) During metaphase, Aurora B (blue) phosphorylates H3(S10) (yellow) on chromosomes (red), acentrics are pushed to the edge of the metaphase plate, and the nuclear envelope (lime green) is partially disassembled. (B) During anaphase, Aurora B, a component of the chromosome passenger complex, is removed from the main chromosomes and relocalizes to the spindle midzone. Phospho-H3(S10) marks on the main nuclei are removed, and HP1 (dark green) is recruited to the main nuclei. However, persistent Aurora B on the acentric and tether continues to phosphorylate H3(S10) and inhibits HP1a recruitment to the acentric/tether. (C) During telophase, nuclear envelope components reform connections with chromatin through HP1a and nuclear envelope reassembly proceeds. However, the exclusion of HP1a from Aurora B-coated tether/acentrics prevents accumulation of nuclear envelope components on the tether/acentrics and at the site where the tether contacts the main nucleus, leading to local delays in nuclear envelope reassembly and the formation of nuclear envelope channels. (D) Successful incorporation of late-segregating acentrics into telophase nuclei through nuclear envelope channels results in euploid daughter cells.

Figure 20

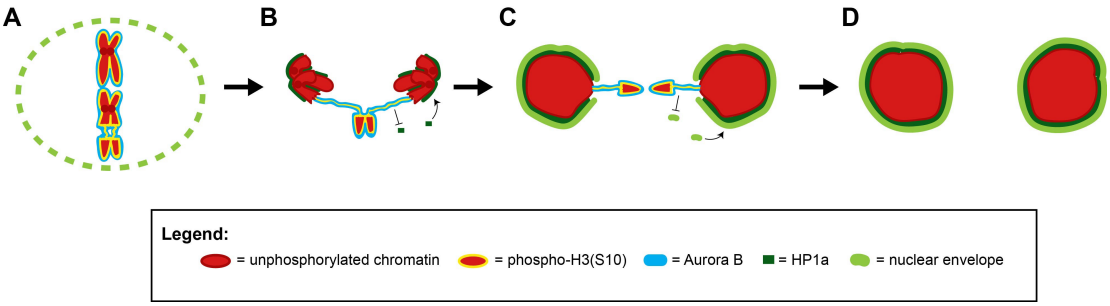

Interestingly, channel formation mediated by HP1a exclusion is similar to the mechanism of human polyomavirus egress from its host nucleus. Viral angoprotein binds to HP1α/HP1a and disrupts its binding with the inner nuclear membrane protein LBR, causing sections of weakened nuclear envelope through which virions leave the nucleus (Okada *et al.* 2005). Thus regulation of chromatin-HP1a-nuclear envelope interactions may represent a conserved method for bypassing the barrier of the nuclear envelope.

By generating acentrics through X-irradiation, we found that the general pattern of HP1a recruitment driving nuclear envelope reassembly on acentrics was not dependent upon the system used to generate acentrics or due to the exact physical nature of an I-CreI-induced acentric (Figure 17). However, we note that while micronuclei derived from I-CreI-induced acentrics were generally HP1a-coated, a higher proportion of micronuclei derived from irradiation-induced acentrics were HP1a-free. It is tempting to speculate that these HP1a-free micronuclei were derived from largely euchromatic acentrics that simply lack a sufficient amount of heterochromatin to recruit HP1a. This observation suggests that Aurora B may mediate acentric entry into daughter nuclei through multiple pathways of which preferential exclusion of HP1a is one. It is possible these HP1a-free acentrics remain capable of recruiting a nuclear envelope through an HP1a-independent pathway, perhaps involving an interaction between LEM domain-containing inner nuclear membrane proteins and the DNA-crosslinking factor barrier-to-autointegration factor (Haraguchi *et al.* 2001; Samwer *et al.* 2017).

To support our finding that HP1a promotes nuclear envelope assembly *in vivo*, we examined its role in assembling the nuclear envelope on normal intact chromatin. We observed HP1a localize to the leading edge of segregating chromosomes before nuclear envelope reassembly (Figure 18). As previously reported, we observed nuclear envelope reassembly initiate on the leading edge of chromosomes segregating to daughter neuroblasts, proceeding to wrap around and complete reassembly on the midzone-proximal face of the nascent nucleus (Robbins and Gonatas 1964; Katsani *et al.* 2008; Karg *et al.* 2015). However, reducing HP1a levels disrupts the preferential nuclear envelope assembly on the pole-proximal face of the segregating chromosomes (Control = 70% pole-proximal initiation; HP1a depletion = 47.5% pole-proximal initiation) (Figure 19). This result is complementary to a growing body of evidence demonstrating HP1 proteins may play key roles in nuclear envelope reassembly. For example, in mammalian cells, HP1α/HP1a recruits PRR14 to segregating chromosomes where it tethers heterochromatin to the nuclear envelope (Poleshko *et al.* 2013), and *in vitro* experimentation shows HP1β/HP1b to be important for recruiting nuclear envelope components to interphase-like chromatin (Kourmouli *et al.* 2000). In addition, depletion of the PP1γ subunit Repo-Man leads to retained phospho-H3(S10) marks on chromatin, loss of HP1α/HP1a recruitment to mitotic chromosomes, and defects in nuclear envelope reassembly (Vagnarelli *et al.* 2011). One mechanism by which HP1a might bias nuclear envelope reassembly to initiate on the leading edge of segregating chromosomes is by enhancing the natural ability of nuclear envelope components to bind to chromatin, possibly through its

interaction with the inner nuclear membrane protein, LBR (Ulbert *et al.* 2006; Ye and Wormann 1996).

Despite the clear preference for initiation of nuclear envelope reassembly on the leading edge of chromosomes segregating to daughter neuroblasts, we observed no such preference on the chromosomes segregating to the daughter GMC (Figure 19). It is possible this difference is due to the relatively small size of the GMC daughter, or that in *Drosophila* neuroblast divisions, the endoplasmic reticulum, from which the nuclear envelope extends during mitotic exit, is asymmetrically localized to the spindle pole of the neuroblast daughter (Smyth *et al.* 2015).

Our data also address a key question regarding nuclear envelope channel formation: how do late-segregating acentrics near the spindle midzone act at a distance to influence nuclear envelope reassembly dynamics on main nuclei near the poles? In our system, we believe there are two pools of Aurora B: a constitutive midzone-based pool (Fuller *et al.* 2008; Afonso *et al.* 2014), and a tether-based pool, which stretches from the acentric to the main nucleus (Royou *et al.* 2010). Given that nuclear envelope channels are only observed on the main nuclei when acentrics and the tether-based pool of Aurora B are present, we proposed that the pool of Aurora B responsible for channel formation is the tether-based Aurora B (Karg *et al.* 2015). Our observation of phospho-H3(S10) "hotspots" on the main nuclei at sites closest to acentrics is consistent with the hypothesis that tether-based Aurora B activity controls channel formation (Figure 13A, yellow arrowheads). Since the midzone pool of Aurora B is confined away from the main telophase nuclei, it is probable that these

hotspots are due to the activity of Aurora B along tethers, which stretch from acentrics and contact main nuclei at sites closest to the acentrics. These phospho-H3(S10) hotspots could then locally prevent HP1a association and nuclear envelope reassembly. Thus, while nuclear envelope reassembly can still proceed around the rest of the nucleus, it is inhibited at the site of these hotspots, resulting in channels.

In summary, our results reveal a novel mechanism by which genome integrity is maintained. Late-segregating acentric fragments pose a significant hazard, as they are at high risk of forming micronuclei that induce dramatic rearrangements in the genome (Fenech *et al.* 2000; Zhang *et al.* 2015; Ly *et al.* 2017)**.** Consequently it is likely that cells have evolved mechanisms to prevent the formation of micronuclei. Here, we provide evidence for one such mechanism in which Aurora B-mediated inhibition of HP1a-chromatin association during anaphase/telophase prevents the formation of micronuclei from late-segregating acentric fragments.

Material and Methods

Fly stocks

All stocks were raised on standard *Drosophila* food (Sullivan *et al.* 2000). Chromosome dynamics were monitored using H2Av-RFP (stock #23651, Bloomington *Drosophila* Stock Center (BDSC), Bloomington, IN). The following Gal4 drivers were used: elav-Gal4 (Lin and Goodman 1994), Wor-Gal4 (Cabernard and Doe 2009), and Actin-Gal4 (#25708, BDSC; (Ito *et al.* 1997)). To monitor nuclear envelope dynamics, we expressed UAS-lamin-GFP (#7376, BDSC) driven by

elav-Gal4. HP1a localization was assessed through use of GFP-HP1a (#30561, BDSC). UAS-ial-shRNA (#28691, BDSC) driven by Wor-Gal4 was used to deplete Aurora B. UAS-Su(Var)205-shRNA (#33400) driven by either Actin-Gal4 or elav-Gal4, depending on the experiment, was used to deplete HP1a.

Fixed neuroblast cytology

Crawling female 3rd instar larvae bearing either hs-I-CreI and Wor-Gal4 or hs-I-CreI, Wor-Gal4, and UAS-ial-shRNA were heat shocked for 1 hour at 37°C. Following 1 hour recovery at room temperature, brains were dissected in 0.7% NaCl then fixed in 3.7% formaldehyde for 30 min. Brains were washed in 45% acetic acid in PBS for 3 min then placed between siliconized coverslips and glass slides in 60% acetic acid in PBS. Brains were squashed by tracing over coverslips with watercolor paper. Slides were frozen in liquid nitrogen for 10 min and then washed in 20% ethanol for 10 min at -20°C. After washing with PBST (10 min) and PBS (2 X 5 min), slides were blocked in a 5% dried milk solution in PBST for 1 hour. Samples were incubated with rabbit anti-histone phospho-H3(S10) antibody (abcam #ab5176) at a 1:500 dilution overnight at 4°C. Samples were subsequently washed in PBST before incubation with goat anti-rabbit-alexa488 (ThermoFisher #A-11008) at a 1:300 dilution for 1 hour at room temperature. Slides were washed in PBST, counterstained with DAPI in vectashield, and imaged the following day. Procedure adapted from (Bonaccorsi *et al.* 2003; Cenci *et al.* 2003).

Quantitative immunofluorescence imaging

Fixed slides were imaged on a Leica DMI6000B wide-field inverted microscope equipped with a Hamamatsu EM CCD camera (ORCA C9100-02) with a binning of 1 and a 100x Plan-Apochromat objective with NA 1.4. For experiments determining the ratio of phospho-H3(S10)/DNA on the acentrics vs. on the main nuclei, phospho-H3(S10)/DNA pixel intensity was determined in ImageJ (National Institutes of Health, Bethesda, MD) by drawing individual region of interests (ROIs) around both main nuclei and the acentrics (as determined from DAPI staining) from sum projections of all z-slices in which the nuclei and acentrics were in focus. Corrected total fluorescence (CTF) was calculated for each ROI (acentrics and nuclei) for both DAPI and phospho-H3(S10) channels by subtracting the product of the ROI area and the mean pixel intensity of an arbitrarily-selected background region from the measured integrated density of the ROI. For each division set, CTFs were averaged for the two main nuclei and for the acentrics when more than one acentric ROI was drawn. Phospho-H3(S10)/DAPI ratios were calculated by dividing the CTF of phospho-H3(S10) by the CTF of DAPI for the averaged acentrics and the averaged nuclei. To determine the fold change for acentrics vs. main nuclei phospho-H3(S10)/DAPI ratios, the phospho-H3(S10)/DAPI ratio of acentrics was divided by that of the main nuclei for each imaged division.

To compare phospho-H3(S10) levels on acentrics in I-CreI vs. I-CreI; Aurora B RNAi neuroblasts, control and Aurora B-depleted brains were imaged at the same

laser settings. Quantification of phospho-H3(S10)/DAPI ratios were calculated as detailed above.

Live neuroblast cytology

For experiments involving acentrics, crawling female 3rd instar larvae bearing hs-I-CreI, elav-Gal4, H2Av-RFP, and a combination of GFP-HP1, UAS-Lamin-GFP, and/or UAS-Su(Var)205-dsRNA were heat shocked for 1 hour at 37°C. Larvae were allowed to recover for at least 1 hour following heat shock. For experiments with no acentrics, female 3rd instar larvae bearing elav-Gal4, H2Av-RFP, and a combination of GFP-HP1, UAS-Lamin-GFP, and/or UAS-Su(Var)205-dsRNA were used. Brains were dissected in PBS and gently squashed between a slide and coverslip (Buffin *et al.* 2005). Neuroblasts along the periphery of the squashed brain provided the best imaging samples. Slides were imaged for up to 1 hour.

Data from time-lapse imaging experiments were acquired with both a Leica DMI6000B wide-field inverted microscope equipped with a Hamamatsu EM CCD camera (ORCA C9100-02) with a binning of 1 and a 100x Plan-Apochromat objective with NA 1.4 and an inverted Nikon Eclipse TE2000-E spinning disk (CSLI-X1) confocal microscope equipped with a Hamamatsu EM-CCD camera (ImageE MX2) with a 100X 1.4 NA oil immersion objective. Successive time points were filmed at 20 sec for the wide-field microscope and 8 sec for the spinning disk microscope. Spinning disk images were acquired with MicroManager 1.4 software.

Small molecule inhibition of Aurora B kinase

For experiments involving the depletion of Aurora B kinase, following dissection, brains were washed in a 25.5μM solution containing Binucleine-2 (Sigma B1186) for 5 min, after which brains were squashed in PBS between a slide and coverslip. For control experiments, dissected brains were washed in 0.15% DMSO (final concentration of DMSO in solution used to dissolve Binucleine-2) for 5 min and then squashed in PBS between a slide and coverslip. Neuroblasts entering anaphase were selected for imaging, and slides were imaged for only one division.

Quantitative GFP-HP1a analysis

Live neuroblasts expressing H2Av-RFP, GFP-HP1a, and I-CreI were imaged with a Nikon Eclipse TE2000-E spinning disk (CSLI-X1) confocal microscope equipped with a Hamamatsu EM-CCD camera (ImageE MX2) with a 100X 1.4 NA oil immersion objective. Neuroblasts treated with DMSO and DMSO + Binucleine-2 were imaged with the same laser settings. GFP-HP1a pixel intensity was calculated by creating sum projections of movies and then measuring the background-subtracted integrated density of GFP signal on the acentric region. Measurements began at the initial point of acentric segregation and continued for 160 sec.

Temperature-regulated expression of RNAi and lethality studies

Flies bearing either Actin-Gal4 or Actin-Gal4 and UAS-Su(Var)205-dsRNA were grown at room temperature (measured as 22^{o}C) until they reached 3rd instar

stage. At this point, larvae were collected into vials and either allowed to continue to grow at room temperature or were shifted to grow at 29^{o}C. Survivability was determined by counting the number of adult flies that eclosed in each vial.

Irradiation studies

Crawling 3rd instar female larvae were placed in an empty plastic vial and irradiated with 605 rads using a Faxitron CP160 X-ray machine. Larvae were allowed to recover for at least 1 hour before brains were dissected and mitotic neuroblasts were imaged as described above.

Statistical analyses

Statistical analyses were determined by chi-square tests (Figure 12C, Figure 13C, E-F; Figure 16E-F, Figure 19C and E) and t-tests (Figure 12C, 19D and Figure 15B) performed in R (R Core Team (2014)). For analyses involving chi-square tests, we assumed a null hypothesis that there should be no difference in values between control and experimental conditions. Therefore, in these cases, the values measured for the control conditions served as the theoretical predictions for what we should observe in the experimental conditions. We then compared the actual values measured in the experimental conditions to these theoretical predictions and determined the significance of difference with a chi-square test.

Figure preparation

Figures were assembled using ImageJ software and Adobe Illustrator (Adobe, San Jose, CA). Graphs were assembled in Microsoft Excel (Microsoft, Redmond, WA). Selected stills from experiments involving live imaging were adjusted for brightness and contrast using ImageJ to improve clarity.

CHAPTER 3: ESCRT-III-mediated membrane fusion drives late-segregating chromosome fragments through nuclear envelope channels

Abstract

Mitotic cells must form a single nucleus during telophase or else exclude part of their genome into damage-prone micronuclei. While much research has detailed how micronuclei arise from cells entering anaphase with lagging broken or misoriented chromosomes, cellular mechanisms that allow late-segregating chromosomes to rejoin daughter nuclei remain relatively unexplored. Here, we find that late-segregating acentric chromosome fragments that rejoin telophase daughter nuclei are associated with nuclear membrane but devoid of lamin and nuclear pore complexes. Using a combination of confocal and lattice light sheet microscopy, we show that acentrics pass through membrane-, lamin-, and nuclear pore-based channels in the nuclear envelope that extend and retract as acentrics enter daughter nuclei. Furthermore, membrane on acentrics fuses to membrane on daughter nuclei. Fusion is mediated by the conserved membrane fusion gene *comatose/NSF* and the ESCRT-III component *shrub/CHMP4B*. We show that fusion between the membrane on acentrics and the membrane on daughter nuclei facilitates reintegration of the acentrics into the daughter nuclei. Taken together, these results suggest a previously unsuspected role for membrane fusion events in the formation of a single nucleus during mitotic exit and the maintenance of genomic integrity.

Introduction

The goal of mitosis is to produce two genetically identical daughter cells. Failure to undergo accurate mitosis results in aneuploidy and the loss of key genetic information. To guarantee accurate production of daughters, cells have evolved mechanisms ensuring proper genome replication and segregation. However, simply segregating sister chromatids equally to each daughter cell is insufficient to maintain euploidy. Instead, the entire segregating chromosome complement must also be gathered into a single daughter nucleus (Zhang et al., 2015; Ly et al., 2017; Samwer et al., 2017). Failure to form a single nucleus results in the formation one or more micronuclei, unstable structures that can undergo chromothripsis, a type of catastrophic DNA damage in which the micronuclear DNA is shattered, rearranged, and then reincorporated into the genome (Stephens et al., 2011; Crasta et al., 2012; Zhang et al., 2015; Ly et al., 2017). Chromothripsis results in aneuploidy (Zhang et al., 2015). Multiple studies link chromothripsis to the development and progression of cancer, and the presence of micronuclei has long been considered a hallmark of cancer cells (Stephens et al., 2011; Santos et al., 2010; Bonassi et al., 2011).

Lagging of whole or fragmented chromosomes during anaphase is perhaps the most common origin of micronuclei (Fenech et al., 2011). Lagging chromosomes can be "locked out" of daughter nuclei if they remain distinct from the main nuclei at the time when the nuclear envelope reassembles around the main chromosome complement. During nuclear envelope reassembly, nuclear membrane is recruited to chromatin, the nuclear lamina is reestablished, and nuclear pore complexes reform.

Different domains of nuclear membrane are then sealed together via the action of conserved membrane fusion proteins such as *N*-ethylmaleimide sensitive factor (NSF) and the endosomal sorting complexes required for transport (ESCRT)-III complex (Baur et al., 2007; Vietri et al., 2015; Olmos et al., 2015). The reassembled nuclear envelope would be expected to act as a physical barrier that prevents lagging chromosome entry into the daughter nucleus and therefore result in the formation of a micronucleus.

While lagging chromosomes certainly pose a significant risk to the genetic integrity of a dividing cell, in actuality, not every lagging chromosome is destined to form a micronucleus. In some instances, lagging chromosomes enter telophase daughter nuclei, preserving euploidy. For example, lagging whole chromosomes can rejoin daughter nuclei in human colorectal cancer cells (Huang et al., 2012) and fission yeast (Pidoux et al., 2000; Sabatinos et al., 2015). In addition, late-segregating acentric fragments sometimes rejoin daughter nuclei in cultured mammalian cells (Liang et al., 1993) and several insect species, including *Chortophaga* (Carlson, 1938) and *Drosophila* (Royou et al., 2010; Bretscher and Fox, 2016).

These examples suggest the presence of mechanisms that alter normal mitotic events to allow the inclusion of late-segregating chromatids into daughter nuclei, maintaining genome integrity. While many studies have documented how a micronucleus could contribute to genomic instability (Terradas et al., 2009; Crasta et al., 2012; Terradas et al., 2012; Hatch et al., 2013; Zhang et al., 2015; Ly et al., 2017;

de Castro et al., 2017; Maass et al., 2018; Liu et al., 2018), the mechanisms that instead facilitate incorporation of lagging chromosomes into daughter nuclei to maintain euploidy remain underexplored. Here, we address this issue by studying the reintegration of late-segregating acentric chromosome fragments in *Drosophila* neuroblast divisions, which rejoin daughter nuclei with high fidelity (Royou et al., 2010).

Acentric behavior in *Drosophila* can be studied with transgenic flies containing a heat-shock inducible I-CreI endonuclease (Rong et al., 2002). I-CreI generates double-stranded DNA breaks in the rDNA repeats at the base of the X chromosome and results in fragments with persistent γH2Av foci that are incapable of recruiting key kinetochore components and are therefore truly acentric (Royou et al., 2010). Despite lacking a centromere, acentrics undergo a delayed but successful poleward segregation, mediated by a protein-coated DNA tether that connects the acentrics to the main chromosome mass (Royou et al., 2010) and microtubules that bundle around the segregating acentric (Karg et al., 2017). Because acentric segregation is severely delayed, by the time acentrics begin their initial segregation poleward, the nuclear envelope has already begun to reform on daughter nuclei (Karg et al., 2015). Surprisingly, the presence of acentrics and their associated tether triggers the formation of highly localized channels in the nuclear envelope through which the acentrics pass to rejoin daughter nuclei (Karg et al., 2015; Warecki and Sullivan, 2018).

Initial poleward segregation of acentrics and nuclear envelope channel formation are clearly important steps in allowing reintegration of late-segregating acentrics into daughter nuclei. However, it is unclear how these two processes are linked to ensure passage of the acentrics through the channels. Here we find that acentric velocity decreases when acentrics first enter nuclear envelope channels, suggesting the presence of an additional mechanism involved in acentric reintegration. We also show that the nuclear envelope channel is highly dynamic, extending outward to reach toward segregating acentrics and retracting back as acentrics enter channels. Finally, we find that acentrics reintegrating into daughter nuclei recruit nuclear envelope membrane despite lacking lamin and nuclear pore complexes (Afonso et al., 2014; Karg et al., 2015). In addition, we find that the conserved membrane fusion protein Comt/NSF and the ESCRT-III component Shrub/CHMP4B are required for efficient entry of acentrics into daughter nuclei. Taken together, these results suggest a novel mechanism for nuclear membrane fusion in maintaining genome integrity in which fusion between membrane on acentrics and membrane on daughter nuclei guides poleward-segregating acentrics through nuclear envelope channels and into daughter nuclei.

Results

Velocity of poleward-segregating acentrics decreases as acentrics pass through nuclear envelope channels

I-CreI-induced acentrics segregate equally to each daughter cell and move poleward through the combined action of protein-coated DNA tethers and bundled microtubules in *Drosophila* neuroblasts (Royou et al., 2010; Karg et al., 2017). Acentrics then pass through channels in the nuclear envelopes of telophase daughter nuclei to rejoin the undamaged chromosomes (Karg et al., 2015). To explore the functional link between initial acentric segregation, nuclear envelope reassembly and acentric reintegration into daughter nuclei, we imaged live *Drosophila* neuronal stem cells (neuroblasts) from third-instar larvae. These larvae bore H2Av-RFP, and Lamin-GFP transgenes and heat-shock inducible I-CreI. This enabled us to observe chromosome and nuclear envelope dynamics and to generate X chromosome acentrics, respectively (Figure 21). We exclusively imaged female *Drosophila* larvae, which produce four acentric X chromosome fragments upon I-CreI induction (Rong et al., 2002).

Errors in initial poleward segregation often manifest in an unequal partitioning of acentrics to each daughter cell (Karg et al., 2017). Therefore, we determined whether divisions in which acentrics were unequally partitioned had an increased rate of micronuclei formation. However, we found no correlation between unequal acentric segregation and micronuclei formation (Figure 21A). Euploid daughter cells that received two acentrics (arrows) were just as likely to reincorporate their acentrics

into daughter nuclei through nuclear envelope channels (arrowhead; 67%; N = 12) as aneuploid daughter cells that received either one or three acentrics (67%; N = 9). This suggests that initial poleward segregation and reintegration into daughter nuclei may be mechanistically uncoupled.

Additionally, we observed that acentrics (arrows) slowed as they passed through nuclear envelope channels (arrowheads) compared to their poleward movement from the metaphase plate (Figure 21B-D). In the division shown in Figure 21B (see Movie 14), the acentric moving toward the bottom nucleus moved at an average of roughly 12 nm/sec as it segregated from the metaphase plate to the beginning of the nuclear envelope channel. As the acentric passed through the channel, its velocity decreased to about 4 nm/sec. To determine if this slowing is a consistent feature of acentric segregation, we measured the velocity changes in our live-imaging of 23 acentrics that reentered daughter nuclei. We deemed the period of acentric segregation from their movement off the metaphase plate to their first contact with nuclear envelope channels as their "initial poleward phase" and the period of acentric movement from when acentrics first contact nuclear envelope channels to when the nuclear envelope has completely surrounded acentrics as their "channel passage phase." We calculated distance by measuring from the furthest tip of the acentric to the nearest point on the daughter nucleus (see Figure 21C). Overall, we found that acentrics moved through the initial poleward phase with an average velocity of about 10 nm/sec (N = 23; SD = 3 nm/sec), while they moved through the channel passage phase with an average velocity of about 7 nm/sec (N = 23; SD = 5

nm/sec) (Figure 21D). This decrease in acentric velocity while passing through channels was statistically different from acentric velocity during initial poleward segregation as determined by a paired t-test ($p = 0.004$). On average, acentrics began to contact channels around 149 sec (N = 23; SD = 40 sec) after they began poleward segregation. Taken together, these results suggest that acentric poleward segregation prior to reaching the nuclear envelope and acentric passage through the nuclear envelope involve distinct forces and perhaps distinct mechanisms.

Figure 21. Velocities of poleward-segregating acentrics decrease as acentrics pass through nuclear envelope channels. (A) Percentage of neuroblast divisions in which acentrics formed micronuclei when segregating equally to each daughter cell (left) and when segregating unequally to each daughter cell (right). Additionally, stills from movies of mitotic neuroblasts expressing I-CreI, H2Av-RFP (magenta), and Lamin-GFP (green) when acentrics (arrows) segregated equally (left) and unequally (right) and entered daughter nuclei through channels in the nuclear envelope (arrowheads). Scale bar is 2 μm. (B) Stills from a movie (see Movie 14) of a mitotic neuroblast expressing I-CreI, H2Av-RFP (magenta) and Lamin-GFP (green). Acentrics (arrows) moved off the metaphase plate and towards daughter nuclei during the "initial poleward phase" (0-270 sec) before entering nuclear envelope channels (arrowheads) and being surrounded by a complete nuclear envelope (270-396 sec) during the "channel passage phase." Time is written in seconds after initial acentric poleward movement. Scale bar is 2 μm. Yellow dashed boxes indicate magnified regions. (C) Diagram illustrating how acentric velocities were measured. The time between when acentrics first move poleward and when they enter nuclear envelope channels is deemed the "initial poleward phase." The time between when acentrics first enter channels and when the nuclear envelope reassembles completely around them is termed the "channel passage phase." Distance was measured between the furthest point on the acentric and the closest point on the daughter nucleus (red brackets). Velocity was calculated as the difference in measured distances at the beginning and ending of each phase divided by the time it took for acentrics to complete each phase. (D) Velocities of acentrics during their initial poleward phase (left) and during their channel passage phase (right). Each dot represents one acentric. Lines connect the measured initial poleward and channel passage velocities of the same acentric. The velocities of 18/23 acentrics decreased from their initial poleward phase to their channel passage phase (blue dots). The velocities of 5/23 acentrics increased from their initial poleward phase to their channel passage phase (red dots). Boxes represent interquartile ranges and lines represent medians of the measured data. Asterisk indicates statistical significance ($p = 0.004$) determined by a paired t-test.

Figure 21

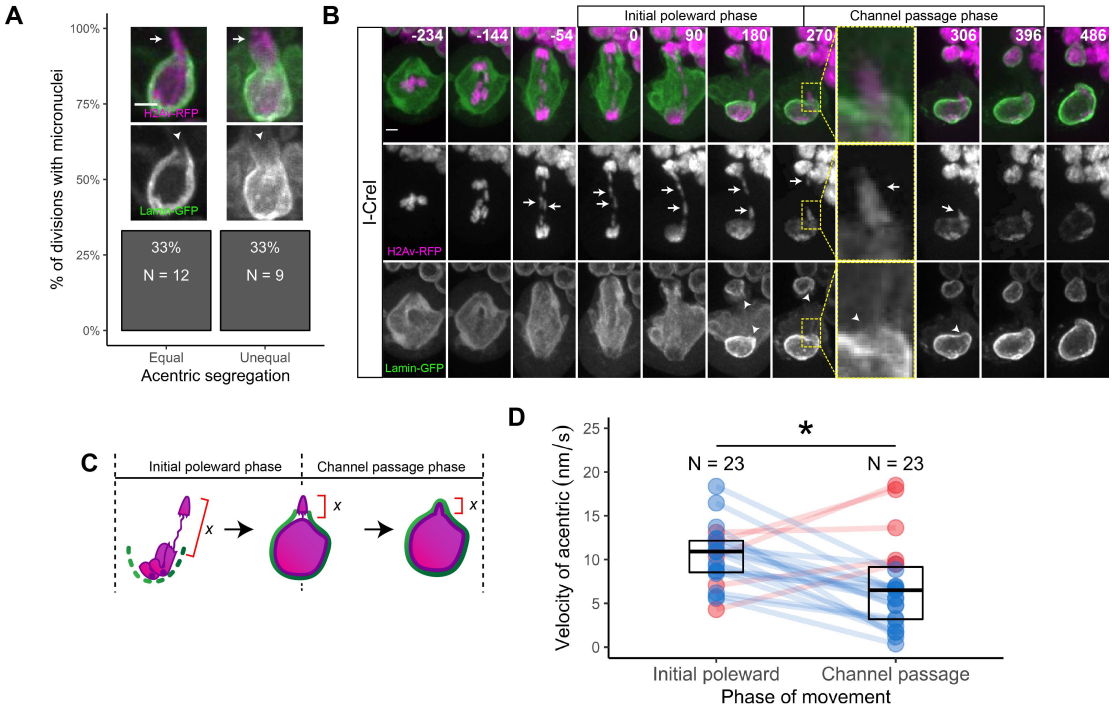
A
100%
75%
50%
25%
0%
% of divisions with micronuclei
H2Av-RFP
Lamin-GFP
33%
N = 12
33%
N = 9
Equal
Unequal
Acentric segregation
B
Initial poleward phase
Channel passage phase
-234
-144
-54
0
90
180
270
306
396
486
I-CreI
H2Av-RFP
Lamin-GFP
C
Initial poleward phase
Channel passage phase
x
x
x
D
*
N = 23
N = 23
Velocity of acentric (nm/s)
25
20
15
10
5
0
Initial poleward
Channel passage
Phase of movement

Nuclear envelope channels extend towards acentrics and retract as acentrics rejoin daughter nuclei

Because velocity decreases as acentrics pass through nuclear envelope channels, we hypothesized that the environment of the channel itself may contribute to the observed change in acentric velocity. We therefore imaged neuroblasts expressing I-CreI, H2Av-RFP, and Lamin-GFP and performed a detailed analysis of the dynamics of channels at the time when acentrics passed through them to reenter daughter nuclei (Figure 22).

Figure 22A (see Movie 15) shows the typical dynamics of nuclear envelope channels as acentrics enter and pass through to rejoin daughter nuclei. As acentrics (arrows) segregated, we observed lamin assembly on the poleward side of daughter nuclei as has been previously reported (Katsani et al., 2008; Warecki and Sullivan, 2018). Nuclear envelope channels (arrowheads) were clearly visible in the lamin as acentrics approached daughter nuclei. We observed lamin extend outwards from channels (brackets) and towards acentrics. Lamin extensions did not completely envelop the acentric but only extended partway along the segregating acentric, leaving the midzone-facing tip of the acentric lamin-free. As the acentrics passed through channels, the lamin extensions retracted toward the daughter nuclei. After this retraction, lamin completed reassembly around the distal tips of the acentrics to ensure the acentrics and daughter nuclei were completely surrounded by an intact nuclear envelope.

We measured the longest length of the lamin extensions during acentric segregation and the length of the retracted extension at the time of completion of lamin reassembly for all divisions imaged (Figure 22B). On average, we found that lamin extended 1.9 μm (N = 18; SD = 0.5 μm) away from daughter nuclei at their longest extension. Upon complete lamin reassembly, extensions were 1.5 μm (N = 18; SD = 0.7 μm) away from daughter nuclei. The retraction of lamin extensions was statically significant as determined by a paired t-test ($p = 0.005$). We hypothesized that the observed variation in the lamin extension length might be due to variation in the distance of each acentric from its daughter nucleus. However, we observed only a weak positive correlation ($r = 0.23$) between the distances of the nearest point on the acentric to the daughter nucleus at the time when channels begin to form and of the longest lamin extension measured (Figure 22C). We observed a mild positive correlation ($r = 0.32$) between the distance the lamin extensions retracted and the distance acentrics travelled during the time of retraction (Figure 22D).
This suggests that the extension and retraction of the lamin may be mechanistically linked to acentric passage through the channel.

Acentric entry through channels is associated with global disruptions in nuclear morphology

We subsequently asked how the lamin extensions from channels affected the overall morphology of daughter nuclei. We performed lattice light-sheet microscopy on neuroblasts expressing I-CreI, H2Av-RFP, and Lamin-GFP (Figure 22E). In this

experiment, we observed neuroblasts that divided without acentrics, neuroblasts that divided with acentrics that entered daughter nuclei through nuclear envelope channels, and neuroblasts that divided with acentrics that formed micronuclei due to a lack of nuclear envelope channels on the daughter nuclei. We focused our attention on the phase when lamin reassembly had just completed encompassing the daughter nucleus. In general, we found that daughter nuclei from divisions with no acentrics were fairly smooth and spherical. In contrast, divisions with acentrics (arrows) that entered daughter nuclei through nuclear envelope channels often exhibited global disruptions in morphology: they were wrinkled and adopted an elongated shape. Surprisingly, we sometimes also observed nuclear envelope protrusions in regions of the daughter nucleus opposite to the acentric entry-point (asterisk). Daughter nuclei from divisions with acentrics that formed micronuclei due to a lack of channels exhibited an intermediate morphology and were somewhat elongated but not as wrinkled as nuclei from divisions with acentrics that had entered through channels.

To quantify these observations, we measured the sphericity of each daughter nucleus (Figure 22F; also see Methods). Perfect spheres have a sphericity of 1. Daughter nuclei from divisions with no acentrics had an average sphericity of 0.823 (SD = 0.010; N = 6). The average sphericity of daughter nuclei from divisions with acentrics that entered nuclei through channels decreased to 0.731 (SD = 0.059; N = 7), a statistically significant decrease ($p = 0.003$) by a Mann-Whitney-Wilcoxon test. Daughter nuclei from divisions with acentrics that formed micronuclei due to the absence of channels had an average sphericity of 0.804 (SD = 0.039; N = 3) with a

range of values corresponding to both outcomes. Taken together, these data suggest that lamin reassembly around daughter nuclei is globally altered when nuclear envelope channels form in response to the presence of acentrics.

Figure 22. Lamin extends from nuclear envelope channels and retracts as acentrics rejoin daughter nuclei. (A) Stills from a movie (see Movie 15) of a mitotic neuroblast expressing I-CreI, H2Av-RFP (magenta) and Lamin-GFP (green). As acentrics (arrows) approached nuclear envelope channels (arrowheads), lamin extended outward from the channels towards the acentric (brackets). As the acentrics passed through channels to rejoin nuclei, these lamin extensions retracted back. Time is written in seconds after initial acentric poleward movement. Scale bars is 2 μm. Yellow dashed boxes indicate magnified regions. (B) Lengths of lamin extensions at their longest point during acentric segregation (left) and at the time the nuclear envelope has completed reassembly (right). Each dot represents the length of a lamin extension from one nucleus. Lines connect the extension lengths at their longest value and at completed nuclear envelope reassembly for the same nucleus. The lengths of 16/18 lamin extensions decreased from their longest value during acentric segregation to complete nuclear envelope reassembly (blue dots). The lengths of 2/18 lamin extensions increased from their longest value during acentric segregation to complete nuclear envelope reassembly (red dots). Boxes represent interquartile ranges and lines represent medians of the measured data. Asterisk indicates statistical significance ($p = 0.005$) determined by a paired t-test. (C) Correlation between the distance of the nearest point on the acentric to the nucleus at the time of channel formation (x-axis) and to the longest length of the lamin extension during acentric segregation (y-axis). Each dot represents one acentric/nucleus pair. Blue dots represent acentric/nucleus pairs whose lamin extensions decreased by the time of complete nuclear envelope reassembly. Red dots represent acentric/nucleus pairs whose lamin extensions increased by the time of complete nuclear envelope reassembly. The black line is the regression line for all data points. (D) Starting at the time of maximum lamin extension, the correlation between the distance an acentric travels (x-axis) and the distance the lamin extension retracts during the same time period (y-axis). Each dot represents one acentric/nucleus pair. Blue dots represent acentric/nucleus pairs whose lamin extensions decreased by the time of complete nuclear envelope reassembly. Red dots represent acentric/nucleus pairs whose lamin extensions increased by the time of complete nuclear envelope reassembly. The black line is the regression line for all data points. (E) Three-dimensional reconstructions from movies of mitotic neuroblasts expressing I-CreI, H2Av-RFP (magenta), and Lamin-GFP (green) imaged on a lattice light-sheet microscope (left panels). Constructed surface models of the nuclear envelope are shown to the right of each image. Images are representative of I-CreI-expressing neuroblasts that had no acentrics (left), had acentrics and nuclear envelope channels (middle), or had acentrics (arrows) and no channels (right). While divisions with no acentrics and divisions with acentrics but no channels formed smooth daughter nuclei, divisions with acentrics and channels had daughter nuclei that were wrinkled and protruded, including at locations far from where the acentric had entered (asterisk). Scale bars are 2 μm. (F) Measurement of the sphericity of the nuclear envelopes of daughter nuclei from neuroblasts expressing I-CreI that had no acentrics (left), acentrics and channels (middle), or acentrics but no channels (right). Divisions with

both acentrics and channels had daughter nuclei with relatively lower sphericities than those from divisions with no acentrics and divisions with acentrics but no channels. Boxes represent interquartile ranges and lines represent medians of the measured data. Asterisk indicates statistical significance ($p = 0.003$) by a Mann-Whitney-Wilcoxon test. The difference between divisions with channels and divisions with micronuclei was not statistically different ($p = 0.07$) as was the difference between divisions without acentics and divisions with micronuclei ($p = 0.5$), determined by Mann-Whitney-Wilcoxon tests.

Figure 22

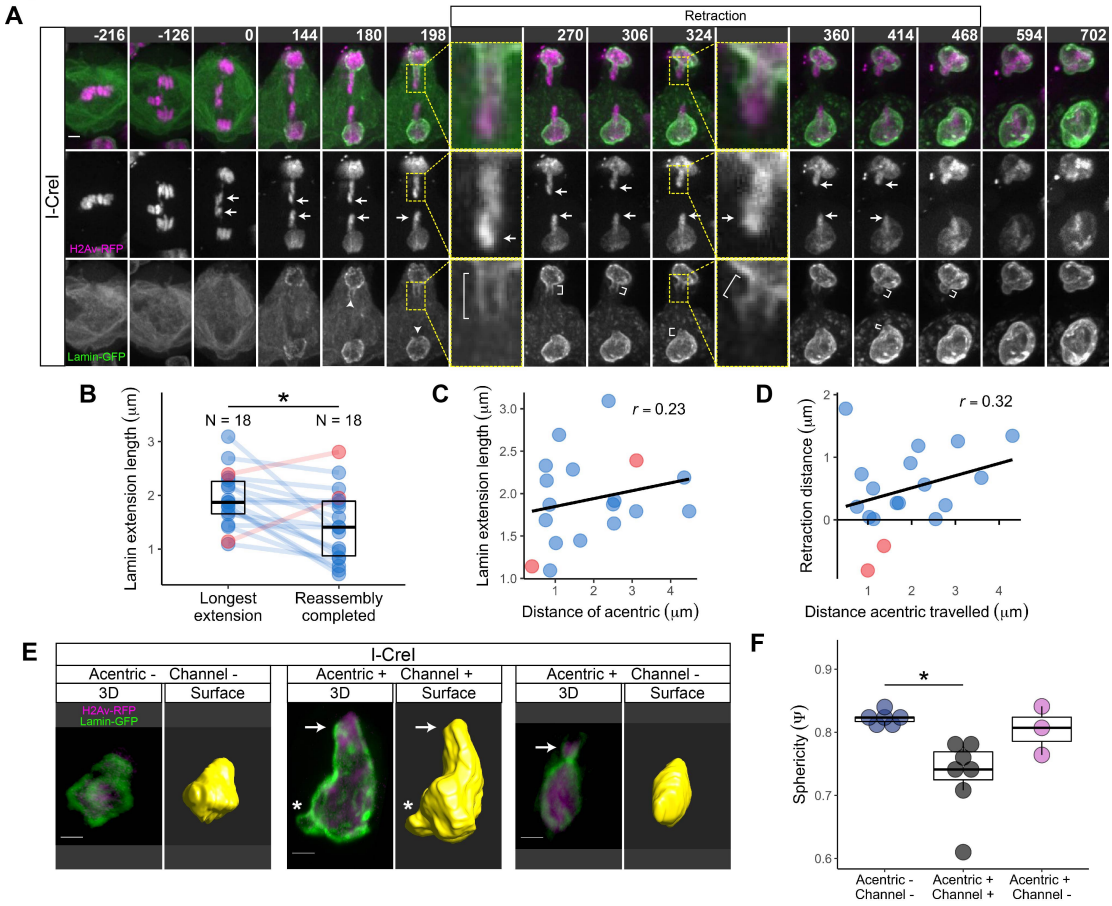
A
Retraction
-216
-126
0
144
180
198
270
306
324
360
414
468
594
702
I-CreI
H2Av-RFP
Lamin-GFP
B
Lamin extension length (μm)
N = 18
N = 18
Longest extension
Reassembly completed
C
Lamin extension length (μm)
r = 0.23
Distance of acentric (μm)
D
Retraction distance (μm)
r = 0.32
Distance acentric travelled (μm)
E
I-CreI
Acentric - Channel -
Acentric + Channel +
Acentric + Channel -
3D
Surface
H2Av-RFP
Lamin-GFP
F
Sphericity (Ψ)
Acentric - Channel -
Acentric + Channel +
Acentric + Channel -

Late-segregating acentrics are associated with nuclear envelope membrane but not lamina or nuclear pore complexes

Due to the observed extension and retraction of lamin as acentrics contact and pass through nuclear envelope channels, we next examined whether the acentrics were associated with certain components of the nuclear envelope and whether the reassembling nuclear envelope mediates acentric reintegration into daughter nuclei. The nuclear envelope consists of the lamina, a double phospholipid bilayer, nuclear pore complexes, and a subset of proteins that are embedded in the inner nuclear membrane (INM) termed INM proteins (for review, see Schooley et al., 2012). At the beginning of mitosis, these structures disassemble and remodel as the nuclear envelope breaks down. We and others have shown that while lamin and nuclear pore complexes can reassemble on telophase daughter nuclei, lagging chromatin remains free of these two components (Afonso et al., 2014; Karg et al., 2015; de Castro et al., 2017; Liu et al., 2018). Interestingly, lagging whole chromosomes that form micronuclei recruit a nuclear membrane despite initially lacking lamin or nuclear pore complexes (Liu et al., 2018; de Castro et al., 2017; Maass et al., 2018). However, it is unknown whether lagging acentrics that rejoin daughter nuclei also recruit a nuclear membrane. To explore the behavior of different components of the nuclear envelope during acentric segregation and reintegration into daughter nuclei, we live-imaged dividing neuroblasts expressing I-CreI, H2Av-RFP, and either Lamin-GFP, GFP-Nup107, or Protein Disulfide Isomerase (PDI)-GFP (Figure 23). PDI is a luminal endoplasmic reticulum (ER) protein. The lumen of the ER is continuous with the

perinuclear space between the outer nuclear membrane and the INM, and so marking luminal ER proteins is a strategy to visualize nuclear membrane dynamics (Bobinnec et al., 2003; Bergman et al., 2015; Yao et al., 2018).

First, we examined lamina reformation during divisions with acentrics. We monitored lamin dynamics by imaging neuroblasts expressing Lamin-GFP, a ubiquitously-expressed lamin orthologous to mammalian Lamin B (Reimer et al., 1995) (Figure 23A, see Movie 16). As we had previously found, segregating acentrics (arrows) remained free of Lamin-GFP when daughter nuclei (arrowheads) accumulated Lamin-GFP (Karg et al., 2015). We quantified this observation for all imaged divisions by measuring the fluorescence intensities of the Lamin-GFP signals around both the main nuclei and the acentrics for 342 sec (20 time points) from when acentrics began segregating poleward (Figure 24). We found that Lamin-GFP signal intensity increased around the main nuclei as nuclear envelope reassembly began, but Lamin-GFP signal intensity around acentrics remained relatively low and constant (Figure 23A').

We next monitored nuclear pore complex reassembly when neuroblasts divided with acentrics. The nuclear pore complex is composed of nucleoporins, among which Nup107 is a component of the core Nup107-160 subcomplex (Walther et al., 2003). We monitored nuclear pore complex dynamics by imaging neuroblasts expressing GFP-Nup107 (Figure 23B, see Movie 17). As we observed before (Karg et al., 2015), segregating acentrics (arrows) were mostly free of GFP-Nup107 while daughter nuclei (arrowheads) accumulated GFP-Nup107. We sometimes detected

GFP-Nup107 localize to acentrics as they neared daughter nuclei, similar to the behavior of lamin extensions we had previously observed. We quantified the fluorescence intensities of the GFP-Nup107 signals on the main nuclei and acentrics for 342 sec for all divisions imaged. As we observed with the nuclear lamina, we found GFP-Nup107 signal intensities increased around the main nuclei when the nuclear envelope began reassembling, while GFP-Nup107 signal intensity around acentrics remained low and constant (Figure 23B').

Finally, we monitored nuclear membrane recruitment in divisions with acentrics using PDI-GFP (Figure 23C, Movie 18). In contrast to Lamin-GFP and GFP-Nup107, which were not recruited to late-segregating acentrics, we observed PDI-GFP signal on daughter nuclei and in varying levels on acentrics (arrows). Late-segregating acentrics first recruited PDI-GFP soon after they moved off the metaphase plate. We quantified the fluorescence intensities of PDI-GFP signals on acentrics and main nuclei for 342 sec from when acentrics began poleward movement for all divisions imaged. Unlike with the signal intensities for Lamin-GFP and GFP-Nup107, PDI-GFP signal intensity around the main nuclei decreased as cells progressed from anaphase to telophase (Figure 23C'). Presumably, the observed decrease in PDI-GFP signal intensity around main nuclei was due to the fluorophore photobleaching, as it has been well-established that nuclear membrane is recruited to reforming nuclei (Chaudhary and Courvalin, 1993; Ellenberg et al., 1997). In contrast to the Lamin-GFP and GFP-Nup107 signal intensities on segregating acentrics, which were lower than those on the main nuclei and remained constant

while signal intensity around the main nuclei increased, we found that PDI-GFP signal intensity around acentrics was higher than that of main nuclei and stayed constant while the signal intensity around the main nuclei decreased (Figure 23C'). Given the observed decrease in PDI-GFP signal intensity on the main nuclei during the time period of nuclear envelope reassembly, we interpret the high, constant PDI-GFP signal intensity on acentrics as indicative of PDI-GFP recruitment to acentrics.

Despite the high levels of PDI-GFP on late-segregating acentrics, we observed acentrics reenter daughter nuclei through highly localized gaps in all three major components of the nuclear envelope surrounding daughter nuclei, including in the PDI-GFP signal (Figure 23D, arrows). While the main nuclei were almost completely coated with a layer of PDI-GFP, the acentrics exhibited highly variable association with PDI-GFP, with some acentrics almost completely surrounded by PDI-GFP while others had only one or two sides coated (compare acentrics in Figures 23C-E). In addition, the PDI-GFP signal associated with acentrics was dynamic and could dissociate and reassociate with acentrics as they moved towards daughter nuclei (Figure 23E). In comparison, the PDI-GFP that localized to main nuclei was relatively static. As acentrics began to pass through the channels formed in the nuclear membrane around main nuclei, we observed the PDI-GFP signal on acentrics (Figure 23E, arrow) and the PDI-GFP signal on main nuclei (arrow) merge (asterisk). Taken together, these results suggest that late-segregating acentrics rejoining daughter nuclei recruit a nuclear membrane that fuses with the membrane on the daughter

nuclei as acentrics pass through channels in the nuclear envelope to rejoin undamaged chromosomes.

Figure 23. Late-segregating acentrics are associated with nuclear envelope membrane but not lamina or nuclear pore complexes. (A-C) Stills from movies of mitotic neuroblasts expressing I-CreI, H2Av-RFP (magenta) and either Lamin-GFP (A, see Movie 16; green), GFP-Nup107 (B, see Movie 17; cyan), or PDI-GFP (C, see Movie 18; yellow). Images are max projections. Daughter nuclei (arrowheads) accumulated Lamin-GFP, GFP-Nup107, and PDI-GFP during late anaphase/early telophase. However, acentrics (arrows) did not associate with Lamin-GFP, often did not associate with GFP-Nup107, but did associate with PDI-GFP (yellow arrows). We sometimes observed GFP-Nup107 localize to acentrics near daughter nuclei (Figure 2B; 144-234 sec). Scale bars are 2 μm. Yellow dashed boxes indicate magnified regions. (A'-C') Fluorescent intensity of Lamin-GFP (A'), GFP-Nup107 (B'), or PDI-GFP (C') measured on the nuclei (black lines) and on the acentrics (purple lines). Lines represent averages. Dark shaded regions represent +/- SE. Light shaded regions represent +/- 2 x SE. Dashed green lines represent the previously measured average time when acentrics begin passing through channels (149 sec post acentric segregation). Lamin-GFP and GFP-Nup107 fluorescence intensity increased over time as the nuclear envelope reformed on daughter nuclei but remained consistently low on acentrics. PDI-GFP fluorescence intensity decreased during the time corresponding to nuclear envelope reassembly on daughter nuclei but was consistently high on acentrics. (D) Stills from movies of mitotic neuroblasts expressing I-CreI, H2Av-RFP, and either Lamin-GFP (left panel), GFP-Nup107 (middle panel), or PDI-GFP (right panel). Each Image is a single z-slice of one daughter nucleus. Channels in the nuclear envelope (arrows) formed in all three major components of the nuclear envelope, allowing acentrics to enter daughter nuclei. Scale bar is 2 μm. (E) Stills from a movie of a mitotic neuroblast expressing I-CreI, H2Av-RFP, and PDI-GFP. As the acentric approached the daughter nucleus, nuclear membrane on the acentric and daughter nucleus (arrows) fused (asterisk). Time is written in seconds after initial acentric poleward movement. Each image is a single Z-slice. Scale bar is 2 μm.

Figure 23

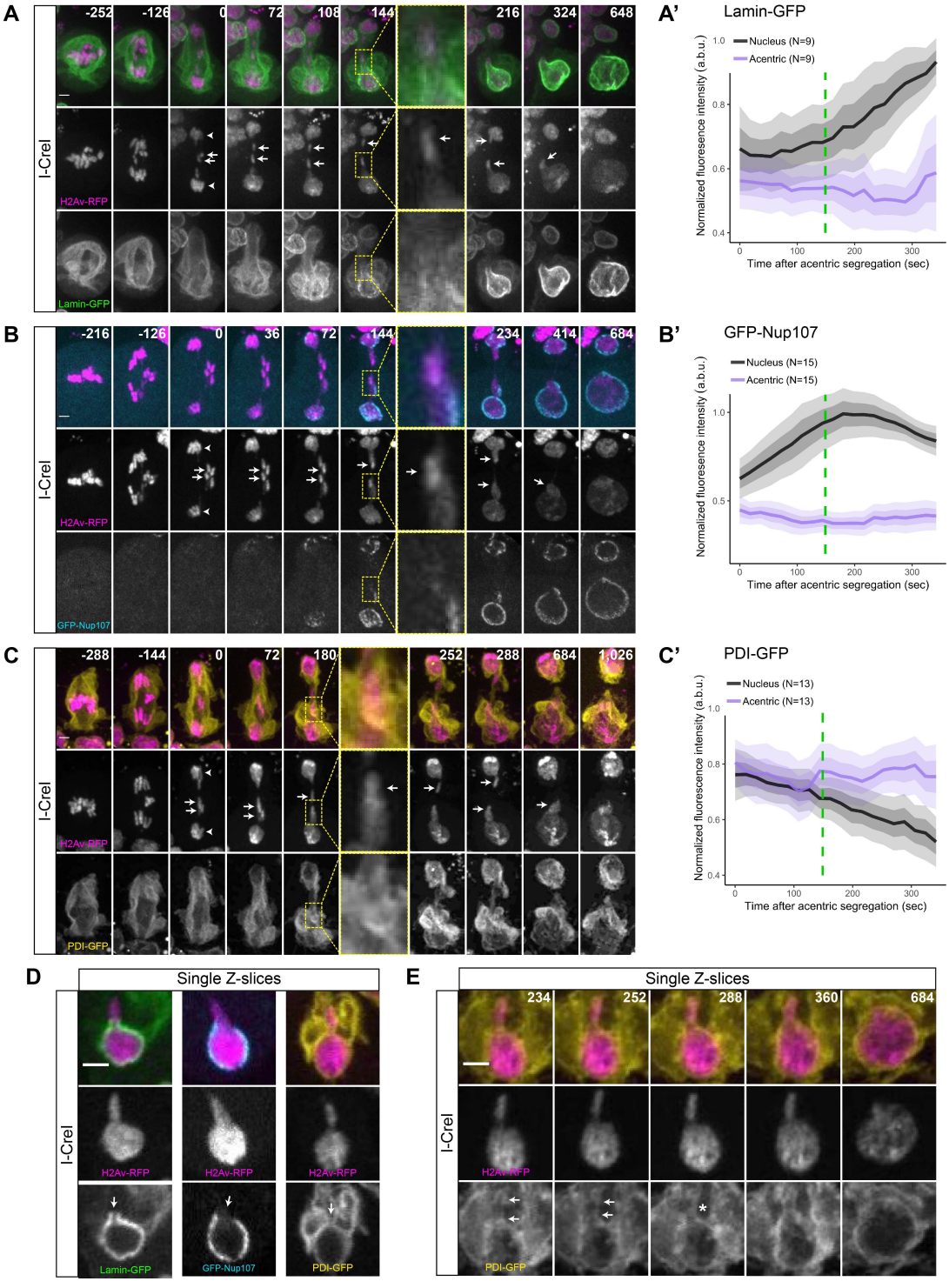
A
-252
-126
0
72
108
144
216
324
648
I-CreI
H2Av-RFP
Lamin-GFP
A'
Lamin-GFP
Nucleus (N=9)
Acentric (N=9)
Normalized fluorescence intensity (a.b.u.)
Time after acentric segregation (sec)
B
-216
-126
0
36
72
144
234
414
684
GFP-Nup107
B'
GFP-Nup107
Nucleus (N=15)
Acentric (N=15)
C
-288
-144
0
72
180
252
288
684
1,026
PDI-GFP
C'
PDI-GFP
Nucleus (N=13)
Acentric (N=13)
D
Single Z-slices
E
Single Z-slices
234
252
288
360
684

Figure 24. Schematic of fluorescence intensity quantification. (A) Diagram illustrating where fluorescence intensity quantifications were measured. A region of interest was drawn around the nucleus (dashed black line) and each acentric (dashed purple lines). The fluorescence intensity of the nuclear envelope marker was then measured. Values were normalized (see Methods). (B) Theoretical graph depicting the normalized fluorescence intensity on nuclei (black line) and acentrics (purple line) over time. The red box represents the hypothetical values measured from (A).

Figure 24

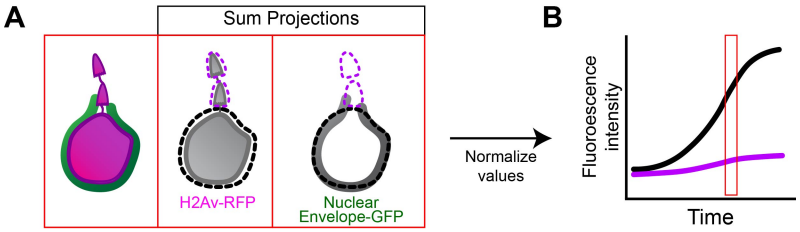

Membrane fusion proteins Comt/NSF and Shrub/CHMP4B are required for efficient acentric reintegration into daughter nuclei

Because of the apparent fusion between nuclear membrane on late-segregating acentrics and nuclear membrane surrounding main nuclei as acentrics pass through nuclear envelope channels, we hypothesized that membrane fusion genes may play an important role in acentric reintegration into daughter nuclei. The time required for fusion events between membrane on acentrics and membrane on nuclei may also explain the marked decrease in the velocity of acentrics as they pass through nuclear envelope channels. During nuclear envelope reassembly in divisions lacking lagging chromatin, the ER restructures to extend membrane that first contacts and then spreads over decondensing chromatin to form the nuclear membrane (Ellenberg at al., 1997). Canonical membrane fusion genes, including NSF and soluble NSF attachment protein receptor (SNARE) proteins, mediate fusion of distinct nuclear membrane sections to form a continuous membrane sheet around daughter nuclei (Baur et al., 2007). Nuclear membrane fusion also requires the ESCRT-III complex (Vietri et al., 2015; Olmos et al., 2015). We hypothesized that membrane fusion events between nuclear membrane on acentrics and nuclear membrane on the main nuclei would require a similar set of proteins.

To determine if membrane fusion is required for efficient acentric reintegration into daughter nuclei, we performed a candidate-based RNA interference (RNAi) screen where we depleted single membrane fusion proteins and used live-imaging to monitor if the rate of acentrics forming micronuclei increased compared to

control divisions. We also included several proteins involved in ER organization and function in our screen. In total, we depleted 12 different proteins. We classified acentrics as forming micronuclei if they visibly failed to rejoin daughter nuclei. We considered hits from this screen to be proteins that when knocked down resulted in a greater than two-fold increase in the measured rate of micronuclei formation for control divisions. The results of this screen are summarized in Table 1. In control divisions, acentrics segregated equally in 89% of divisions (N = 27). We observed acentrics form micronuclei in only about 17% (N = 24) of control divisions. Figure 25A (see Movie 19) shows a typical control division in which the acentrics (arrows) successfully rejoin daughter nuclei. Of note, we observed significant increases in the rate of acentrics forming micronuclei when the levels of Comt/NSF (46%), Rtnl2/RTN2 (53%), or Shrub/CHMP4B (50%) were decreased with RNAi compared to control divisions (Table 1).

Table 1. Summary of results from candidate-based RNAi screen for genes involved in acentric reintegration into daughter nuclei. Micronucleation and equal segregation rates for lines used in the candidate-based RNAi screen for genes involved in acentric entry into daughter nuclei. Stock numbers are based off the Bloomington *Drosophila* Stock Center

Table 1

Genotype	Stock #	Micronuclei	Equal Segregation
y1v1	1509	17% (N = 24)	89% (N = 27)
Rtnl2 RNAi	58208	53% (N = 32)	89% (N = 35)
Shrub RNAi	38305	50% (N = 24)	67% (N = 21)
Comt RNAi	31666	46% (N = 46)	89% (N = 44)
Comt RNAi	31470	43% (N = 40)	73% (N = 40)
***comt6*/+**	26708	62% (N = 13)	64% (N = 11)
Snap24 RNAi	28719	38% (N = 8)	83% (N = 6)
Membrin RNAi	50515	33% (N = 12)	86% (N = 7)
Snap RNAi	29587	33% (N = 18)	56% (N = 18)
Spastin RNAi	53331	33% (N = 24)	70% (N = 20)
Atlastin RNAi	36736	33% (N = 18)	75% (N = 20)
Usnp RNAi	25862	31% (N = 16)	67% (N = 9)
***Rtnl1*/+**	12425	31% (N = 13)	75% (N = 8)
Syb RNAi	38234	27% (N = 20)	80% (N = 20)
Snap 25 RNAi	34377	23% (N = 13)	67% (N = 9)

Figure 25. Comt/NSF, Rtnl2/RTN2, and Shrub/CHMP4B are required for efficient acentric reintegration into daughter nuclei. (A-D) Stills from movies of mitotic neuroblasts expressing I-CreI and H2Av-RFP (gray) only (A, see Movie 19), or expressing I-CreI and H2Av-RFP in combination with RNAi against Comt (B, see Movie 20), Rtnl2 (C, see Movie 21), or Shrub (D, see Movie 22). Each panel is composed of a row of max projections (top row) above their corresponding sum projections that are pseudo-colored to illustrate differences in Z-position (bottom row; red = upper Z-planes, blue = lower Z-planes). Acentrics (arrows) segregated poleward and reentered daughter nuclei in control movies. However, acentrics in dividing neuroblasts expressing RNAi against Comt, Rtnl2, or Shrub initially segregated but failed to reintegrate into daughter nuclei and instead formed micronuclei (arrowheads). Time is written in seconds after initial acentric poleward movement. Scale bars are 2 μm. Yellow dashed boxes indicate magnified regions. Asterisks indicate statistical significance to control as determined by chi-square tests (B: $p = 0.016$; C: $p = 0.005$; D: $p = 0.014$). (A'-D') Distance of acentrics from main nuclei in control (A'-D'; black line), Comt-depleted (B'; purple line), Rtnl2-depleted (C'; purple line), and Shrub-depleted (D'; purple line) neuroblasts. Lines represent averages. Dark shaded regions represent +/- SE. Light shaded regions represent +/- 2 x SE. Dashed green lines represent the previously measured average time when acentrics begin passing through channels (149 sec post acentric segregation). Although initially following a similar trajectory as acentrics in control neuroblasts, acentrics in both Comt- and Rtnl2-depleted neuroblasts ultimately remained further apart from daughter nuclei at 400 sec after initial acentric segregation than those in control divisions. The point of divergence was approximately the measured time when acentrics begin passing through channels. In contrast, the trajectory of acentrics in Shrub-depleted neuroblasts, which likewise remained further apart from daughter nuclei at 400 sec after initial acentric segregation than those in control divisions, diverged from acentrics in control neuroblasts soon after initial acentric segregation.

Figure 25

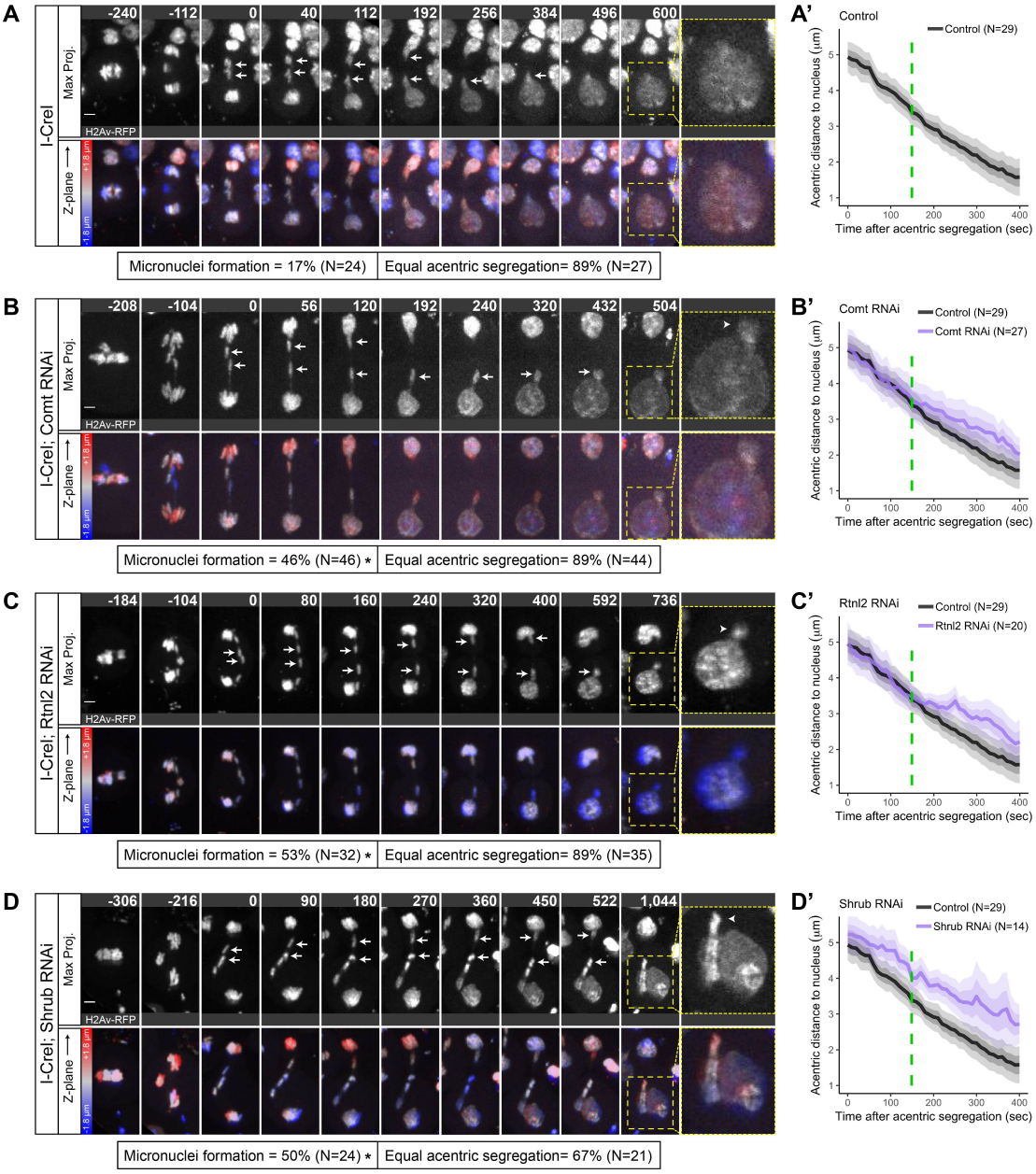
A
I-CreI
Max Proj.
Z-plane
H2Av-RFP
-240
-112
0
40
112
192
256
384
496
600
Micronuclei formation = 17% (N=24)
Equal acentric segregation= 89% (N=27)
A'
Control
Control (N=29)
Acentric distance to nucleus (μm)
Time after acentric segregation (sec)
B
I-CreI; Comt RNAi
-208
-104
0
56
120
192
240
320
432
504
Micronuclei formation = 46% (N=46) *
Equal acentric segregation= 89% (N=44)
B'
Comt RNAi
Control (N=29)
Comt RNAi (N=27)
C
I-CreI; Rtnl2 RNAi
-184
-104
0
80
160
240
320
400
592
736
Micronuclei formation = 53% (N=32) *
Equal acentric segregation= 89% (N=35)
C'
Rtnl2 RNAi
Control (N=29)
Rtnl2 RNAi (N=20)
D
I-CreI; Shrub RNAi
-306
-216
0
90
180
270
360
450
522
1,044
Micronuclei formation = 50% (N=24) *
Equal acentric segregation= 67% (N=21)
D'
Shrub RNAi
Control (N=29)
Shrub RNAi (N=14)

Figure 25B (see Movie 20) shows a typical Comt-depleted neuroblast division in which an acentric (arrows) forms a micronucleus (arrowhead). Comt is one of two *Drosophila* homologs of NSF, a protein that disassembles trans-SNARE complexes and allows repeated cycles of membrane fusion (Ordway et al., 1994). In Comt-depleted neuroblasts, sister acentrics were equally segregated in 89% (N = 44) of divisions imaged (compare to control divisions: 89%), indicating that Comt-depletion does not affect the initial poleward segregation of acentrics. However, RNAi-depletion of Comt resulted in a dramatic increase in acentrics failing to reintegrate into daughter nuclei, leading to the formation of micronuclei (micronuclei formed in 46% of divisions; N = 46; compare to control divisions: 17%). We confirmed this result by using a second RNAi line against Comt and again observed a high rate of micronuclei formation (43%; N = 40; control: 17%). Additionally, we used the well-characterized *comt6* temperature-sensitive mutant (Krishnan et al., 1996; Sanyal and Krishnan, 2012) and likewise observed acentrics form micronuclei at a high rate in heat shocked *comt6*/+ heterozygotes (62%, N=13; control: 17%) (Table 1).

Figure 25C (see Movie 21) shows a typical Rtnl2-depleted neuroblast division in which an acentric (arrows) forms a micronucleus (arrowhead). Rtnl2 is likely the *Drosophila* ortholog of human RTN2 (Thurmond et al., 2019), a reticulon family protein involved in the restructuring of the ER (Voeltz et al., 2006; Montenegro et al., 2012). In Rtnl2-depleted neuroblasts, acentrics were also equally segregated 89% (N = 35) of the time (compare to control divisions: 89%), indicating that Rtnl2 is not involved in initial acentric segregation. However, upon RNAi-depletion of Rtnl2,

acentrics failed to enter daughter nuclei and instead formed micronuclei in 53% (N = 32) of divisions filmed (compare to control divisions: 17%).

Figure 25D (see Movie 22) shows a typical Shrub-depleted neuroblast division in which an acentric (arrows) forms a micronucleus (arrowhead). Shrub is the *Drosophila* ortholog of charged multivesicular body protein (CHMP)4B, a major component of the ESCRT-III complex (Sweeney et al., 2006). In Shrub-depleted neuroblasts, we observed decreased equal acentric segregation (67%; N = 21) compared to controls (89%), suggesting that Shrub may be involved in the initial segregation of acentrics. RNAi depletion of Shrub also resulted in acentrics forming micronuclei in 50% (N = 24) of divisions imaged (compare to control divisions: 17%). However, equivalent high rates of micronuclei formation were observed in divisions in which acentrics were partitioned equally (5/12) and in which acentrics were partitioned unequally (4/7). This suggests that the increased rate of micronuclei formation was not due to any defect in initial acentric poleward segregation.

We next determined whether the increased micronucleation observed upon depletion of Comt, Rtnl2, and Shrub were due to differences in the initial distances of acentrics from daughter nuclei or differences in timing of acentric segregation (Figure 26). While acentrics in Shrub-depleted neuroblasts were initially slightly further from daughter nuclei, we found no statistically significant differences in the initial distances of acentrics from daughter nuclei between control neuroblasts and Comt-, Rtnl2-, or Shrub-depleted neuroblasts (Figure 26A). Moreover, for each condition, acentrics that formed micronuclei were not initially further away from daughter

nuclei than acentrics that entered nuclei. We also found no statistically significant differences in the time from anaphase onset to acentric segregation between all the conditions, although acentrics from Rtnl2-depleted divisions segregated slightly later than controls (Figure 26B). In general, we observed no definitive correlation that linked the time between anaphase onset and acentric segregation to the ability of an acentric to enter the nucleus. Table 2 summarizes these data. Taken together, these results indicate that the increased micronucleation we observed upon RNAi depletion of Comt, Rtnl2, and Shrub was not due to defective initial behavior of segregating acentrics.

Figure 26. Micronuclei formation is not correlated to changes in distance of acentrics from nuclei or time of acentric segregation. (A-B) Comparison of the distances of acentrics from daughter nuclei (A) and the times between anaphase onset and acentric segregation (B). Each dot represents one acentric. Blue dots represent acentrics that rejoin daughter nuclei. Red dots represent acentrics that form micronuclei. For each condition, there is no strong correlation between acentrics that form micronuclei and how far acentrics are from main nuclei at the time of acentric segregation. For each condition, there is no strong correlation between acentrics that form micronuclei and how long after anaphase acentrics began to segregate. Boxes represent interquartile ranges and lines represent medians of the measured data.

Figure 26

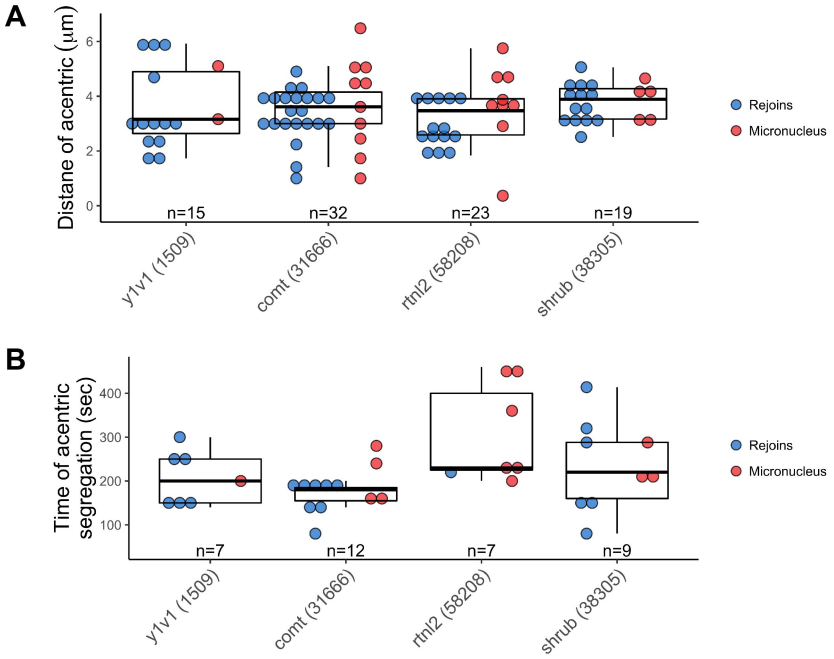

Table 2. Key characteristics of hits from the candidate-based RNAi screen. Micronucleation and equal segregation rates, the average distance of acentrics from daughter nuclei at the time of acentric segregation, and the time from anaphase onset to acentric segregation are shown for each hit from our screen

Table 2

Genotype	Stock #	Micronuclei	Equal segregation	Distance of acentric to nucleus (μm)	Time of acentric segregation (sec)
y1v1	1509	17% (N = 24)	89% (N = 27)	3.6 (SD = 1.5; N = 15)	200 (SD = 60; N = 7)
Comt RNAi	31666	46 % (N = 46)	89% (N = 44)	3.5 (SD = 1.2; N = 32)	180 (SD = 50; N = 12)
Rtnl2 RNAi	58208	53% (N = 32)	89% (N = 35)	3.2 (SD = 1.2; N = 23)	300 (SD = 110; N = 7)
Shrub RNAi	38305	50% (N = 24)	67% (N = 21)	3.8 (SD = 0.7; N = 19)	230 (SD = 103; N = 9)

To more thoroughly understand when acentric reintegration was affected in Comt-, Rtnl2-, and Shrub- depleted neuroblasts, we measured the distance of the lagging end of the acentric to the nearest point on the main nucleus every 10 sec for 400 sec after acentrics began their initial poleward movement for an additional set of control and Comt-, Rtnl2-, and Shrub-depleted divisions (Figure 25A'-D'). We then compared the trajectory of acentrics in Comt-, Rtnl2-, and Shrub-depleted divisions to the trajectory of acentrics in control divisions (Figure 25A'-D'; black line). We reasoned that acentrics failing to enter daughter nuclei should exhibit a measurable increase in distance from main nuclei than those that reenter nuclei (Figure 27). In Comt-depleted divisions, the trajectory of acentrics (Figure 25B'; purple line) initially matched the trajectory of acentrics from control divisions. However, at the time when acentrics in control divisions begin to enter into nuclear envelope channels (previously measured at 149 sec after acentrics begin their poleward movement; dashed green line), acentrics from Comt-depleted neuroblasts began to become measurably further away from daughter nuclei. This pattern was also seen for acentrics from Rtnl2-depleted divisions (Figure 25C'; purple line): acentrics from Rtnl2-depleted neuroblasts closely matched the trajectory of acentrics from control divisions until the point when acentrics from control divisions enter channels (149 sec; dashed green line), at which point acentrics from Rtnl2-depleted neuroblasts began to become measurably further away from daughter nuclei. Interestingly, acentrics from Shrub-depleted neuroblasts (Figure 25D'; purple line) exhibited a distinct trajectory even during the initial segregation stages. However, after the point

when acentrics from control divisions enter channels (149 sec; dashed green line), the trajectory of acentrics from Shrub-depleted neuroblasts became even further away from the trajectory of control acentrics than during the initial segregation period.

Taken together, these results indicate that Comt and Rtnl2, and Shrub are required for efficient acentric entry during the final stage of acentric integration, suggesting that nuclear membrane fusion and ER restructuring events are important mechanisms that ensure late-segregating acentrics pass through nuclear envelope channels.

Figure 27. Schematic detailing the measured distance between acentrics and daughter nuclei as acentrics segregate toward nuclei. (A) Diagram illustrating that acentrics rejoining daughter nuclei will have a decreasing distance between the tail of the acentric and the closest point on the daughter nucleus. As time progresses, and the acentric completely reenters the daughter nucleus, the distance between the tail of the acentric and the daughter nucleus will approach 0. (B) Diagram illustrating that acentrics forming micronuclei will have a decreasing distance between the tail of the acentric and the closest point on the daughter nucleus until the acentric reaches the location where it is incapable of entering the daughter nucleus. As time progresses, the acentric will remain distinct from the main nucleus, and the distance between the tail of the acentric and the daughter nucleus will be measured as greater than 0.

Figure 27

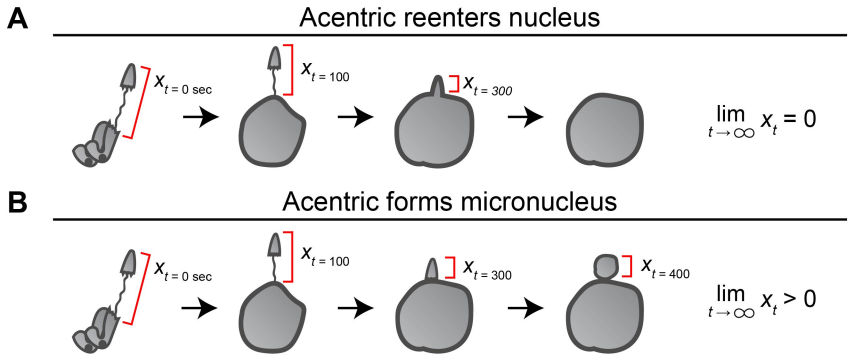

Shrub/CHMP4B localizes to acentrics as they reintegrate into daughter nuclei

To determine the role of Shrub/CHMP4B in acentric reintegration into daughter nuclei, we analyzed the location of Shrub in neuroblasts dividing with acentrics. We reasoned that if Shrub were involved in acentric reintegration, we would observe Shrub localize to acentrics beginning to contact daughter nuclei. Therefore, we performed live imaging on neuroblasts expressing I-CreI, H2Av-RFP, and Shrub-GFP and quantified when Shrub-GFP localized to acentrics and daughter nuclei (Figure 28).

Figure 28A (see Movie 23) shows the typical pattern of Shrub-GFP localization during the division of a neuroblast with acentrics. At the time when the acentrics began their initial poleward movement, Shrub-GFP did not localize to either the acentrics (arrows) or the daughter nuclei (arrowheads). In contrast, at the time when the acentrics began to rejoin daughter nuclei, Shrub-GFP puncta localized both to acentrics (arrowheads) and strongly to daughter nuclei. Shrub-GFP puncta localized along the periphery of daughter nuclei, presumably mediating fusion of nuclear membrane on daughter nuclei as previously described (Vietri et al., 2015; Olmos et al., 2015). Shrub-GFP puncta localized to the main body of the acentric and also specifically at the point where the acentric contacted the daughter nucleus prior to reintegration (Figure 28A, 180 sec; arrowhead).

We quantified the amount of Shrub-GFP puncta localized to acentrics and daughter nuclei for all divisions imaged (Figure 28B). We observed very low Shrub-GFP localization on acentrics (purple line) and on nuclei (black line) in the time

period between 90 sec before and 90 sec after acentrics began their poleward movement. During this time period, only 2/15 acentrics were associated with more than 1 Shrub-GFP punctum at any given time, and 6/15 acentrics were associated with Shrub-GFP puncta at consecutive time points. Similarly, only 4/15 daughter nuclei were associated with more than 1 Shrub-GFP punctum at any given time, and 8/15 daughter nuclei were associated with Shrub-GFP puncta at consecutive time points. The average number of GFP-puncta on acentrics and daughter nuclei at the time when acentrics began moving poleward was 0 (N = 15; SD = 0) and 0.33 (N = 15; SD = 0.47) respectively.

In contrast, we observed increased Shrub-GFP localization to both acentrics and daughter nuclei in the time period between 90 sec before and 90 sec after acentrics first contacted daughter nuclei. During this time period, 11/14 acentrics were associated with more than 1 Shrub-GFP punctum at any given time, and 12/14 acentrics were associated with Shrub-GFP puncta at consecutive time points. Likewise, 14/14 daughter nuclei were associated with more than 1 Shrub-GFP punctum at any given time, and 14/14 daughter nuclei were associated with Shrub-GFP puncta at consecutive time points. The average number of Shrub-GFP puncta on acentrics and daughter nuclei at the time when acentrics contacted daughter nuclei was 0.86 (N = 14; SD= 0.76) and 4.08 (N = 1.75; SD = 1.75) respectively. The average number of Shrub-GFP puncta on acentrics was highest at 72 sec after acentrics contacted daughter nuclei (1.64; N = 14; SD = 1.17). The average number

of Shrub-GFP puncta on daughter nuclei was highest at 54 sec after acentrics contacted daughter nuclei (4.54; N = 14; SD = 2.37).

Taken together, these results indicate that Shrub/CHMP4B localizes to reintegrating acentrics. Therefore, Shrub/CHMP4B is in the correct place at the correct time to mediate the fusion between membrane on acentrics and membrane on daughter nuclei that allows acentric reintegration into daughter nuclei.

Figure 28. Shrub/CHMP4B localizes to acentrics as they reintegrate into daughter nuclei. (A) Stills from a movie (see Movie 23) of a mitotic neuroblast expressing I-CreI, H2Av-RFP (magenta), and Shrub-GFP (green). At the time when acentrics began their initial poleward movement, neither acentrics (arrows) nor daughter nuclei were associated with any Shrub-GFP puncta. When acentrics began to rejoin daughter nuclei, Shrub-GFP puncta localized to both acentrics and daughter nuclei (arrowheads), including to the location where the acentric is contacting the daughter nucleus. Time is written in seconds after initial acentric poleward movement. Scale bar is 2 µm. Yellow dashed boxes indicate magnified regions. (B) Average number of Shrub-GFP puncta that localized to acentrics (purple line) and to nuclei (black line) when acentrics initially segregated poleward (left) and when acentrics rejoined daughter nuclei (right). For 90 sec before and after when acentrics initially segregated poleward, little to no Shrub-GFP puncta localized to acentrics or nuclei. For 90 sec before and after acentrics began to contact and reintegrate into nuclei, Shrub-GFP puncta frequently localized to acentrics and to daughter nuclei. Lines represent averages. Dark shaded regions represent +/- SE. Light shaded regions represent +/- 2 x SE.

Figure 28

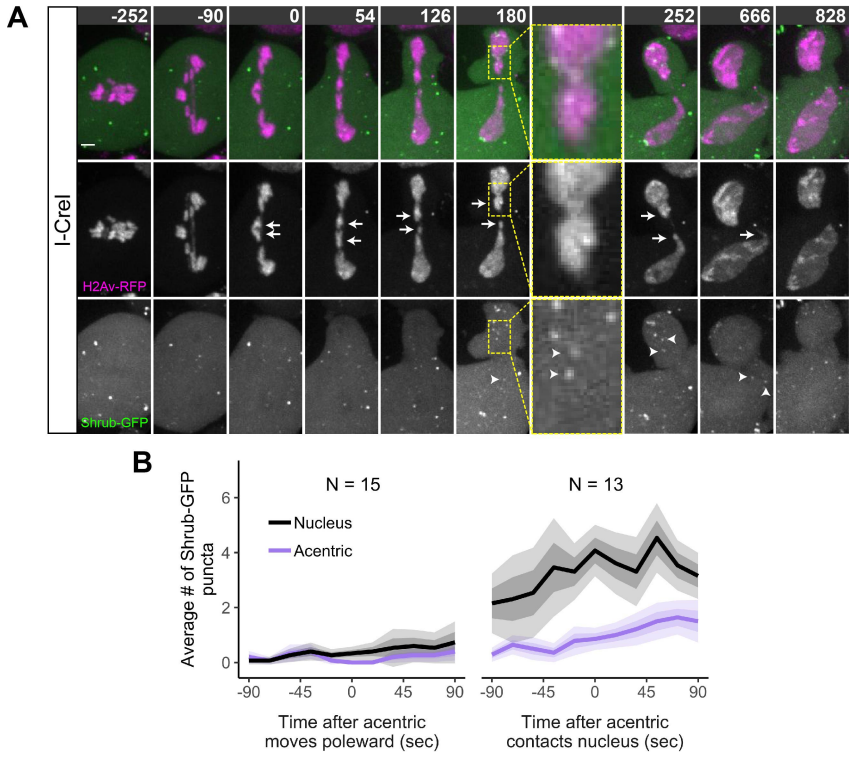

Discussion

Chromosome fragments enter telophase nuclei through channels in all major components of the nuclear envelope

Cells dividing with lagging whole or broken chromosomes risk losing or damaging a significant part of their genome if these wayward chromosomes are not included in daughter nuclei. Chromosomes and chromosome fragments that fail to incorporate into a daughter nucleus form micronuclei, which can undergo chromothripsis (Zhang et al., 2015; Ly et al., 2017). Chromothripsis leads to the development of aneuploidy and is linked to the progression of cancer (Bonassi et al., 2011). While lagging chromosomes are relatively rare in healthy cells due to the evolution of safeguards such as the spindle assembly checkpoint (for review, see Sacristan and Kops, 2015) and the DNA damage response (Mikhailov et al., 2002), they are much more frequent in cancer cells, in which these safeguards are often compromised (Thompson and Compton, 2008). For example, colorectal cancer cells frequently bypass these checkpoints to divide with lagging chromosomes (Stewénius et al., 2005; Green and Kaplan, 2003). Intriguingly, not every lagging chromosome forms a micronucleus: some reincorporate into daughter nuclei to maintain euploidy. In cultured colorectal cancer cells for example, some lagging chromosomes can reintegrate into daughter nuclei up to 38% of the time (Huang et al., 2012). In addition, lagging whole chromosomes can enter daughter nuclei in fission yeast (Pidoux et al., 2000; Sabatinos et al., 2015), and late-segregating acentric fragments are capable of

reintegrating into telophase daughter nuclei in PTK2 (Liang et al., 1993), grasshopper (Carlson, 1938), and *Drosophila* cells (Royou et al., 2010; Bretscher and Fox, 2016).

In spite of the fact that incorporation of late-segregating chromosomes and chromosome fragments into daughter nuclei has been documented in multiple systems, the mechanisms that facilitate entry remain relatively unexplored. Previous work has established that late-segregating acentric fragments remain connected to daughter nuclei through DNA tethers in *Drosophila* neuroblasts (Royou et al., 2010). BubR1 kinase, Polo kinase, Aurora B kinase, and INCENP coat these tethers (Royou et al., 2010). Poleward movement of acentrics is mediated by microtubules (Karg et al., 2017), and acentrics enter daughter telophase nuclei by passing through highly localized channels in the layers of lamin and nuclear pore complexes that assemble around daughter nuclei (Karg et al., 2015). Aurora B kinase, a well-established inhibitor of nuclear envelope formation, activity along the tether is integral to the formation of these channels (Karg et al., 2015; Warecki and Sullivan, 2018).

These studies lead to questions regarding channel formation, structure, and closure. The data presented here demonstrate that channels result from local inhibition of the reassembly of all three major components of the nuclear envelope at the sites of channel formation. Acentrics enter daughter nuclei by passing through clear gaps in the nuclear membrane surrounding daughter nuclei as well as in the lamina and nuclear pore complexes (Figure 23). This indicates that nuclear envelope channels are specialized structures in the nuclear envelope that allow acentric entry into daughter nuclei. Moreover, as discussed below, we conclude that the

reassembling nuclear envelope is not just a passive structure to be bypassed via passage through channels but is actively involved in incorporating acentrics into daughter nuclei as well.

Acentric incorporation involves localized extension and retraction of the nuclear lamina

We found that late-segregating acentric fragments moved off the metaphase plate at a higher velocity than when passing through nuclear envelope channels (Figure 21). Initial acentric movement poleward occurs through the action of microtubules that bundle around the acentrics (Karg et al, 2017). During this initial, microtubule-mediated phase of acentric movement, we measured an average acentric velocity of 10 nm/sec (N = 23; SD = 3 nm/sec), which corresponds to previously reported segregation rates of undamaged chromosomes in *Drosophila* S2 cells (9.8 nm/sec; de Lartigue et al., 2011). The attenuated velocities of acentrics (7 nm/sec; N = 23; SD = 5 nm/sec) indicate different and/or additional forces are imposed on these chromosome fragments as they pass through channels. This finding also suggests distinct mechanisms drive the acentric through the channel.

Insight into the mechanisms driving acentric channel passage comes from our observation that lamin extends outward from nuclear envelope channels and towards the poleward-segregating acentrics (Figure 22). Nuclear envelope-chromatin connections might promote acentric movement. The transmission of force from the cytoskeleton across the nuclear envelope to chromatin via the linker of

nucleoskeleton and cytoskeleton (LINC) complex requires nuclear envelope-chromatin connections (Tajik et al., 2016). LINC-mediated forces lead to chromatin stretching in response to mechanical stress (Tajik et al., 2016) and the characteristic rapid chromosome movements necessary for homolog pairing in meiosis (Ding et al., 2007; Schmitt et al., 2007; Conrad et al., 2008; Sato et al., 2009). In accord with a model in which nuclear envelope-chromatin connections promote acentric movement, we observed the lamin extensions retract back toward nuclei as acentrics passed through channels. It is tempting to speculate that the retraction of lamin extensions is evidence of a mechanical link between the lamin extensions and the acentric. Retracting lamin extensions "taking over" from microtubules to drive acentrics into nuclei could also explain the different velocities of acentrics moving off the metaphase plate and entering daughter nuclei. However, the mild correlation we measured between lamin retraction and acentric movement suggests that factors in addition to lamin extension and retraction drive acentrics through nuclear envelope channels.

The signals guiding lamin extension remain unclear, but one possibility is based on studies demonstrating that the reassembling nuclear envelope recognizes chromosomes via the Ran-GTP gradient emanating from chromatin (for review, see Hetzer et al., 2002), and lamin can bind both directly and indirectly to chromatin (Goldberg et al., 1999). In neuroblast divisions with acentrics, highly localized Aurora B kinase activity along the tether initially prevents the recruitment of lamin to the acentric and to the site of channel formation (Warecki and Sullivan, 2018). It is

possible that the lamin we observe extending from channels towards acentrics might therefore represent an attempt to reestablish lamin-DNA connections once Aurora B is cleared from the acentric guided by the local Ran-GTP gradient originating from the acentric.

Acentrics are encompassed by a membrane distinct from the nuclear envelope

In contrast to the behavior of the nuclear envelope components at the site of channels, in which all three major components were excluded from the sites of acentric entry to form nuclear envelope channels, we observed nuclear membrane localize to late-segregating acentrics despite the absence of lamin and nuclear pore complexes (Figure 23). The discrepancy in the ability of core and non-core components of the nuclear envelope to localize to lagging chromosomes was previously observed in cancer cells in which lagging whole chromosomes subsequently formed micronuclei (Liu et al., 2018). In these cells, the inability of micronuclei to recruit a fully functional nuclear envelope was proposed as the first step on the path toward chromothripsis. In contrast, in *Drosophila*, the exclusion of lamin and nuclear pore complexes from lagging chromosome fragments is important for the inclusion of the fragments into daughter nuclei and the maintenance of euploidy (Afonso et al., 2014; Karg et al., 2015). Lagging acentrics that fail to exclude lamin form micronuclei at high rates (Karg et al., 2015). Therefore, the exclusion of key nuclear envelope components from late-segregating chromosomes may represent both a blessing and a curse for a dividing cell: laggards that are free of non-core components are better

equipped to rejoin daughter nuclei; however, should the laggards fail to enter daughter nuclei, the resulting micronuclei would be particularly susceptible to chromothripsis and subsequent aneuploidy.

Membrane fusion drives the final stage of acentric incorporation into daughter nuclei

Despite the presence of nuclear membrane encompassing lagging acentrics, we observed efficient entry of membrane-coated acentrics into daughter nuclei. We hypothesized that membrane fusion between membrane on acentrics and membrane on daughter nuclei would be required for acentric integration into daughter nuclei. In accord with this hypothesis, we observed decreased acentric entry into daughter nuclei when cells were depleted of the conserved membrane fusion proteins Comt/NSF and Shrub/CHMP4B (Figure 25). In the canonical model of membrane fusion, the assembly of SNAREs on opposing membranes into a trans-SNARE complex mediates fusion of the membranes. NSF uses ATP hydrolysis to disassemble the trans-SNARE complex, freeing SNAREs for additional rounds of membrane fusion (for review, see Ryu et al., 2016). SNARE and NSF membrane fusion activity are essential for proper nuclear envelope reassembly: mutants result in membrane targeting to but not sealing around daughter nuclei (Baur et al., 2007). Since NSF disassembles trans-SNARE complexes, the involvement of Comt/NSF in efficient acentric entry into daughter nuclei suggests the involvement of SNARE proteins as well. However, the SNARE RNAi lines we tested did not result in increased micronucleation in our screen. This could be due to a defective RNAi line,

possible functional redundancy among the SNAREs, and/or the involved SNARE(s) not being included in our screen. Nevertheless, we believe the failure of acentric entry into daughter nuclei in Comt-depleted neuroblasts is due to an inability of these cells to undergo repeated rounds of SNARE-mediated membrane fusion necessary to fuse the membrane on acentrics to the membrane on nuclei.

Like Comt/NSF, Shrub/CHMP4B has conserved membrane fusion functions. CHMP4B is a major component of the ESCRT-III complex, which mediates membrane fusion in many processes, including cytokinesis (Carlton and Martin-Serrano, 2007; Morita et al., 2007), viral budding (Arii et al., 2018; Johnson et al., 2018), and plasma membrane repair (Jimenez et al., 2014). Recent work has shown that ESCRT-III also mediates membrane sealing during nuclear envelope reassembly (Vietri et al., 2015; Olmos et al., 2015) and nuclear envelope repair (Denais et al., 2016; Raab et al., 2016). Previous studies have shown that ESCRT-III localizes to lagging chromosomes that form micronuclei (Liu et al., 2018) and to micronuclei in interphase (Sagona et al., 2014; Willan et al., 2019). In these cells, ESCRT-III seals the nuclear membrane around the lagging chromosome, preventing their entry into daughter nuclei and resulting in the formation of micronuclei (Liu et al., 2018). Membrane sealing prevents proper recruitment of nuclear pore complexes and can subsequently lead to increased chromothripsis (Liu et al., 2018). In addition, ESCRT-III activity on micronuclei in interphase might also be linked to micronuclei degradation through autophagy (Sagona et al., 2014).

In contrast to these reports, in which ESCRT-III activity results in the damage to or loss of key genetic information, we believe ESCRT-III activity on late-segregating acentrics in *Drosophila* neuroblasts promotes maintenance of euploidy. We observed a failure of acentrics to enter into daughter nuclei in Shrub/CHMP4B-depleted neuroblasts. In our Shrub-depleted cells, acentrics exhibited segregation defects in addition to a decreased ability to reenter nuclei. However, increased micronucleation in Shrub-depleted neuroblasts could not be explained due to either the increased distance of Shrub-depleted acentrics from daughter nuclei or their unequal segregation off the metaphase plate. Neither of these variables correlated with increased micronucleation (Figure 26). We hypothesize that the failure of acentrics to enter daughter nuclei when Shrub is depleted is likely due to the same inability to fuse membrane on acentrics to membrane on daughter nuclei as we believe occurs in Comt-depleted cells. This could mechanistically explain the previously reported increase in in the frequency of cells with micronuclei observed when ESCRT-III components are depleted (Willan et al., 2019). Additionally, we found Shrub localized to acentrics during acentric reintegration into daughter nuclei but not during acentric initial poleward movement (Figure 28), suggesting the main activity of Shrub on acentrics is during reintegration.

We believe the Shrub-mediated acentric reintegration into daughter nuclei is most analogous to ESCRT-III's role in nuclear envelope repair. In our system, Shrub/CHMP4B-mediated membrane fusion between membrane on acentrics and membrane on nuclei is the first step in surrounding the acentric and the daughter

nucleus in the same nuclear envelope. At this stage, a continuous sheet of membrane surrounds the acentric and the nucleus. Most of the nucleus is encircled by lamin and nuclear pore complexes with the exception of a gap at the site of the channel (Figure 23). This geometry is reminiscent of transient nuclear envelope rupture events that can occur in migrating cancer cells (Denais et al., 2016). In these cells, mechanical pressure on nuclei creates lamin- and nuclear pore complex-free membrane blebs through which chromatin protrudes. Subsequent rupture of the membrane at these sites is followed by the restoration of nuclear envelope integrity through the action of ESCRT-III (Raab et al., 2016; Denais et al., 2016). ESCRT-III can similarly repair ruptured membranes that occur on interphase micronuclei (Willan et al., 2019), highlighting that ESCRT-III's nuclear membrane repair activity is not limited to primary nuclei. Because of the striking similarity in the morphology of the ruptured nucleus to that of a telophase daughter nucleus on which a nuclear envelope channel has formed, it is possible that the ESCRT-III complex recognizes channels as if they were nuclear envelope ruptures and subsequently performs the same membrane sealing actions in both cases, thereby fusing the acentric-associated membrane with the daughter nucleus-associated membrane.

A key unresolved issue is to identify the factors that govern ESCRT-III activity on reintegrating acentrics. Addressing this issue might explain why ESCRT-III activity on lagging chromosomes in human cells promotes the formation of damage-prone micronuclei (Liu et al., 2018), while ESCRT-III activity on lagging acentric fragments in *Drosophila* promotes the entry of those fragments into daughter

nuclei. In budding yeast and human cells, ESCRT-III assembles on telophase chromatin through interactions between one of its components, CHMP7, and the nuclear membrane (Olmos et al., 2016) and LEM2, an INM protein (Gu et al., 2017). CHMP7 then recruits additional ESCRT-III components to form a functional complex. Because nuclear membrane is recruited to both lagging whole chromosomes destined to form micronuclei (Liu et al., 2018) and to acentrics rejoining daughter nuclei, we would imagine that CHMP7 recruitment is similar in these two cases. A potential candidate for differentially regulating ESCRT-III activity on lagging whole chromosomes and acentric fragments is Aurora B kinase. In humans and *Drosophila*, Aurora B inhibits ESCRT-III activity during abscission through phosphorylation of CHMP4C (Carlton et al., 2012; Capalbo et al., 2012). It has been proposed that CHMP4C phosphorylation prevents formation of active ESCRT-III polymers (Capalbo et al., 2012). Aurora B initially localizes to the DNA tethers connecting acentrics to daughter nuclei (Royou et al., 2010) and is necessary for channel formation (Karg et al., 2015). Presumably, there is no Aurora B-coated tether connecting the lagging whole chromosome back to the main nucleus. In this view, perhaps Aurora B specifically on the acentric and tether inhibits formation of a fully functional ESCRT-III complex until acentrics near daughter nuclei. Thus, membrane sealing is delayed until reintegration. On whole lagging chromosomes in human cells, ESCRT-III may be active much earlier and might therefore lead to "premature" membrane sealing and micronuclei formation.

The Shrub/CMP4B we observe localize to reintegrating acentrics may be involved in additional processes besides fusing membrane on acentrics to membrane on daughter nuclei. Channel formation requires the disruption of nuclear pore complex assembly (Karg et al., 2015). It is possible that localized inhibition of nuclear pore complex assembly results in malformed nuclear pore complexes specifically where the acentric will enter the nucleus. In budding yeast, ESCRT-II/III component Chm7/CHMP7 is involved in sealing nuclear membrane around improperly formed nuclear pore complexes (Webster et al., 2016; Bauer et al., 2015). It is possible that ESCRT-III localizing to acentrics performs a similar function once acentrics begin to enter nuclei if channel formation had resulted in improper nuclear pore complexes.

Finally, we found that efficient acentric reintegration was dependent upon the endoplasmic reticulum protein Rtnl2/RTN2 (Figure 25). Rtnl2 is a member of the reticulon family, a group of proteins that play crucial roles in restructuring the endoplasmic reticulum throughout the cell cycle, including during mitosis (Voeltz et al., 2006). Reticulon proteins stabilize areas of high membrane curvature (Voeltz et al., 2006), and altering the levels of different reticulons in the cell can affect the dynamics of nuclear envelope reassembly (Anderson and Hetzer, 2008). It is possible that Rtnl2 is required to form or to stabilize curved nuclear membranes that may manifest as acentrics enter daughter nuclei. Failure to form these curved membranes in Rtnl2 knockdowns may prevent fusion between acentric-associated and daughter nuclei-associated membrane ultimately resulting in micronuclei formation.

Acentric entry into daughter nuclei results in global changes to nuclear morphology

Surprisingly, as the acentric entered the telophase nucleus, we often observed global disruptions in the organization of the nuclear envelope in addition to the local perturbations at the sites of acentric entry. While the elongated shape of nuclei was expected due to the lamin extended from channels, we were surprised by the presence of additional blebs distant from this site and an overall wrinkled appearance to the nuclei. One explanation for the global nuclear dysmorphia after acentrics rejoined daughter nuclei could be that restructuring the entire nuclear envelope is required to provide sufficient membrane, lamin and other components for the extensions. Abnormal nuclear shape might also result from acentric movement after it has been fully encompassed by a nuclear envelope. I-CreI creates double-stranded DNA breaks in the pericentric heterochromatin of the X chromosome (Rong et al., 2002). I-CreI induction does not affect the viability of the fly (Royou et al., 2010), suggesting that the break between the acentric and the centric fragments is eventually repaired. In *Drosophila*, heterochromatic breaks are moved to the nuclear periphery and are tethered to nuclear envelope components before they are repaired (Ryu et al., 2015). During homolog pairing in budding yeast meiosis, movement of chromosomes tethered to the nuclear envelope is correlated with nuclear envelope blebbing (Koszul et al., 2008). Thus, the nuclear blebbing we observe after acentrics enter daughter nuclei through channels could be due to repair events occurring at the nuclear envelope that rejoin the acentric and centric fragments.

Misshapen nuclei have long been observed in diseased and cancerous cells, including both primary tumors and cultured cell lines (Zink et al., 2004). Nuclear blebs are common in human diseases caused by mutations in A/C-type lamins, termed laminopathies (for review, see Capell and Collins, 2006). In these diseases, blebs are marked by the presence of A-type lamins and the absence of B-type lamins (Goldman et al., 2004). In addition to laminopathies, cancer cells also frequently form nuclear envelope blebs absent of Lamin B. For example, the prostate cancer-derived LNCaP and PC-3 cell lines have abnormal nuclear envelopes characterized by Lamin B-free blebs (Helfand et al., 2012). Intriguingly, both LNCaP and PC-3 cells often divide with lagging chromosomes (Wang and Kung, 2012; Cosenza et al., 2017), and abnormal nuclear blebs in these cells were only detected following cell division (Helfand et al., 2012). It would be interesting to see if these cancer cells undergo similar nuclear envelope reassembly modifications that facilitate the incorporation and repair of lagging and broken chromosomes.

There is a key difference between the blebbing observed in cancer cells and those observed in our system. In the former, lamin B is largely undetected in blebs (Helfand et al., 2012; Goldman et al., 2004), while in our system, we observe blebs forming with Lamin Dm0, the *Drosophila* ortholog of B-type lamins (Reimer et al., 1995). Computer modeling suggests that lamin B-free blebs form due to the result of local domains of lamin A expanding and adopting a distinct curvature (Funkhouser et al., 2013). Lamin A blebbing is associated with high energy states where the blebs originate (Funkhouser et al., 2013). We suspect that lamin Dm0-positive blebs

present when acentrics enter nuclei through channels are caused by localized bending and stretching of lamin Dm0. We would likewise expect the presence of lamin Dm0-positive blebs (Figure 22E; asterisk) to indicate an energetically unfavorable nuclear shape. If so, the energy required to bend and bleb the lamin Dm0 might be a sign of an active mechanism for incorporating acentrics into daughter nuclei.

Smaller than blebs, nuclear herniations are caused when malformed and/or malfunctioning nuclear pore complexes are sealed behind a nuclear membrane (Webster et al., 2016). Because we observe local defective nuclear pore complex assembly on acentrics and at the sites of channel formation, it is possible these surveillance mechanisms contribute to the abnormal nuclear shapes observed when acentrics enter daughter nuclei. However, it is hard to imagine how surveillance of defective nuclear pore complex assembly at the site of channels might lead to herniations elsewhere along the nuclear envelope unless global nuclear pore complex assembly was also disrupted. We do not believe there is a global disruption of nuclear pore complex assembly in our system, as we observe strong peripheral GFP-Nup107 localization along the rest of the nucleus. Furthermore, nuclei with acentrics passing through channels still remain capable of sequestering GFP-NLS, albeit at lower levels compared to normal nuclei, which is likely due to the formation of channels (Montembault et al., 2017). We therefore do not believe that the lamin blebs are caused by membrane sealing around malformed nuclear pore complexes.

The work presented here focuses on the final steps in which late segregating chromatids enter daughter nuclei. In summary, our results support a model in which

fusion of the reassembling nuclear membrane drives entry of chromosome fragments into daughter nuclei (Figure 29). To our knowledge, this represents a novel mechanism by which cells dividing with lagging chromosomes are able to maintain their genome integrity.

Figure 29. Model for membrane fusion-mediated acentric reintegration into daughter nuclei. Acentrics (magenta arrow) lag behind on the metaphase plate while the undamaged sister chromatids segregate. Acentrics remain connected to daughter nuclei by a previously described DNA tether (Royou et al., 2010). In late anaphase, acentrics begin segregating poleward via the action of microtubules (not shown). In telophase, all three major components of the nuclear envelope (dark green arrow: lamin, blue arrow: nuclear pore complexes, and yellow arrow: membrane) assemble on daughter nuclei, but only membrane assembles on acentrics. Nuclear envelope channels form in the lamin, nuclear pore complex, and membrane on daughter nuclei to provide a passageway through which acentrics can enter nuclei. Membrane fusion proteins such as NSF and ESCRT-III (light green arrow) localize to acentrics and daughter nuclei at the sites where acentrics first contact nuclei and mediate fusion between the membrane that is on acentrics and the membrane that is on daughter nuclei. These membrane fusion events guide acentrics through channels and into nuclei allowing the dividing cell to maintain euploidy.

Figure 29

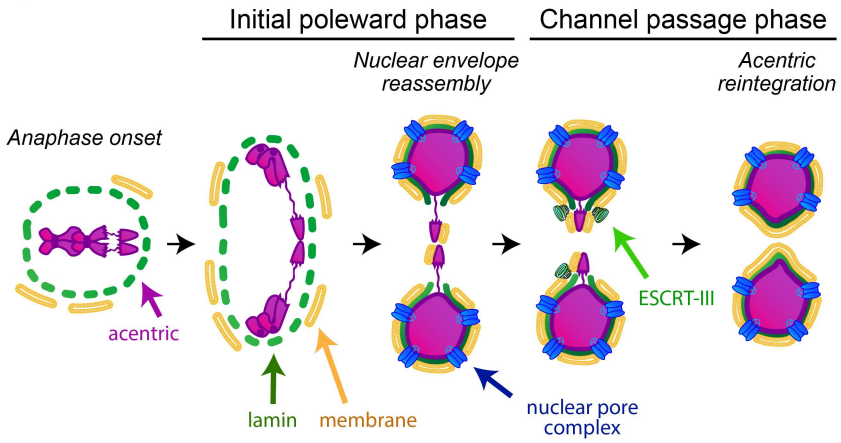

Materials and Methods

Drosophila stocks

All *Drosophila* stocks were raised on brown food (Sullivan et al., 2000). Crosses were performed at 25^{o}C with the exception of crosses involving Shrub-GFP (Figure 28), which were performed at 18^{o}C. Chromosome behavior was monitored using H2Av-RFP (stock #23561; Bloomington *Drosophila* Stock Center (BDSC, Bloomington Indiana). elav-Gal4 (Lin and Goodman, 1994) was used to drive expression of transgenes under control of an upstream activating sequence (UAS). We used the following lines to monitor nuclear envelope components: UAS-Lamin-GFP (#7376; BDSC), GFP-Nup107 (#35514; BDSC), and PDI-GFP (#6839; BDSC). *y1v1* flies (#1509) were used as a control for the RNAi screen (Table 1). The following RNAi lines were used: UAS-Rtnl2-shRNA (#58208; BDSC), UAS-Shrub-shRNA (#38305; BDSC), UAS-Comt-shRNA (#31666, #31470; BDSC), UAS-Snap24-shRNA (#28719; BDSC), UAS-Membrin-shRNA (#50515; BDSC), UAS-Snap-shRNA (#29587; BDSC), UAS-Spastin-shRNA (#53331; BDSC), UAS-Atlastin-shRNA (#36736; BDSC), UAS-Usnp-shRNA (#25862; BDSC), UAS-Syb-shRNA (#38234; BDSC), and UAS-Snap25-shRNA (#34377). We rebalanced RNAi stocks originally segregating Cyo to now segregate Cyo-GFP to allow for selection of the RNAi transgene at the larval stage. In addition, we used the following mutant flies: *comt6* (#26708; BDSC), and *Rtnl1* (#12425; BDSC). Flies containing UAS-Shrub-GFP transgenes were generously provided by Dr. Fen-Biao Gao.

Live neuroblast cytology

For experiments involving live imaging of acentrics, crawling female third-instar larvae were heat shocked for 1h at 37^{o}C. After 1-6h of recovery, brains were dissected in PBS and squashed between a slide and coverslip (Buffin et al., 2005). We filmed neuroblasts along the periphery of the squashed brain. Slides were imaged for up to 1h.

Time-lapse imaging for the RNAi screen was performed using both a Leica DM16000B wide-field inverted microscope equipped with a Hamamatsu EM-CCD camera (ORCA 9100-02) with a binning of 1 and a 100X Plan-Apochromat objective with NA 1.4 and an inverted Nikon Eclipse TE2000-E spinning disk (CSLI-X1; Nikon, Garden City, NY) confocal microscope equipped with a Hamamatsu EM-CCD camera (ImageE MX2) with a 100 x 1.4 NA oil immersion objective. Successive time points were filmed at 20 sec on the wide-field microscope and 10-18 sec on the spinning disk microscope. Spinning disk images were acquired with MicroManager 1.4 software.

All imaging experiments involving distance and fluorescence quantification (Figure 21B-D, Figure 22A-D, Figure 23, Figure 25A'-D', Figure 28) were performed exclusively using the spinning disk microscope. Successive time points for experiments presented in Figures 21B-D, 22A-D, 23, and 28 were filmed at 18 sec. Successive time points for experiments presented in Figure 25A'-D' were filmed at 10 sec.

Lattice Light Sheet Microscopy

We performed lattice light sheet microscopy at the Advanced Imaging Center (AIC) of the Howard Hughes Medical Institute (HHMI) Janelia research campus. Larvae were prepared as described above. After dissection, whole brains were mounted unsquashed in a drop of 2% agar and then imaged in a slide bath containing PBS. Brains were excited by a Special Optics 0.65 NA 3.74 mm working water dipping objective and detected with a Nikon CFI Apo LWD 25X water dipping 1.1 NA objective. Neuroblast divisions were filmed with a Hamamatsu Orca Flash 4.0 v2 sCMOS camera. Time-lapse movies were deskewed and deconvolved (Chen et al., 2014) prior to analysis.

Quantitative measurements

The distances of acentrics to daughter nuclei was calculated either as the distance of the furthest point on the acentric to the nearest point on the daughter nucleus (Figures 21D, 22D, and 25A'-D') or as the distance of the nearest point on the acentric to the nearest point on the daughter nucleus (Figures 22C and 26A). Distances were calculated at the time points indicated in the sections describing each figure. The lengths of lamin extensions were measured from the nearest point on the nucleus to the furthest point of the extension (Figure 22B-D) at the time points mentioned while describing each panel. All distances were measured in 3D space from Z-stacks taken during spinning disk microscopy.

The sphericities of daughter nuclei (Figure 22F) were measured in Imaris v9.2 (Bitplane) by generating contour surfaces of the nuclear envelopes at the time of completed lamin reassembly (Figure 22E, right panels). In brief, we drew regions of interest that aligned to the peripheral fluorescence intensity of Lamin-GFP in successive cross-sections throughout each Z-plane of the nucleus. These regions were then use to construct the surface. Sphericity values were calculated from the constructed surfaces.

The distances of acentrics from daughter nuclei in our RNAi screen (Figure 26A) were measured as described above. Distances were measured at the point when acentrics began their poleward movement. The time of acentric segregation (Figure 26B) was determined by measuring the time between anaphase onset and when acentrics first began their poleward movement. Measurements were performed in Fiji (Schindelin et al., 2012). Distance measurements were only made on movies acquired using spinning disk confocal microscopy, while time measurements were made on movies filmed both with the wide-field and spinning disk microscopes.

Quantitative measurements of nuclear envelope components on acentrics (Figure 23A'-C') were made in Fiji. We created a region of interest around the acentric or nucleus at each time point and measured the background-subtracted fluorescence intensity of the GFP signal from sum projections for the drawn region (Figure 24). Intensities were divided by the areas of the regions of interest. Each acentric was paired with the nucleus to which it was segregating. All values in an

acentric/nucleus pair were then normalized to the highest value in the acentric/nucleus pair.

Statistical analyses

All statistical tests were performed in R (R Core Team 2018). We used the following tests: paired t-tests (Figures 21D, 22B), independent two-sample t-tests (Figure 26), Mann-Whitney-Wilcoxon tests (Figure 22F), and chi-square tests (Figure 25). Additionally, we calculated the Pearson's correlations for data presented in Figure 2C-D in R.

Figure Preparation

Figures were assembled in Adobe Illustrator (Adobe, San Jose, CA). Imaging data was processed in Fiji. Selected stills were adjusted for brightness and contrast to improve clarity. Images for experiments involving lattice light sheet microscopy were processed and analyzed using Imaris. Graphs were created in R using the ggplot2 package (Wickham, 2016).

Bibliography

Abbas T., Keaton M. A., and Dutta A. (2013). Genomic instability in cancer. *Cold Spring Harb Perspect Biol* 5: a012914. https://doi.org/10.1101/cshperspect.a012914.

Afonso, O., Matos, I., Pereira, A.J., Aguiar, P., Lampson, M.A., *et al*. (2014). Feedback control of chromosome separation by a midzone Aurora B Gradient. *Science* 345: 332-336. https://doi.org/10.1126/science.1251121

Ahmad K., and Golic K. G. (1998). The transmission of fragmented chromosomes in Drosophila melanogaster. *Genetics* 148: 775-792.

Anderson, D.J. and Hetzer, M.W. (2008). Reshaping of the endoplasmic reticulum limits the rate for nuclear envelope formation. *J Cell Biol* 182: 911-924. https://doi.org/10.1083/jcb.200805140

Arii, J., Watanabe, M., Maeda, F., Tokai-Nishizumi, N., Chihara, T., *et al*. (2018). ESCRT-III mediates budding across the inner nuclear membrane and regulates its integrity. *Nat Commun* 9: 3379. https://doi.org/10.1038/s41467-018-05889-9

Bajer, A. (1957). Cine-micrographic studies of chromosome movements in β-irradiated cells. *Chromosoma* 9: 319-331. https://doi.org/10.1007/BF02568084

Bauer, I., Brune, T., Preiss, R., and Kölling, R. (2015). Evidence for a Nonendosomal Function of the Saccharomyces cerevisiae ESCRT-III-Like Protein Chm7. *Genetics* 201: 1439-1452. https://doi.org/10.1534/genetics.115.178939

Baur, T., Ramadan, K., Schlundt, A., Kartenbeck, J., and Meyer, H.H. (2007). NSF- and SNARE-mediated membrane fusion is required for nuclear envelope formation and completion of nuclear pore complex assembly in Xenopus laevis egg extracts. *J Cell Sci* 120: 2895-2903. https://doi.org/10.1242/jcs.010181

Bergman, Z.J., Mclaurin, J.D., Eritano, A.S., Johnson, B.M., Sims, A.Q., *et al*. (2015). Spatial Reorganization of the Endoplasmic Reticulum during Mitosis Relies on Mitotic Kinase Cyclin A in the Early *Drosophila* Embryo. *PLoS One* 10:e0117859. https://doi.org/10.1371/journal.pone.0117859

Bobinnec, Y., Marcaillou, C., Morin, X., and Debec, A. (2003). Dynamics of the endoplasmic reticulum during early development of Drosophila melanogaster. *Cell Motil Cytoskeleton* 54: 217-25. https://doi.org/10.1002/cm.10094

Bonaccorsi, S., Giansanti, M.G., and Gatti, M. (2000). Spindle assembly in *Drosophila* neuroblasts and ganglion mother cells. *Nat Cell Biol* 2: 54-56. https://doi.org/10.1038/71378

Bonassi, S., El-Zein, R., Bolognesi, C., and Fenech, M. (2011). Micronuclei frequency in peripheral blood lymphocytes and cancer risk: evidence from human studies. *Mutagenesis* 26: 93-100. https://doi.org/10.1093/mutage/geq075

Bretscher, H.S., and Fox, D.T. (2016). Proliferation of Double-Strand Break-Resistant Polyploid Cells Requires Drosophila FANCD2. *Dev Cell* 37: 444-457. https://doi.org/10.1016/j.devcel.2016.05.004

Buffin, E., Lefebvre, C., Huang, J., Gagou, M.E., Karess, R.E. (2005). Recruitment of Mad2 to the kinetochore requires the Rod/Zw10 complex. *Curr Biol* 15: 856-861. https://doi.org/10.1016/j.cub.2005.03.052

Cabenard, C., and Doe, C.Q. (2009). Apical/basal spindle orientation is required for neuroblast homeostasis and neuronal differentiation in *Drosophila*. *Dev Cell* 17: 134-141. https://doi.org/10.1016/j.devcel.2009.06.009

Capalbo, L., Montembault, E., Takeda, T., Bassi, Z.I., Glover, D.M., *et al*. (2012). The chromosomal passenger complex controls the function of endosomal sorting complex required for transport-III Snf7 proteins during cytokinesis. *Open Biol* 2: 120070. https://doi.org/10.1098/rsob.120070

Capell, B.C., and Collins, F.C. (2006). Human laminopathies: nuclei gone genetically awry. *Nat Rev Genet* 7: 940-952. https://doi.org/10.1038/nrg1906

Carlson, J.G. (1938). Mitotic Behavior of Induced Chromosomal Fragments Lacking Spindle Attachments in the Neuroblasts of the Grasshopper. *Proc Natl Acad Sci U S A* 24: 500-507.

Carlton, J.G., and Martin-Serrano, J. (2007). Parallels between cytokinesis and retroviral budding: a role for the ESCRT machinery. *Science* 316: 1908-1912. https://doi.org/10.1126/science.1143422

Carlton, J.G., Caballe, A., Agromayor, M., Kloc, M., and Martin-Serrano, J. (2012). ESCRT-III governs the Aurora B-mediated abscission checkpoint through CHMP4C. *Science* 336: 220-225. https://doi.org/10.1126/science.1217180

Carmena, M., Wheelock, M., Funabiki, H., and Earnshaw, W.C. (2012). The chromosomal passanger complex (CPC): from easy rider to the godfather of mitosis. *Nat Rev Mol Cell Biol* 13: 789-803. https://doi.org/1038/nrm3474

Celik, D.A., Koşar, P.A., Ozçelik, N., and Eroğlu, E. (2013). Cytogenetic finding of breast cancer cases and their first-degree relatives. *J Breast Cancer* 13: 285-290. https://doi.org/10.4048/jbc.2013.16.3.285

Cenci, G., Siriaco, G., Raffa, G.D., Kellum, R., and Gatti, M. (2003). The *Drosophila* HOAP protein is required for telomere capping. *Nat Cell Biol* 5: 82-84. https://doi.org/10.1038/ncb902

Chaudhary, N., and Courvalin, J.C. (1993). Stepwise reassembly of the nuclear envelope at the end of mitosis. *J Cell Biol* 122: 295-306.

Chen, B.C., Legant, W.R., Wang, K., Shao, L., Milkie, D.E., *et al*. (2014). Lattice light-sheet microscopy: imaging molecules to embryos at high spatiotemporal resolution. *Science* 346: 1257998. https://doi.org/10.1126/science.1257998

Cimini, D., Fioravanti, D., Salmon, E.D., and Degrassi, F. (2002). Merotelic kinetochore orientation vs. chromosome mono-orientation in the orgin of lagging chromosomes in human primary cells. *J Cell Sci* 115: 507-515.

Cipressa, F., and Cenci, G. (2013). DNA damage response, checkpoint activation and dysfunctional telomeres: face to face between mammalian cells and Drosophila. *Tsitologiia* 55: 211-217.

Conrad, M.N., Lee, C.Y., Chao, G., Shinohara, M., Kosaka, H., *et al*. (2008). Rapid Telomere movement in meiotic prophase is promoted by NDJ1, MPS3, and CSM4 and is modulated by recombination. *Cell* 133: 1175-1187. https://doi.org/10.1016/j.cell.2008.04.047

Cosenza, M.R., Cazzola, A., Rossberg, A., Schieber, N.L., Konotop, G. *et al*. (2017). Asymmetric Centriole Numbers at Spindle Poles Cause Chromosome Missegregation in Cancer. *Cell Rep* 20: 1906-1920. https://doi.org/10.1016/j.celrep.2017.08.005.

Crasta, K., Ganem, N.J., Dagher, R., Lantermann, A.B., Ivanova, E.V., *et al*. (2012). DNA breaks and chromosome pulverization from errors in mitosis. *Nature* 482: 53-58. https://doi.org/10.1038/nature10802

Daigle, N., Beaudouin, J., Hartnell, L., Imreh, G., Hallberg, E., *et al*. (2001). Nuclear pore complexes form immobile networks and have a very low turnover in live mammalian cells. *J Cell Biol* 154: 71-84. https://doi.org/10.1083/jcb.200101089

de Castro, I.J., Gil., R.S., Ligammari, L., Di Giacinto, M.L., and Vagnarelli, P. (2017). CDK1 and PLK1 coordinate the disassembly and reassembly of the

nuclear envelope in vertebrate mitosis. *Oncotarget* 9: 7763-7773. https:/doi.org/10.18632/oncotarget.23666

de Lartigue, J., Brust-Mascher, I., and Scholey, J.M. (2011). Anaphase B spindle dynamics in Drosophila S2 cells: Comparison with embryo spindles. *Cell Div* 6. https://doi.org/10.1186/1747-1028-6-8

Denais, C.M., Gilbert, R.M., Isermann, P., McGregor, A.L., te Lindert, M., *et al*. (2016). Nuclear envelope rupture and repair during cancer cell migration. *Science* 352: 353-358. https://doi.org/10.1126/science.aad7297

Derive, N., Landmann, C., Montembault, E., Claverie, C., Pierre-Elies, P., *et al*. (2015). Bub3-BubR1-dependent sequestration of Cdc20Fizzy at DNA breaks facilitates the correct segregation of broken chromosomes. *J Cell Biol* 211: 517-532. https://doi.org/10.1083/jcb.201504059

Ding, X., Xu, R., Yu, J., Xu, T., Zhuang, Y., *et al*. (2007). SUN1 is required for telomere attachment to nuclear envelope and gametogenesis in mice. *Dev Cell* 12:863-872. https://doi.org/10.1016/j.devcel.2007.03.018

Doe, C.Q. (2008). Neural stem cells: balancing self-renewal with differentiation. *Development* 135: 1575-1587. https://doi.org/10.1242/dev.014977

Dormann, H.L., Tseng, B.S., Allis, C.D., Funabiki, H., and Fischle, W. (2006). Dynamic regulation of effector protein binding to histone modifications: the biology of HP1 switching. *Cell Cycle* 5: 2842-2851. https://doi.org/10.4161/ec5.24.3540

Doucet, C.M., and Hetzer, M.W. (2010). Nuclear pore biogenesis into an intact nuclear envelope. *Chromosoma* 119: 469-477. https://doi.org/10.1007/s00412-010-0289-2

Douglas, M.E., Davies, T., Joseph, N., and Mishima, M. (2010). Aurora B and 14-3-3 coordinately regulate clustering of centralspindlin during cytokinesis. *Curr Biol* 20: 927-933. https://doi.org/10.1016/j.cub.2010.03.055

Duffy, J.B. (2002). GAL4 system in Drosophila: a fly geneticist's Swiss army knife. *Genesis* 34: 1-15. https://doi.org/10.1002/gene.10150

Dultz, E., Zanin, E., Wurzenberger, C., Braun, M., Rabut, G., *et al*. (2008). Systematic kinetic analysis of mitotic dis- and reassembly of the nuclear pore in living cells. *J Cell Biol* 180: 857-865

Elledge, S. (1996). Cell cycle checkpoints: preventing an identity crisis. *Science* 274: 1664-1672. https://doi.org/10.1126/science.274.5293.1664

Ellenberg, J., Siggia, E.D., Moreira, J.E., Smith, C.L., Presley, J.F. *et al*. (1997). Nuclear membrane dynamics and reassembly in living cells: targeting of an inner nuclear membrane protein in interphase and mitosis. *J Cell Biol* 138: 1193-1206.

Fasulo, B., Koyama, C., Yu, K.R., Homola, E.M., Hsieh, T.S., *et al*. (2012). Chk1 and Wee1 kinases coordinate DNA replication, chromosome condensation, and anaphase entry. *Mol Biol Cell* 23: 1047-1057. https://doi.org/10.1091/mbc.E11-10-0832

Fenech, M. (2000). The in vitro micronucleus technique. *Mutat Res* 455: 81-95. https://doi.org/10.1016/S0027-5107(00)00065-8

Fenech, M., Kirsch-Volders, M., Natarajan, A.T., Surralles, J., Crott, J.W., *et al*. (2011). Molecular mechanisms of micronucleus, nucleoplasmic bridge and nuclear bud formation in mammalian and human cells. *Mutagenesis* 26: 125-132. https://doi.org/10.1093/mutage/geq052

Funkhouser, C.M., Sknepnek, R., Shimi, T., Goldman, A.E., Goldman, R.D., *et al*. (2013). Mechanical model of blebbing in nuclear lamin meshworks. *Proc Natl Acad Sci U S A* 110: 3248-3253. https://doi.org/10.1073/pnas.1300215110

Fischle, W., Tseng, B.S., Dormann, H.L., Ueberheide, B.M., Garcia, B.A., *et al*. (2005). Regulation of HP1-chromatin binding by histone H3 methylation and phosphorylation. *Nature* 438: 1116-1122. https://doi.org/10.1038/nature04219

Forbes, D.J., Kirschner, M.W., and Newport, J.W. (1983). Spontaneous formation of nucleus-like structures around bacteriophage DNA microinjected into Xenopus eggs. *Cell* 34: 13-23.

Fuller, B.G., Lampson, M.A., Foley, A.E., Rosasco-Nitcher, S., Le, K.V., *et al*. (2008). Midzone activation of aurora B in anaphase produces intracellular phosphorylation gradient. *Nature* 453: 1132-1136. https://doi.org/10.1038/nature06923

Galgoczy, D.J., and Toczyski, D.P. (2001). Checkpoint adaptation precedes spontaneous and damage-induced genomic instability in yeast. *Mol Cell Biol* 21: 1710-1718. https://doi.org/10.1128/MCB.21.5.1710-1718.2001

Giasanti, M.G., Gatti, M., and Bonaccorsi, S. (2001). The role of centrosomes and astral microtubules during asymmetric division of Drosophila neuroblasts. *Development* 128: 1137-1145.

Giet, R., and Glover, D.M. (2001). Drosophila aurora B kinase is required for histone H3 phosphorylation and condensin recruitment during chromosome condensation and to organize the central spindle during cytokinesis. *J Cell Biol* 152: 669-682.

Goldberg, M., Harel, A., Brandeis, M., Rechsteiner, T., Richmond, T.J., *et al*. (1999). The tail domain of lamin Dm0 binds histones H2A and H2B. *Proc Natl Acad Sci U S A* 96: 2852-2857.

Goldman, R., Shumaker, D.K., Erdos, M.R., Eriksson, M., Goldman, A.E., *et al*. (2004). Accumulation of mutant lamin A causes progressive changes in nuclear architecture in Hutchinson-Gilford progeria syndrome. *Proc Natl Acad Sci U S A* 101: 8963-8968. https://doi.org/10.1073/pnas.0402943101

Golic, M.M., and Golic, K.G. (2011). A simple and rapid method for constructing ring-X chromosomes in Drosophila melanogaster. *Chromosoma* 120: 159-164. https://doi.org/10.1007/s00412-010-0297-2

Gonzalez, C., Casal Jimenez, J., Ripoli, P., and Sunkel, C.E. (1991). The spindle is required for the process of sister chromatid separation in Drosophila neuroblasts. *Exp Cell Res* 192: 10-15.

Green, R.A., and Kaplan, K.B. (2003). Chromosome instability in colorectal tumor cells is associated with defects in microtubule plus-end attachments caused by a dominant mutation in APC. *J Cell Biol* 163: 949-961. https://doi.org/10.1083/jcb.200307070.

Gruneberg, U., Neef, R., Honda, R., Nigg, E.A., and Barr, F.A. (2004). Relocation of Aurora B from centromeres to the central spindle at the metaphase to anaphase transition requires MKlp2. *J Cell Biol* 166: 167-172.

Gu, M., LaJoie, D., Chen, O.S., von Appen, A., Ladinsky, M.S., *et al*. (2017). LEM2 recruits CHMP7 for ESCRT-mediated nuclear envelope closure in fission yeast and human cells. *Proc Natl Acad Sci U S A* 114: E2166-E2175. https://doi.org/10.1073/pnas.1613916114

Güttinger, S., Laurell, E., Kutay, U. (2009). Orchestrating nuclear envelope disassembly and reassembly during mitosis. *Nat Rev Mol Cell Biol* 10: 178-191. https://doi.org/10.1038/nrm2641

Haraguchi, T., Koujin, T., Segura-Totten, M., Lee, K.K., Matsuoka, Y., *et al*. (2001). BAF is required for emerin assembly into the reforming nuclear envelope. *J Cell Sci*. 114: 4575-4585.

Hatch, E.M., Fischer, A.H., Deerinck, T.J., and Hetzer, M.W. (2013). Catastrophic nuclear envelope collapse in cancer cell micronuclei. *Cell* 154: 47-60. https://doi.org/10.1016/j.cell.2013.06.007

Helfand, B.T., Wang, Y., Pfleghaar, K., Shimi, T., Taimen, P., *et al*. (2012). Chromosomal regions associated with prostate cancer risk localize to lamin B-deficient microdomains and exhibit reduced genet transcription.

Hetzer, M., Gruss, O.J., and Mattaj, I.W. (2002). The Ran GTPase as a marker of chromosome position in spindle formation and nuclear envelope assembly. *Nat Cell Biol* 4: E177-E184. https://doi.org/10.1038/ncb0702-e177

Hirota, T., Lipp, J.J., Toh, B.H., and Peters, J.M. (2005). Histone H3 serine 10 phosphorylation by Aurora B causes HP1 dissociation from heterochromatin. *Nature* 438: 1176-1180. https://doi.org/10.1038/nature04254

Hsu, J.Y., Sun, Z.W., Li, X., Reuben, M., Tatchell, K., *et al*. (2000). Mitotic phosphorylation of histone H3 is governed by Ipl1/aurora kinase and Glc7/PP1 phosphatase in budding yeast and nematodes. *Cell* 102: 279-291. https://doi.org/10.1016/S0092-8674(00)00034-9

Huang, Y., Hou, H., Yi, Q., Zhang, Y., Chen, D., *et al*. (2011). The fate of micronucleated cells post X-irradiation detected by live cell imaging. *DNA Repair (Amst)* 10: 629-638. https://doi.org/10.1016/j.dnarep.2011.04.010

Huang, Y., Jiang, L., Yi, Q., Lv, L., Wang, Z., *et al*. (2012). Lagging chromosomes entrapped in micronuclei are not 'lost' by cells. *Cell Res* 22: 932-935. https://doi.org/10.1038/cr.2012.26

Ito, K., Awano, W., Suzuki, K., Hiromi, Y., and Yamamoto, D. (1997). The Drosophila mushroom body is a quadruple structure of clonal units each of which contains a virtually identical set of neurons and glial cells. *Development* 124: 761-771.

Ji, W., Bian, Z., Yu, Y., Yuan, C., Liu, Y., *et al*. (2013). Expulsion of micronuclei containing amplified genes contributes to a decrease in double minute chromosomes from malignant tumor cells. *Int J Cancer* 134: 1279-1288. https://doi.org/10.1002/ijc.28467

Jiang, Y., and Reichert, H. (2013). Analysis of neural stem cell self-renewal and differentiation by transgenic RNAi in Drosophila. *Arch Biochem Biophys* 534: 38-43. https://doi.org/10.1016/j.abb.2012.08.003

Jimenez, A.J., Maiuri, P., Lafaurie-Janvore, J., Divoux, S., Piel, M., *et al*. (2014). ESCRT machinery is required for plasma membrane repair. *Science* 343: 1247136. https://doi.org/10.1126/science.1247136

Johnson, D.S., Bleck, M., and Simon, S.M. (2018). Timing of ESCRT-III protein recruitment and membrane scission during HIV-1 assembly. *Elife* 7: e36221. https://doi.org/10.7554/eLife.36221

Kanda, T., and Wahl, G.M. (2000). The dynamics of acentric chromosomes in cancer cells revealed by GFP-based chromosome labeling strategies. *J Cell Biochem Suppl* 35: 107-144. https://doi.org/10.1002/1097-4644(2000)79:35+<107::AID-JCB113>3.0.CO;2-Y

Karg, T., Warecki, B., and Sullivan, W. (2015). Aurora B-mediated localized delays in nuclear envelope formation facilitate inclusion of late-segregating chromosome fragments. *Mol Biol Cell* 26: 2227-2241. https://doi.org/10.1091/mbc.E15-01-0026

Karg, T., Elting, M.W., Vicars, H., Dumont, S., and Sullivan, W. (2017). The chromokinesin Klp3a and microtubules facilitate acentric chromosome segregation. *J Cell Biol* 216: 1597-1608. https://doi.org/10.1083/jcb.201604079

Katsani, K.R., Karess, R.E., Dostatni, N., and Doye, V. (2008). In Vivo Dynamics of *Drosophila* Nuclear Envelope Components. *Mol Biol Cell* 19: 3652-3666. https://doi.org/10.1091/mbc.E07-11-1162

Kaye, J.A., Melo, J.A., Cheung, S.K., Vaze, M.B., Haber, J.E., *et al*. (2004). DNA breaks promote genomic instability by impeding proper chromosome segregation. *Curr Biol* 14: 2096-2106

Kirsch-Volders, M., Plas, G., Elhajouli, A., Lukamowicz, M., Gonzalez, L., *et al*. (2011). The in vitro MN assay in 2011: origin and fate, biological significance, protocols, high throughput methodologies, and toxicological relevance. *Arch Toxicol* 85: 873-899. https://doi.org/10.1007/s00204-011-0691-4

Koszul, R., Kim, K.P., Prentiss, M., Kleckner, N., and Kameoka, S. (2008). Meiotic chromosomes move by linkage to dynamic actin cables with transduction of force through the nuclear envelope. *Cell* 133: 1188-1201. https://doi.org/10.1016/j.cell.2008.04.050

Kotadia, S., Montembault, E., Sullivan, W., and Royou, A. (2012). Cell elongation is an adaptive response for clearing long chromatid arms from the cleavage plane. *J Cell Biol* 199: 745-753. https://doi.org/10.1083/jcb.201208041

Kourmouli, N., Theodoropoulos, P.A., Dialynas, G., Bakou, A., Politou, A.S., *et al*. (2000). Dynamic associations of heterochromatin protein 1 with the nuclear envelope. *EMBO J* 19: 6558-6568. https://doi.org/10.1093/emboj/19.23.6558

Krishnan, K.S., Chakravarty, S., Rao, S., Raghuram, V., and Ramaswami, M. (1996). Alleviation of the temperature-sensitive paralytic phenotype of shibire(ts) mutants in Drosophila by sub-anesthetic concentrations of carbon dioxide. *J Neurogenet* 10: 221-238.

LaFountain, J.R. Jr, Oldenbourg, R., Cole, R.W., and Rieder, C.L. (2001). Microtubule flux mediates poleward motion of acentric chromosome fragments during meiosis in insect spermatocytes. *Mol Biol Cell* 12: 4054-4065. https://doi.org/10.1091/mbc.12.12.4054

Liang, H., Wright, W.H., Cheng, S., He, W., and Berns, M.W. (1993). Micromanipulation of Chromosomes in PTK2 Cells Using Laser Microsurgery (Optical Scalpel) in Combination with Laser-Induced Optical Force (Optical Tweezers). *Exp Cell Res* 204: 110-120. https://doi.org/10.1006/excr.1993.1015

Lin, D.M., and Goodman, C.S. (1994). Ectopic and increased expression of Fasciclin II alters motorneuron growth cone guidance. *Neuron* 13: 507-523. https://doi.org/10.1016/0896-6273(94)90022-1

Liu, S., Kwon, M., Mannino, M., Yang, N., Renda, F., *et al*. (2018). Nuclear envelope assembly defects link mitotic errors to chromothripsis. *Nature* 561: 551-555. https://doi.org/10.1038/s41586-018-0534-z

Lu, L., Ladinsky, M.S., and Kirchhausen, T. (2011). Formation of the postmitotic nuclear envelope from extended ER cisternae precedes nuclear pore assembly. *J Cell Biol* 194: 425-440. https://doi.org/10.1083/jcb.201012063

Ly, P., Teitz, L.S., Kim, D.H., Shoshani, O., Skaletsky, H., *et al*. (2017). Selective Y centromere inactivation triggers chromosome shattering in micronuclei and repair by non-homologous end joining. *Nat Cell Biol* 19: 68-75. https://doi.org/10.1083/jcb.201012063

Maass, K.K., Rosing, F., Ronchi, P., Willmund, KV., Devens, F., *et al*. (2018). Altered nuclear envelope structure and proteasome function of micronuclei. *Exp Cell Res* 371: 353-363. https://doi.org/10.1016/j.yexcr.2018.08.029

Maggert, K.A., and Golic, K.G. (2005). Highly efficient sex chromosome interchanges produced by I-CreI expression in Drosophila. *Genetics* 171: 1103-1114. https://doi.org/10.1534/genetics.104.040071

Malkova, A., Ivanov, E.L., and Haber, J.E. (1996). Double-strand break repair in the absence of RAD51 in yeast: a possible role for break-induced DNA replication. *Proc Natl Acad Sci U S A* 93: 7131-7136. https://doi.org/10.1073/pnas.93.14.7131

Martins, T., Kotadia, S., Malmanche, N., Sukel, C.E., Sullivan, W. (2013). Strategies for outcrossing and genetic manipulation of Drosophila compound autosome stocks. *G3 (Bethesda)* 3: 1-4. https://doi.org/10.1534/g3.112.004481

McManus, K.J., and Hendzel, M.J. (2006). The relationship between histone H3 phosphorylation and acetylation throughout the mammalian cell cycle. *Biochem Cell Biol* 84: 640-657. https://doi.org/10.1139/o06-086

Meyer, H., Drozdowska, A., Dobrynin, G. (2010). A role for Cdc48/p97 and Aurora B in controlling chromatin condensation during exit from mitosis. *Biochem Cell Biol* 88: 23-28. https://doi.org/10.1139/o09-119

Mikhailov, A., Cole, R.W., and Rieder, C.L. (2002). DNA damage during mitosis in human cells delays the metaphase/anaphase transition via the spindle-assembly checkpoint. *Curr Biol* 12: 1797-1806.

Montembault, E., Claverie, M.C., Bouit, L., Landmann, C., Jenkins, J., *et al*. (2017). Myosin efflux promotes cell elongation to coordinate chromosome segregation with cell cleavage. *Nat Commun* 8: 326. https://doi.org/10.1038/s41467-017-00337-6

Montenegro, G., Rebelo, A.P., Connell, J., Allison, R., Babalini, C., *et al*. (2012). Mutations in the ER-shaping protein reticulon 2 cause the axon-degenerative disorder hereditary spastic paraplegia type 12. *J Clin Invest* 122: 538-544. https://doi.org/10.1172/JCI60560

Morita, E., Sandrin, V., Chung, H.Y., Morham, S.G., Gygi, S.P., *et al*. (2007). Human ESCRT and ALIX proteins interact with proteins of the midbody and function in cytokinesis. *EMBO J* 26: 4215-4227. https://doi.org/10.1038/sj.emboj.7601850

Newport, J.W., Wilson, K.L., and Dunphy, W.G. (1990). A lamin-independent pathway for nuclear envelope assembly. *J Cell Biol* 111: 2247-2259. https://doi.org/10.1083/jcb.111.6.2247

Norden, C., Mendoza, M., Dobbelaere, J., Kotwaliwale, C.V., Biggins, S., *et al*. (2006). The NoCut pathway links completion of cytokinesis to spindle midzone function to prevent chromosome breakage. *Cell* 125: 85-98.

Okada, Y., Suzuki, T., Sunden, Y., Orba, Y., Kose, S., *et al*. (2005). Dissociation of heterochromatin protein 1 from lamin B receptor induced by human polyomavirus agnoprotein: role in nuclear egress of viral particles. *EMBO Rep* 6: 452-457. https://doi.org/10.1038/sj.embor.7400406

Oliveira, R.A., Kotadia, S., Tavares, A., Mirkovic, M., Bowlin, K., *et al*. (2014). Centromere-independent accumulation of cohesion at ectopic

Olmos, Y., Hodgson, L., Mantell, J., Verkade, P., and Carlton, J.G. (2015). ESCRT-III controls nuclear envelope reformation. *Nature* 522: 236-239. https://doi.org.10.1038/nature14503.

Olmos, Y., Perdrix-Rosell, A., and Carlton, J.G. (2016). Membrane Binding by CHMP7 Coordinates ESCRT-III-Dependent Nuclear Envelope Reformation. *Curr Biol* 26: 2635-2641. https://doi.org/10.1016/j.cub.2016.07.039

Onischenko, E.A., Gubanova, N.V., Kiseleva, E.V., an Halberg, E. (2005). Cdk1 and okadaic acid-sensitive phosphatases control assembly of nuclear pore complexes in *Drosophila* embryos. *Mol Biol Cell* 16: 5152-5162. https://doi.org/10.1091/mbc.e05-07-0642

Ordway, R.W., Pallanck, L., and Ganetzky, B. (1994). Neurally expressed Drosophila genes encoding homologs of the NSF and SNAP secretory proteins. *Proc Natl Acad Sci U S A* 91:5715-5719.

Paredes, S., and Magger, K.A. (2009). Expression of I-CreI endonuclease generates deletions within the rDNA of Drosophila. *Genetics* 181: 1161-1671. https://doi.org/10.1534/genetics.108.099093

Pidoux, A., Uzawa, S., Perry, P.E., Cande, W.Z., and Allshire, R.C. (2000). Live analysis of lagging chromosomes during anaphase and their effect on spindle elongation rate in fission yeast. *J Cell Sci* 113: 4177-4191.

Poleshko, A., Mansfield, K.M., Burlingame, C.C., Andrake, M.D., Shah, N.R., *et al*. (2013). The human protein PRR14 tethers heterochromatin to the nuclear lamina during interphase and mitotic exit. *Cell Rep* 5: 292-301. https://doi.org/10.1016/j.celrep.2013.09.024

Polioudaki, H., Kourmouli, N., Drosou, V., Bakou, A., Theodoropoulos, P.A., *et al*. (2001). Histones H3/H4 form a tight complex with the inner nuclear membrane

protein LBR and heterochromatin protein 1. *EMBO Rep* 2: 920-925: https://doi.org/10.1093/embo-reports/kve199

Puerto, S., Ramírez, M.J., Marcos, R., Creus, A., and Surrallés, J. (2001). Radiation-induced chromosome aberrations in huan euchromatic (17cen-p53) and heterochromatic (1cen-1q12) regions. *Mutagenesis* 16: 291-296. https://doi.org/10.1093/mutage/16.4.291

R Core Team (2014). R: A language and statistical environment for statistical computing. R Foundation for Statistical Computing, Vienna, Austria. http://www.R-project.org

Raab, M., Gentili, M., de Belly, H., Thiam, H.R., Vargas, P., *et al*. (2016). ESCRT III repairs nuclear envelope ruptures during cell migration to limit DNA damage and cell death. *Science* 352: 359-362. https://doi.org/10.1126/science.aad7611

Ramadan, K., Bruderer, R., Spiga, F.M., Popp, O., Baur, T., *et al*. (2007). Cdc48/p97 promotes reformation of the nucleus by extracting the kinase Aurora B from chromatin. *Nature* 450: 1258-1262. https://doi.org/10.1038/nature06388

Rebollo, E., Sampaio, P., Januschke, J., Llamazares, S., Varmark, H., *et al*. (2007). Functionally unequal centrosomes drive spind orientation in asymmetrically dividing Drosophila neural stem cells. *Dev Cell* 12: 467-474.

Reimer, D., Stuurman, N., Berrios, M., Hunter, C., Fisher, P.A., *et al*. (1995). Expression of Drosophila lamin C is developmentally regulated: analogies with vertebrate A-type lamins. *J Cell Sci* 108: 3189-98.

Rhind, N., and Russell, P. (2012). Signaling pathways that regulate cell division. *Cold Spring Harb Perspect Biol* 4: a005942. https://doi.org/10.1101/cshperspect.a005942

Robbins, E., and Gonatas, N.K. (1964). The Ultrastructure of a mammalian cell during the mitotic cell cycle. *J Cell Biol* 21: 429-463. https://doi.org/10.1083/jcb.21.3.429

Robinson, J.T., Wojcik, E.J., Sanders, M.A., McGrail, M., and Hays, T.S. (1999). Cytoplasmic dynein is required for the nuclear attachment and migration of centrosomes during mitosis in Drosophila. *J Cell Biol* 146: 597-608.

Rong, Y.S., Titen, S.W., Xie, H.B., Golic, M.M., Bastiani, M., *et al*. (2002). Targeted mutagenesis by homolgous recombination in D. melanogaster. *Genes Dev* 16: 1568-1581. https://doi.org/ 10.1101/gad.986602

Roots, R., Kraft, G., and Gosschalk, E. (1985). The formation of radiation-induced DNA breaks: the ratio of double-strand breaks to single-strand breaks. *Int J Radiat Oncol Biol Phys* 11: 259-265. https://doi.org/10.1016/0360-3016(85)90147-6

Royou, A., H. Macias, H., and Sullivan, W. (2005). The Drosophila Grp/Chk1 DNA damage checkpoint controls entry into anaphase. *Curr Biol* 15: 334-339. https://doi.org/10.1016/j.cub.2005.02.026

Royou, A., Gagou, M.E., Karess, R., and Sullivan, W. (2010). BubR1- and Polo-coated DNA tethers facilitate poleward segregation of acentric chromatids. *Cell* 140: 235-245. https://doi.org/10.1016/j.cell.2009.12.043

Ryu, J.K., Jahn, R., and Yoon, T.Y. (2016). Review: Progresses in understanding N-ethylaleimide sensitive factor (NSF) mediated disassembly of SNARE complexes. *Biopolymers* 105: 518-531. https://doi.org/10.1002/bip.22854

Ryu, T., Spatola, B., Delabaere, L., Bowlin, K., Hopp, H., *et al*. (2015). Heterochromatic breaks move to the nuclear periphery to continue recombinational repair. *Nat Cell Biol* 17: 1401-11. https://doi.org/10.1038/ncb3258

Sabatinos, S.A., Ranatunga, N.S., Yuan, J.P., Green, M.D., and Forsburg, S.L. (2015). Replication stress in early S phase generates apparent micronuclei and chromosome rearrangement in fission yeast. *Mol Biol Cell* 26: 3439-3450. https://doi.org/10.1091/mbc.e15-05-0318

Sacristan, C., and Kops, G.J. (2015). Joined at the hip: kinetochores, microtubules, and spindle assembly checkpoint signaling. *Trends Cell Biol* 25:21-28. https://doi.org/10.1016/j.tcb.2014.08.006

Sagona, A.P., Nezis, I.P., and Stenmark, H. (2014). Association of CHMP4B and autophagy with micronuclei: implications for cataract formation. *Biomed Res Int* 2014: 974393. https://doi.org/10.1155/2014/974393

Samwer, M., Schneider, M.W.G., Schmalhorst, P.S., Jude, J.G., Zuber, J., *et al*. (2017). DNA cross-bridging shapes a single nucleus from a set of mitotic chromosomes. *Cell* 170: 956-972.e23. https://doi.org/10.1016/j.cell.2017.07.038

Santos, R.A., Teixeira, A.C., Mayorano, M.B., Carrara, H.H.A., Andrade, J.M., *et al*. (2010). Basal levels of DNA damage detected by micronuclei and comet assays in untreated breast cancer patients and healthy women. *Clin Exp Medi* 10: 87-92. https://doi.org/10.1007/s10238-009-0079-4

Sanyal, S., and Krishnan, K.S. (2012). Genetic modifiers of comatose mutations in Drosophila: insights into neuronal NSF (N-ethylmaleimide-sensitive fusion factor) functions. *J Neurogenet* 26: 358-359. https://doi.org/10.3109/01677063.2012.697500

Sato, A., Isaac, B., Phillips, C.M., Rillo, R., Carlton, P.M., *et al*. (2009). Cytoskeletal forces span the nuclear envelope to coordinate meiotic chromosome pairing and synapsis. *Cell* 139: 907-919. https://doi.org/10.1016/j.cell.2009.10.039

Schellhaus, A.K., De Magistris, P., and Antonin, W. (2015). Nuclear reformation at the end of mitosis. *J Mol Biol* 428: 1962-1985. https://doi.org/10.1016/j.jmb.2015.09.016

Schmitt, J., Benavente, R., Hodzic, D., Höög, C., Stewart, C.L., *et al*. (2007). Transmembrane protein Sun2 is involved in tethering mammalian meiotic telomeres to the nuclear envelope. *Proc Natl Acad Sci U S A* 104: 7426-7431. https://doi.org/10.1073/pnas.0609198104

Schindelin, J., Arganda-Carreras, I., Frise, E., Kaynig, V., Longair, M., *et al*. (2012). Fiji: an open-source platform for biological-image analysis. *Nat Methods* 9: 676-682. https://doi.org/10.1038/nmeth.2019

Schooley, A., Vollmer, B., and Antonin, W. (2012). Building a nuclear envelope at the end of mitosis: coordinating membrane reorganization, nuclear pore complex assembly, and chromatin de-condensation. *Chromosoma* 121: 539-54. https://doi.org/10.1007/s00412-012-0388-3

Smurnyy, Y.A., Toms, A.V., Hickson, G.R., Eck, M.J., and Eggert, U.S. (2010). Binucleine 2, an isoform-specific inhibitor of Drosophila Aurora B kinase, provides insights into the mechanism of cytokinesis. *ACS Chem Biol* 5: 1015-1020. https://doi.org/10.1021/cb1001685

Smyth, J.T., Schoborg, T.A., Bergman, Z.J., Riggs, B., and Russan, N.M. (2015). Proper symmetric and asymmetric endoplasmic reticulum partitioning requires astral microtubules. *Open Biol* 5: 150067. https://doi.org/10.1098/rsob.150067

Steen, R.L., Martins, S.B., Taskén, and Collas, P. (2000). Recruiment of protein phosphatase 1 to the nuclear envelope by A-kinase anchoring protein AKAP149 is a prerequisite for nuclear lamina reassembly. *J Cell Biol* 150: 1251-1262. https://doi.org/10.1083/jcb.150.6.1251

Stephens, P.J., Greenman, C.D., Fu, B., Yang, F., Bignell, G.R., *et al*. (2011). Massive Genomic Rearrangement Acquired in a Single Catastrophic Event during Cancer Development. *Cell* 144: 27-40. https://doi.org/10.1016/j.cell.2010.11.055

Stewénius, Y., Gorunova, L., Jonson, T., Larsson, N., Höglund, M., *et al.* (2005). Structural and numerical chromosome changes in colon cancer develop through telomere-mediated anaphase bridges, not through mitotic multipolarity.

Sugimoto, K., Tasaka, H., and Dotsu, M. (2001). Molecular behavior in living mitotic cells of human centromere heterochromatin protein HP1α ectopically expressed as a fusion to red fluorescent protein. *Cell Struct Funct* 26: 705-718. https://doi.org/10.1247/csf.26.705

Sullivan, W., Daily, D.R., Fogarty, P., Yook, K.J., and Pimpinelli, S. (1993). Delays in anaphase initiation occur in individual nuclei of the syncytial Drosophila embryo. *Mol Biol Cell*, 4: 885-896.

Sullivan, W., Ashburner, A., and Hawley, R.S. (2000). *Drosophila Protocols*. Cold Spring Harbor Laboratory Press, Cold Spring Harbor, NY.

Sweeney, N.T., Brenman, J.E., Jan, Y.N., and Gao, F.B. (2006). The coiled-coil protein shrub controls neuronal morphogenesis in Drosophila. *Curr Biol* 16: 1006-11. https://doi.org/10.1016/j.cub.2006.03.067

Tajik, A., Zahng, Y., Wei, F., Sun, J., Jia, Q., *et al*. (2016). Transcription upregulation via force-induced direct stretching of chromatin. *Nat Mater* 15: 1287-1296. https://doi.org/10.1038/nmat4729

Tanaka, T.U., Rachidi, N., Janke, C., Pereira, G., Galova, M., *et al*. (2002). Evidence that the Ipl1-Sli15 (Aurora kinase-INCENP) complex promotes chromosomal bi-orientation by altering kinetochore spindle pole connections. *Cell* 108: 317-329.

Tatsuka, M., Katayama, H., Ota, T., Tanak, T., Odashima, S., *et al*. (1998). Multinuclearity and increased ploidy caused by overexpression of the aurora- and Ipl1-like midbody-associated protein mitotic kinase in human cancer cells. *Cancer Res* 58: 4811-4816.

Terradas, M., Martín, M., Tusell, L., and Ganescà. (2009). DNA lesions sequestered in micronuclei induce a local defective-damage response. *DNA Repair (Amst)* 8: 1225-1234. https://doi.org/10.1016/j.dnarep.2009.07.004

Terradas, M., Martín, M., Hernández, L, Tusell, L., and Ganescà. (2012). Nuclear envelope defects impede a proper response to micronuclear DNA lesions. *Mutat Res* 729: 35-40. https://doi.org/10.1016/j.mrfmmm.2011.09.003

Thompson, S.L., and Compton, D.A. (2008). Examining the link between chromosomal instability and aneuploidy in human cells. *J Cell Biol* 180: 665-672. https://doi.org/10.1083/jcb.200712029

Thurmond, J., Goodman, J.L., Strelets, V.B., Attrill, H., Gramates, L.S., *et al*. (2019). Flybase 2.0: the next generation. *Nucleic Acids Res* 47: D759-D765. https://doi.org/10.1093/nar/gky1003

Titen, S.W., and Golic, K.G. (2008). Telomere loss provokes multiple pathways to apoptosis and produces genomic instability in Drosophila melanogaster. *Genetics* 180: 1821-1832. https://doi/org/10.1534/genetics/108.093625

Ulbert, S., Platani, M., Boue, S., and Mattaj, I.W. (2006). Direct membrane protein-DNA interactions required early in nuclear envelope assembly. *J Cell Biol* 173: 469-476. https://doi.org/10.1534/genetics.108.093625

Vagnarelli, P., Ribeiro, S., Sennels, L., Sanches-Pulido, L., de Lima Alves, F., *et al*. (2011). Repo-man coordinates chromosomal reorganization with nuclear envelope reassembly during mitotic exit. *Dev Cell* 21: 328-342. https://doi.org/10.1016/j.devcel.2011.06.020

Vázquez-Diez, C., Yamagata, K., Trivedi, S., Haverfield, J., and Fitz-Harris, G. (2006). Micronucleus formation causes perpetual unilateral chromosome inheritance in mouse embryos. *Proc Natl Acad Sci U S A* 113: 626-631. https://doi.org/10.1038/nature14408

Vietri, M., Schink, K.O., Campsteijn, C., Wegner, C.S., Schultz, W., *et al*. (2015). Spastin and ESCRT-III coordinate mitotic spindle disassembly and nuclear envelope sealing. *Nature* 522: 231-235. https://doi.org/10.1038/nature14408

Voeltz, G.K., Prinz, W.A., Shibata, Y., Rist, J.M., Rapoport, T.A. (2006). A class of membrane proteins shaping the tubular endoplasmic reticulum. *Cell* 124: 573-586. https://doi.org/10.1016/j.cell.2005.11.047

Walther, T.C., Alves, A., Pickersgill, H., Loïodice, I., Hetzer, M., *et al*. (2003). The conserved Nup107-160 complex is critical for nuclear pore complex assembly. *Cell* 113: 195-206.

Wang, L.Y., and Kung, H.J. (2012). Male germ cell-associated kinase is overexpressed in prostate cancer cells and causes mitotic defects via deregulation

of APC/CCDH1. *Oncogene* 31: 2907-2918. https://doi.org/10.1038/onc.2011.464

Warecki, B., and Sullivan, W. (2018). Micronuclei Formation Is Prevented by Aurora B-Mediated Exclusion of HP1a from Late-Segregating Chromatin in *Drosophila*. *Genetics* 210: 171-187. https://doi.org/ 10.1534/genetics.118.301031

Webster, B.M., Thaller, D.J., Jäger, J., Ochmann, S.E., Borah, S., *et al*. (2016). Chm7 and Heh1 collaborate to link nuclear pore complex quality control with nuclear envelope sealing. *EMBO J* 35: 2447-2467. https://doi.org/10.15252/embj.201694574

Wente, S.R., and Rout, M.P. (2010). The nuclear pore complex and nuclear transport. *Cold Spring Harb Perspect Biol* 2: 1-19. https://doi.org/10.1101/cshperspect.a000562

Wickham, H. (2016). *ggplot2: Elegant Graphics for Data Analysis*. Springer-Verlag, New York.

Willan, J., Cleasby, A.J., Flores-Rodriguez, N., Stefani, F., Rinaldo, C., *et al*. (2019). ESCRT-III is necessary for the integrity of the nuclear envelope in micronuclei but is aberrant at ruptured micronuclear envelopes generating damage. *Oncogenesis* 8: 29. https://doi.org/10.1038/s41389-019-0136-0

Yao, C., Wang, C., Li, Y., Zavortink, M., Archambault, V., *et al*. (2018). Evidence for a role of spindle matrix formation in cell cycle progression by antibody perturbation. *PLoS One* 13: e0208022. https://doi.org/10.1371/journal.pone.0208022

Ye, Q., and Worman, H.J. (1996). Interaction between an integral protein of the nuclear envelope inner membrane and human chromodomain proteins homologous to Drosophila HP1. *J Biol Chem* 271: 14653-14656. https://doi.org/10.1074/jbc.271.25.14653

Ye, Q., Callebaut, I., Pezham, A., Courvalin, J.C., and Worman, H.J. (1997). Domain-specidic interactions of human HP1-type chromodomain proteins and inner nuclear membrane protein LBR. *J Biol Chem* 272: 14983-14989. https://doi.org/10.1074/jbc.272.23.14983

Zhang, C., Z., Spektor, A., Cornilis, H., Francis, J.M., Jackson, E.K., *et al*. (2015). Chromothripsis from DNA damage in micronuclei. *Nature* 522: 179-184. https://doi.org/10.1038/nature14493

Zink, D., Fisher, A.H., and Nickerson, J.A. (2004). Nuclear structure in cancer cells. *Nat Rev Cancer* 4: 677-87. https://doi.org/10.1038/nrc1430